2014-01-29

Origin of the Mid Cretaceous Heavy Oils from the Safaniya Sandstone Reservoir (Wasia Formation), Saudi Arabia

AlGeer, Ranya

UNIVERSITY OF CALGARY

Origin of the Mid Cretaceous Heavy Oils from the Safaniya Sandstone Reservoir (Wasia Formation), Saudi Arabia

by

Ranya Ali AlGeer

A THESIS

SUBMITTED TO THE FACULTY OF GRADUATE STUDIES

IN PARTIAL FULFILMENT OF THE REQUIREMENTS FOR THE

DEGREE OF MASTER OF SCIENCE

DEPARTMENT OF GEOSCIENCE

CALGARY, ALBERTA

JANUARY, 2014

ABSTRACT

Heavy oil, extra heavy oil and natural bitumen deposits dominate the world oil inventory. There are several mechanisms by which heavy oil and natural bitumen form. They could originate by an early expulsion of oil from low-maturity-organic rich carbonate source rocks (Type II-S), or by in-situ natural alteration processes of conventional oils during migration or in the reservoir. Understanding heavy oil and natural bitumen formation mechanisms, and the geological factors controlling their occurrences, is of importance for petroleum exploration and production. While biodegradation has been found to be the main mechanism producing most Albertan Oil Sands, Venezuelan Orinoco belt heavy oils and other biodegraded oil fields, the origin of the Saudi heavy oils is much less clear.

A geochemical characterization of reservoir rock extracts and produced oil across the Mid Cretaceous Safaniya (SFNY) reservoir (Wasia Fm) section in Saudi Arabia was conducted using bulk, molecular and isotopic composition analysis of these oils to assess their origin. The samples are reservoired at a very shallow depth (3373-3480 feet below surface) and are similar in their physical properties and bulk compositions. The results indicate that the occurrence of these heavy petroleums is controlled primarily by maturity. They were mostly generated at an early stage of maturation (vitrinite reflectance (R_C) ≈ < 0.5%) from a high sulfur (7.8% S), carbonate source rock (marine algal Type II-S) deposited under a highly reducing environment.

The data further suggests that the SFNY petroleum probably has experienced incipient biodegradation as mirrored in the unusual selective depletion in the long chain alkylbenzenes (C_{15+}), while similar molecular weight n-alkanes and other paraffins remain intact. The deactivation of microbes in the shallow SFNY reservoir by deep burial in the Miocene and heating to temperatures up to 76°C prior to uplift was probably the reason for the preservation of the SFNY oils from severe biodegradation. Also, the data reveals a significant alteration in the low molecular weight (LMW) polycyclic aromatic hydrocarbons (C_{15-}) of the petroleum towards the oil water contact zone (OWCZ), possibly caused by water washing. However, a broader study on the hydrology of the Arabian basin involving hydrogen and oxygen isotopes, and oil/water partition coefficient measurement under subsurface conditions is needed to better understand interactions between static water and different compound classes of petroleum, and hence to draw

a firm conclusion on whether water washing was the main cause for the compositional gradients observed in the LMW aromatic hydrocarbons of the studied oils from the SFNY reservoir.

ACKNOWLEDGEMENTS

For help in producing this thesis, my deepest and heartfelt thanks to:

- Dr. Stephen Larter, my thesis supervisor, for giving generously of his time and for sharing his wisdom with me. Also, for his ongoing dedication, support, and guidance during the development of this thesis. Dr. Larter's discussions with me and feedback, both in person and via e-mail, were instrumental in helping me complete my thesis and achieve my academic and research goals.

- Dr. Haiping Huang, my thesis co-supervisor, for his ongoing support and, in particular, for his helpful discussions with me. His feedback was critical in further developing my thesis framework and discussion.

- My MSc Supervisory Committee which also included Dr. Dave Robertson and Dr. Ian Gates for their insightful discussions, and invaluable and constructive feedback in improving my thesis.

- The Petroleum Reservoir Group at the University of Calgary, specifically Priyanthi Weerawardhena, Dr. Norka Marcano, Dr. Thomas Oldenburg Dr. LIoyd Snowdon, Susan Dooley, Kim Nightingale and Rayan Snowdon for providing invaluable assistance in many aspects. As well, Steve Taylor and Jesusa Overend-Pontoy from the Applied Geochemistry Group for their support in the Parrbombing and stable isotopes analysis, and the company Gushor for the Iatroscan analysis.

- Dr. Sami Abdulbagi, Dr. Andreas Fuhrmann and Dr. Abid Buhllar with Aramco in Saudi Arabia for their support in data acquisition and for insightful and useful discussions with them about my research.

- Saudi Aramco for believing in my area of research and in demonstrating their trust in me with the award of a scholarship to further pursue my studies in Canada

- To my parents for their unfailing love and support and who journeyed from Saudi Arabia to Calgary to be with me as I began my graduate studies. Their love and encouragement continue to inspire me to be all that I can be.

TABLE OF CONTENTS

LIST OF TABLES

LIST OF FIGURES AND ILLUSTRATIONS

LIST OF SYMBOLS, ABBREVIATIONS AND NOMENCLATURE

Symbol	Definition
API gravity	American Petroleum Institute gravity
bbl/d	Barrel of oil per day
cP	Centipoise
CSS	Cyclic Steam Stimulation
DCM	Dichloromethane
FID	Flame Ionization Detector
GC	Gas Chromatography
GC-MS	Gas Chromatography -Mass Spectrometry
LCABs	Long Chain Alkylbenzenes
Ma	Million Years
mD	Millidarcy
NSO	Nitrogen, sulfur and oxygen compounds
OWCZ	Oil-Water Contact Zone
PAH	Polyaromatic Hydrocarbons
POPI	Pyroltic Oil Productivity Index
ppm	Parts per million
%Rc	Calculated Vitrinite Reflectance
RRF	Relative Response Factor
SARA	Saturated hydrocarbons, Aromatic, Resins and
SFNY	Safaniyah
TCA	Thermochemical Alteration
TSA	Thermochemical Sulfate Reduction
TDS	Total Dissolved Solids
TOC	Total Organic Carbon
V-CDT	Vienna -Canyon Diablo Troilite
V-PDB	Vienna -Pee Dee Belemnite

Chapter One: INTRODUCTION

This thesis concerns the origin of heavy oils from the Mid Cretaceous Safaniya reservoir (Wasia Formation section) part of the X field, in Saudi Arabia. In this section I briefly introduce the general scientific background for my study. This section first describes the formation, migration and accumulation of petroleum and then provides a general overview of the major mechanisms and secondary processes responsible for the formation of highly viscous heavy oil and tar mat deposits.

1.1 Formation, Migration and Accumulation of Petroleum

Petroleum is ultimately derived from the degradation products of ancient organic matter, buried in the primordial mud of swamps, lakes and oceans. The organic matter is predominantly derived from aquatic, microscopic-photosynthetic organism, known as phytoplankton. However, the residues of zooplankton and terrestrial (higher plants) can also contribute to the organic matter input and are capable to be transferred to petroleum (Peters et al., 2005). Coals are another source of fossil fuels and are mostly originated from terrestrial organic matter deposited under oxic to suboxic environment (Hunt, 1979). Tissot and Welte (1978) divided the transformation process of organic matter to petroleum into three stages of maturation, designated diagenesis, catagenesis and metagenesis. A summary of the petroleum generation process is shown in Fig. 1.1.

The diagenesis stage includes physical, biological and chemical reactions, which convert organic matter to kerogen (insoluble fraction of organic matter in common organic solvents). During this stage, organic matter subsiding in sediment sequence (at depths < 2 km) is compacted and preserved from complete destruction by bacterial activity under mild conditions of pressure and temperature. This compaction results in a drastic loss of water at this stage. Microorganisms then convert the organic matter biopolymers (e.g., proteins, cellulose) and lipids into biomonomers (amino acids, sugars, and fatty acids). Irreversible condensation reactions occur between these biomonomers resulting in the formation of brown humic substances called humic substances or melanoidins. With progressive condensation, the kerogen precursors “geopolymers”, are formed and incorporated into the sediments. At the end of the diagenesis stage, the polycondensed organic residue is called kerogen, which likely contains a mixture of preserved refractory

biopolymers and geopolymers and many new structures(Killops and Killops, 2005). The organic matter in this stage mainly generates biogenic methane (CH_4) in addition to water, CO_2 and some heavy asphaltic compounds. The end of this stage corresponds to vitrinite reflectance of about 0.4-0.5% VRo (Tissot and Welte, 1978).

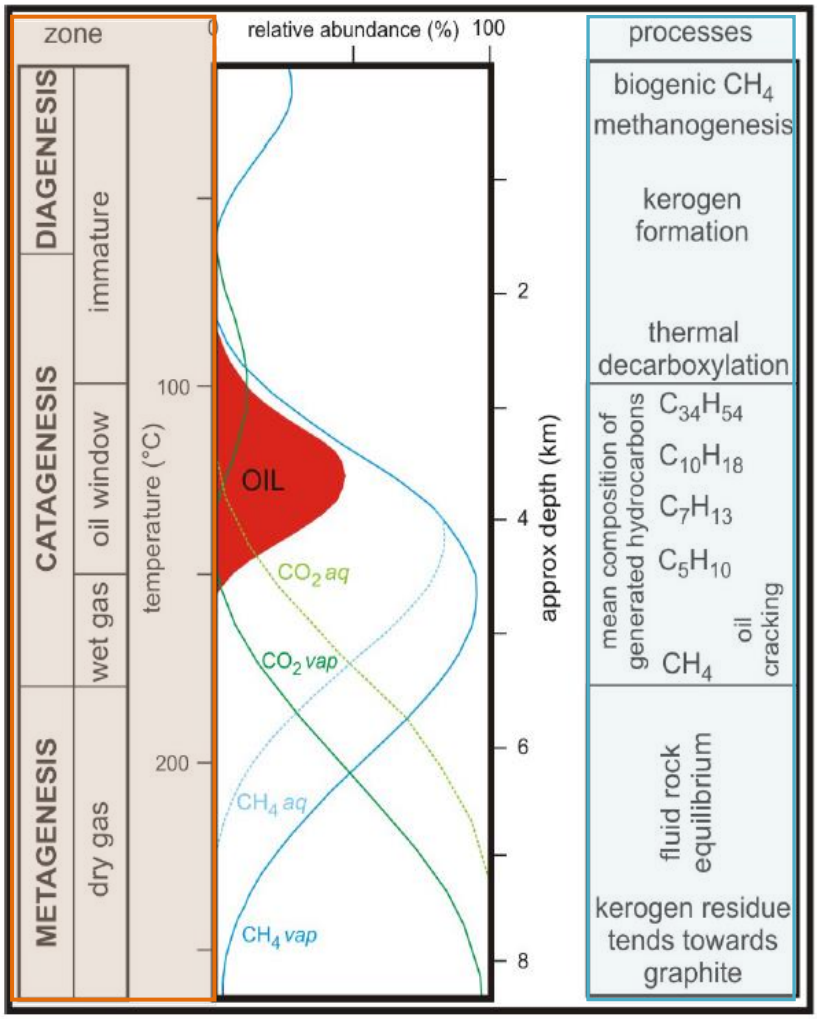

Fig. 1.1 Generalized scheme of thermal transformation of kerogen to petroleum. The Figure shows relative abundances of hydrocarbons, which are generated from sapropelic sources with progressive maturation. The catagenesis stage starts at ~50°C and the onset of oil generation is around 100°C. An average surface temperature of 15°C and ageothermal gradient of 30°C/km have been assumed (modified from Killops and Killops, 2005).

With increasing pressure and temperature as a result of progressive burial, the catagenesis stage starts (VRo 0.6-2%). In this stage, the kerogen and previously generated, during diagenesis, heavy asphaltic compounds are thermally degraded to petroleum as the kerogen attempts to reach thermodynamic equilibrium. The degradation process is accompanied by the loss of oxygen species and water. The catagenesis stage is divided into two zones, the oil window and the wet

gas window. Within the oil window which occurs between 100-150°C (VRo 0.5-1.0%), the organic matter generates only liquid petroleum with intermediate to low molecular weights. The cleavage of C-C and C-O bonds dominates this window, and the newly generated hydrocarbons progressively dilute the previously confined biomarkers within the kerogen structure (Tissot and Welte, 1978). Thus, the early petroleum charge within this window have relatively high molecular weight (~ $C_{34}H_{54}$). However, with increasing thermal maturity the size of the generated hydrocarbon structures decreases. At the last stage of catagenesis, more cleavage of C-C bounds occurs and between 150-180°C a mixture of C_1-C_5 gases is produced. This phase is called the "wet gas" window (VRo 1.3-2%). The amount of generated methane increases with progressive maturation of the kerogen until only this "dry gas" is generated during the metagenesis (>180°C and 2-4% VRo)(Tissot and Welte, 1978).

Once the petroleum is released from the kerogen, it is transported from the source bed to a reservoir where it accumulates. This process is divided into primary and secondary migration with primary migration being defined as the expulsion of the petroleum from the fine-grained source bed into the more porous and permeable carrier beds. The movement of petroleum within the carrier and reservoir rocks is termed secondary migration (Tissot and Welte, 1978). However, England et al. (1987) stated that this distinction of the migration process is artificial. They claimed that most of all petroleum movement in the subsurface happens through the same mechanism. With this mechanism, the petroleum is migrated as a separate phase in water-wet rocks; this movement happens in a focused fashion using only 1-10% of the carrier bed and is governed by the competition of the buoyancy, capillary and hydrodynamic forces. Furthermore, England et al. (1987) pointed out that the only difference between these two movements is that the primary migration is governed by capillary driving forces whereas buoyancy forces play a major role in the secondary movement. As soon as the petroleum enters a reservoir, it is exposed to secondary alteration processes (e.g., biodegradation and water-washing),which might affect its composition, resulting in most of the cases of the formation of heavy viscous oils and/or solid residues.

Because individual derivatives of the original organic matter "biopolymers or biomonomers" are often preserved as biomarkers or are transformed to geopolymers in response to the thermal stress during petroleum generation process, the molecular geochemistry of oil and gas can be used to

infer information about their source rock such as (1) type of kerogen (oil-prone vs. gas-prone); (2) age; lithology; depositional environment; and level of thermal maturity during generation. Furthermore, it can be used to assess the level of degradation processes that altered the petroleum composition during migration or after entrapment in the reservoir. (e.g., Peters and Moldowan, 1993; Lafargue and Barker, 1988; Palmer, 1984; Huang et al., 2004; Peters et al., 2005; Machel, 2001; Wilhelms and Larter, 1994). For example, the biomarker triaromatic and monoaromatic steroids are among the oftenly used parameters in assessing the thermal maturity of source rocks and crude oils. The dominance of monoaromatic steroids over the triaromtic steroids in an oil sample could be an indication of low thermal maturity (Mackenzie, 1984). Various compounds such as as the sterane and diasteranes distribution can be used to characterize the lithology of source rock. The absence or low concentration of diasteranes compared to steranes reflects petroleum generated from clay poor source rock (Rubinstein et al., 1975). The biomarkers C_{31}-C_{35} homohopanes (C_{35} homohopane index) are useful in assessing the redox conditions of a source rock depositional environment. Petroleum from marine sediments deposited under anoxic conditions usually shows a high homohopane index (Ourisson et al., 1984). Also, the relative loss of different classes of compounds (n-alkanes, acyclic isoprenoids, steranes, hopanes and terpanes) in response to microbial attack is successfully employed in ranking the level of biodegradation in biodegraded oils. The selective destruction of n-alkanes in an oil followed by isoprenoids represents a light to moderate biodegradation stage, whereas a severe stage of biodegradation is marked first by the destruction of regular steranes, then by diasteranes and hopanes, aromatic steroids and finally porphyrins (e.g., Peters and Moldowan, 1993; Huang et al., 2004; Peters et al., 2005).

In this thesis, molecular and isotopic geochemistry is used to investigate the origin of heavy oils from the Mid Cretaceous Safaniya reservoir (Wasia Formation section) part of the X field, in Saudi Arabia. Heavy oils, extra heavy oils and natural bitumen constitute more than 65% of the world's total oil resources which are estimated to be between 9 to 13 trillion barrels (Shlumberger, 2006). Despite the difficulties, high costs and environmental impacts associated with heavy oil extraction, transportation and refining, the oil industry is now more focused on exploiting heavy oils to meet the worldwide increase in crude oil demand and to counteract depletion in conventional oil reservoirs. In addition, the challenges associated with natural gas

production, such as exploration risks and economic uncertainties (current low gas price), have made the development of heavy oil resources an attractive and lucrative objective for many producers.

Heavy oils and natural bitumens are characterized by their high viscosity (low mobility), high density (low API gravity), high polar NSO (nitrogen, sulfur and oxygen) compounds and heavy metal content. According to the U.S. Geological Survey (2003), heavy oil is defined as the oil with API gravity and viscosity of 22° and 100 cP, respectively. Whereas the API gravity of extra-heavy oil is below 10° and its viscosity is lower than 10,000 cP. Natural bitumen (e.g., oil sands and tar mats) as a separate category of heavy petroleum is the immobile material with a viscosity over 10,000 cP under reservoir conditions and API gravity less than 10°. Wilhelms and Larter (1994) defined the tar mats as the zones that have a higher concentration of asphaltenes with respect to oil leg (20-60 wt % of C_{15}^{+} compounds) and usually reside close to discontinuities such as oil-water contacts.

Most heavy oils and tar mats are degraded remnants of conventional oils that were altered by in situ natural processes, such as biodegradation, water washing and gas deasphalting (Milner et al., 1977; Blanc and Connan, 1994; Tissot and Welte, 1978). Nevertheless, some of the global heavy oil resources originate from very low mature-organic rich source rock, which is responsible for a very low percentage of heavy oil deposits (Milner et al., 1977; Tissot and Welte, 1978; Tannenbaum and Aizenshtat, 1985). This section provides a general overview of major mechanisms and secondary processes responsible for the formation of highly viscous heavy oil and tar mat deposits.

1.2 Origin of Heavy Oils and Natural bitumen

1.2.1 Early Expulsion of Oil from Immature (Type-IIS) Source Rock

A part of the heavy oil resources in the globe, comes from low mature source rocks. This type of heavy oil commonly resides in association with organic rich carbonates or shales (high sulfur kerogen type-IIS) deposited in a highly reducing environment. The highly reducing conditions leads to the preservation of a significant amount of organic material, which can rapidly change

into petroleum given low thermal stresses. The early expulsion of these low maturity oils is mainly related to the high heteroatomic content (mainly sulfur) in kerogen. Based on kinetic studies of oil generation, it was concluded that the relative weakness of C-S bonds compared to C-C bonds is what results in faster petroleum generation rates from kerogen type-IIS compared to type-II (Tissot et al., 1987; Tomic et al., 1995). However, Lewan et al. (1998) argued that the cleavage of the weaker and limited S-C and S-S bonds cannot account for the cleavage of alkyl C-C bonds to generate the massive petroleum constituents in an early stage of maturation. Hence, he proposed a mechanism that stressed the role of free sulfur radical concentrations in increasing the rate of petroleum formation from a kerogen under low thermal stresses. In this mechanism, the alkyl C-C bonds are activated by hydrogen-removing effects of the sulfur radicals which are produced from the S-C and S-S bonds cleavage during thermal maturation.

The low maturity non-degraded oils are generally characterized by their: (1) low API gravities and high viscosities; (2) low Pr/Ph ratio (predominance of phytane over pristane indicates the strongly reducing conditions); (3) high C15+ content (high proportion of aromatics and polar NSO compounds) leading to lower aliphatic/aromatic hydrocarbon ratios; and (4) high sulfur content due to the fact that carbon-sulfur bonds are weaker and hence easier to crack during the early stage of maturation than carbon-carbon bonds (Orr, 1986).

Although low maturity oils and biodegraded oils show very similar physical properties and gross compositions, and sometimes an unresolved complex mixture "hump" dominates their gas chromatography (GC) traces, they differ from each other by the presence of n-alkanes, which are normally depleted in biodegraded oils at early stages of biodegradation. Moreover, they have different biomarker signatures (Milnur et al., 1977).

1.2.2 Post-Generation Alteration Processes

1.2.2.1 Biodegradation

Biodegradation of petroleum is the alteration of hydrocarbons and other heteroatomic compounds by living organisms (mainly bacteria and archaea) over geological time and has major economic consequences (Milner et al., 1977; Connan, 1984; Blanc and Connan, 1994). Compard with

unaltered petroleum, biodegraded oils have lower API (American Petroleum Institute) gravity, are more viscous, and are richer in sulfur, resins, asphaltenes, acidic compounds and metals (e.g., Ni and V), making them less desirable as a feedstock (Connan, 1984; Head et al., 2003; Wenger and Isaksen, 2002). Until very recently it was generally accepted that the effect of biodegradation on petroleum was mainly caused by aerobic bacteria (Palmer, 1993). However, biodegradation of crude oil is also witnessed in reservoirs where oxygen is not available, and it was later found that anaerobic hydrocarbon degradation is the dominating process in petroleum reservoirs (e.g., Head et al., 2003; Aitken et al., 2004; Jones et al., 2008). In the biodegradation process, hydrocarbons and other heteroaromtic compounds are used as energy source by microorganisims to build biomass, CO_2, partially oxidized residue and organic acids (Head et al., 2003; Peters et al., 2005) through different metabolic pathways. In reservoirs with low concentrations of aqueous sulfate, methanogenic degradation is the primary process, whereas in water containing abundant sulfate, sulfate reduction occurs and hydrogen sulfide is a major by-product (Larter et al., 2006a; Jones et al., 2008). In the latter condition, the possible occurrence of biodegradation can be verified by studying pyrite (iron sulfide) formation in the reservoir, which is inferred to represent the sink for reduced sulfur from sulfate reduction during biodegradation. Moreover, it has been reported the nitrates and ferric iron could act as possible electron acceptors during anaerobic petroleum biodegradation, by denitrifying and ferric iron-reducing bacteria (Heider et al., 1998).

The effects of biodegradation on the molecular composition and physical properties of crude oil and gases are relatively well-known (Connan, 1984). Because biodegradation preferentially consumes light hydrocarbons the residual oil becomes enriched in aromatics and NSO containing compounds resulting in low aliphatic/aromatic hydrocarbon ratios (Connan, 1984; Tissot and Welte, 1978). Typically, the loss of *n*-alkanes relative to branched and cyclic ones is known as the most important indicator of oil biodegradation. This loss is followed by the alteration of isoprenoid, alkylcyclohexanes, alkylated monoaromatic hydrocarbons and more resistant alkylated polyaromatic hydrocarbon components. At severe stages of biodegradation, cyclic biomarker alkanes are altered (Peters and Moldowan, 1993; Wenger et al., 2002). However, according to Larter et al. (2003) and, Peters and Moldowan (1993), alteration of some of the more biodegradation resistant classes of compounds could start before the complete depletion of the more subtle ones to biodegradation.

The criteria used for ranking biodegradation is that advocated by Peters and Moldowan (1993) which was later extended by Wenger et al., (2002). Peters and Moldowan (1993) developed a scale of 1-10 based on the differing resistance of compound classes to microbial attack, with level 1 indicating slightly biodegraded oil (PM 1), while level 10 represents the highest level of alteration (PM 10). Wenger et al. (2002) scale used a more comprehensive suite of compounds to track the changes in oil quality with increasing biodegradation, using very slight, slight to moderate, heavy and severe to describe oil biodegradation levels. Although these scales have successfully provided a useful but general description of level of degradation across different petroleum types, they lacked the resolution when dealing with heavily degraded oils. For example, according to Larter et al. (2012), although a number of analyzed oils from Peace river oil sands have shown dead oil viscosities that ranges from a few thousand cP to > 6 million cP at 20C, they were all described by a degradation level of 5 PM. This lack of resolution is a result of the focus on specific classes of compounds (saturate hydrocarbons), primarily in conventional oils.

Most recently, Larter et al. (2012) developed a new high-resolution scale for ranking biodegradation, especially for heavy oils samples with level PM 4-8, named Manco. The Manco scale differs from the existing scales by using different classes of compounds (alkyl aromatics, alkylthiophenic and steranes) which were found to be useful in tracking compositional gradient in samples that show same degradation level on the existing standard scales. Moreover, the Manco scale uses a semi-quantitative approach and takes into consideration the extent of alteration within a compound class together with a consideration of biodegradation across a range of compound classes. This scale provides for each compound group, 5 levels of increasing degree of degradation with score 0 representing no alteration, score1 for mild alteration , score 2 for intermediate alteration, score 3 for heavy alteration and score 4 for complete depletion of a compound class.

The occurrence of biodegraded oil in the subsurface is constrained to specific geological and geochemical conditions. At shallow depths and temperatures up to about 80°C (176°F), petroleum in subsurface reservoirs is often biologically degraded. Biodegradation requires nutrients (K, N, P) and proceeds in any reservoir that has a water leg. However, it is also possible to find non-degraded oils in shallow reservoirs given that these reservoirs were sterilized (palaeo-

pasteurized) by deep burial to a temperature above 80°C prior to uplift. This high temperature prevented re-colonization by bacteria (Wilhelms et al., 2001a). Also water salinity of formation waters (total dissolved solids, TDS) has an effect on biodegradation. Highly saline formation waters (salinities significantly above the 150 g/l of TDS) may limit biodegradation processes (Wenger and Isaksen (2002). Larter et al. (2006 b) also reported that high water-leg salinities have a second-order inhibitory effect that reduces degradation rates.

Larter et al. (2003) proposed a biodegradation model to explain the large scale compositional gradients at oil columns across heavy oil fields (Fig 1.2). According to this model, biodegradation occurs mostly at the base of oil columns close to the oil-water contact zones, where conditions are appropriate to microbial activity (e.g., availability of free water and nutrients). Also, the model considers the diffusive supply of essential inorganic nutrients (buffered by mineral dissolution) to the biodegradation sites as the rate-limiting factor. Thus, a sufficient porosity and permeability in the reservoir rock fabric and a free water leg is required to allow the diffusion of nutrients to microorganisms at the OWC. Moreover, the model states that reservoir temperature, charge rate, mixing of fresh and degraded oil rates and the ratio between the OWC area and oil volume, are among the primary factors controlling rates of biodegradation and oil compositional variations (Head et al., 2003; Larter et al., 2003; 2006).

Oil biodegradation produces heavy asphaltic oils and therefore was proposed as a possible mechanism for tar mats formation (e.g., Connan, 1984). Nevertheless, Wilhelms and Larter (1994) based on case studies from the North Sea and elsewhere, concluded that due to several reasons, biodegradation is very unlikely to lead to tar mat formation, otherwise tar mats would be more frequent in strongly biodegraded reservoirs than non-degraded reservoirs. Also, they supported their conclusion with evidence that lies within the physical-chemical properties of asphaltenes. As crude oil during the biodegradation process loses its lighter alkane compounds (compounds with lower Hildebrand solubility factor), becoming more aromatic. Therefore, it is expected that biodegradation should stabilize asphaltene solution in biodegraded oils, not precipitate it.

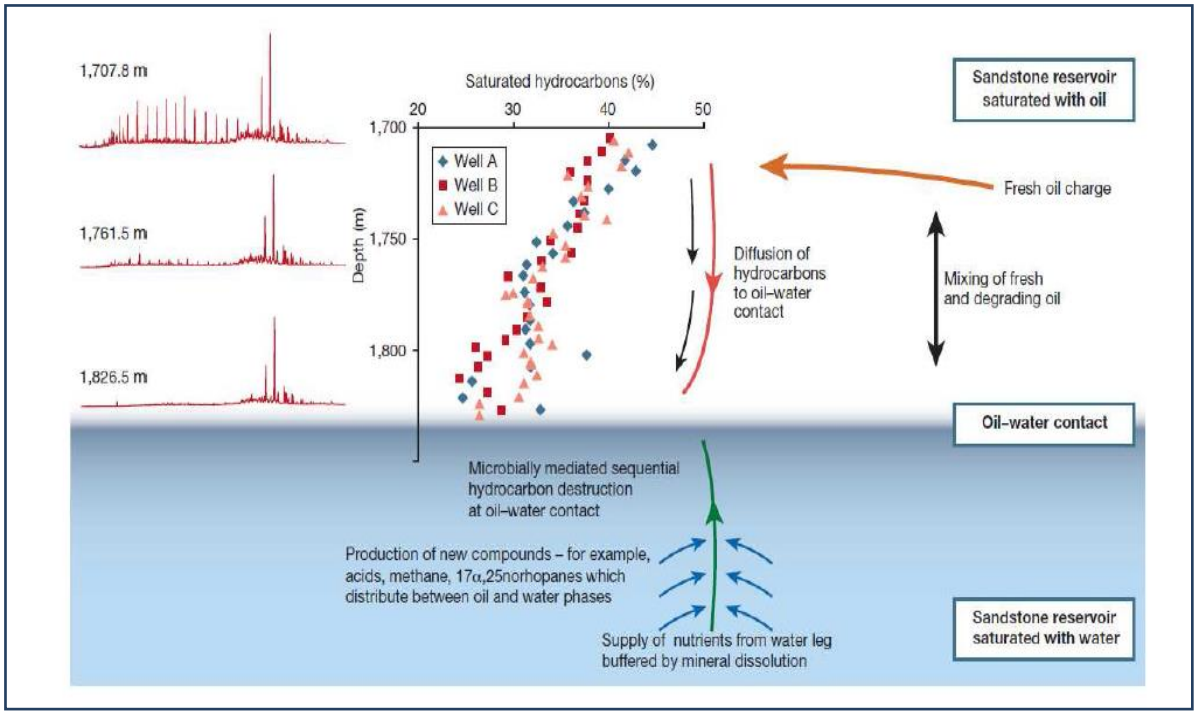

Fig. 1.2 Conceptual model of biodegradation: Compositional gradients in biodegraded oil column results from: hydrocarbon degradation at or near the oil-water contact, diffusion of hydrocarbons towards the oil-water contact and mixing of degraded oil and fresh oil recharge at the top of the reservoir (after Head et al., 2003).

1.2.2.2 Water-washing

Water-washing causes removal of the more soluble light hydrocarbons, aromatics and other compounds from petroleum through contact with formation waters in reservoirs or during migration (Peters and Moldowan, 1993). However, Lafargue and Barker (1988) concluded that water-washing effects on petroleum must be negligible during migration due to the presence of relatively high concentrations of water-soluble molecules, benzene and toluene, in most petroleums. They found that the most water washing occurs after accumulation along with biodegradation providing the necessary conditions. It is difficult to determine the degree of water washing in shallow cool reservoirs (< 80°C) since it is usually associated with biodegradation (Blanc & Connan 1994). Yet, the effect of water washing becomes more pronounced in hot reservoir > 80°C where the microbes are deactivated by high tempretures (Palmer, 1984; Lafargue & Barker, 1988).

Water washing affects the geochemical composition and bulk physical properties of petroleum

(increasing the density, sulfur, NSOs and asphaltene content of the washed hydrocarbon). Water washing removes the more water soluble aromatic hydrocarbons, especially benzene, toluene, ethylbenzene and xylenes (BTEX compounds) (Blanc & Connan 1994; Palmer, 1993). Therefore, these compounds can be used as indicators of water washing, despite the fact that they are also biodegradable.

A series of experiments was conducted by Palmer (1984) and Kuo (1994) on core extracts to study the influence of water washing on petroleum. Water washing leads to selective depletion of dibenzothiophene followed by removal of aromatic hydrocarbons while steranes and terpanes remain unaffected except for the increase and decrease in the amounts of 17α(H)norhopane and 18α(H)trisnorhopane, respectively. Several parameters have been proposed in the literature to identify and evaluate the level of water washing in the absence of biodegradation. They are: (1) reduction of aromatics and *n*-alkanes while the content of naphthenes remains unchanged, (2) decrease in C_{15+} aromatics while the amount of C_{15+} alkanes stays constant and (3) reduction in the amount of sulfur bearing aromatics (especially dibenzothiophene) as the C_{15}-C_{20} saturate fraction maintains the same content (Lafargue & Barker, 1988; Blanc & Connan, 1994).

Although Hunter (1989) suggested that the high cation content and Fe^{3+} concentration in waters induces precipitation in polymer systems and precipitation of asphaltenes, respectively, Wilhelms & Larter (1994) believed that the interaction between oil and water is not one of the main processes generating tar mats because a tar mat is not present at all OWCs, nor do they exclusively occur at OWCs, although it cannot be totally overruled. Moreover, Lafargue and Barker (1988), based on laboratory experiments, negate the viability of water washing process as a mechanism for tar mat formation.

1.2.2.3 Thermal Alteration (Thermal Cracking)

Thermal alteration is a disproportionation reaction that can further degrade reservoired oils into gaseous and light hydrocarbons on one hand and an insoluble carbon-rich solid residue (pyrobitumen) on the other hand. The reaction involves condensation of aromatic compounds and, decarboxylation, dehydration and desulfuration of the NSO fraction generating carbon dioxide (CO_2), water and hydrogen sulfide (H_2S). This process is caused by temperature increase

due to additional burial of the reservoired oils. In the deepest more mature zones of the reservoir, only pyrobitumen, methane and non-hydrocarbon gases including hydrogen sulfide (H_2S) are found (Rogers et al., 1974; Blanc and Connan, 1994; Tissot and Welte, 1978). The effect of thermal cracking of petroleum and the effect of the thermal maturation processes goes in the same direction. Both processes generate high API gravity oils. Yet, the presence of highly mature pyrobitumen in a reservoir is an indicative of cracking processes (Tissot and Welte, 1978).

Dahl et al. (1999) pointed out an upper temperature limit (threshold temperature) for oil accumulation before it is thermally cracked: 150 °C is usually assumed as an average value. However, higher values (175-204 °C) for oil stability have been reported in other studies (Horsfield et al., 1992). Therefore, it is important to calculate the subsidence (burial) and temperature histories (maximum palaeo-temperatures) of a reservoir and compare it to present-day temperature to determine whether or not cracking has occurred.

1.2.2.4 Thermochemical Sulfate Reduction (TSR)

TSR is a redox reaction whereby dissolved sulfate (SO_4^{--}) is reduced to H_2S by reaction with organic matter. The products of TSR are hydrogen sulfide (H_2S), carbon dioxide (CO_2), altered and oxidized hydrocarbons, solid bitumen (pyrobitumen), and possibly metal sulfides, carbonates, and elemental sulfur. The production of H_2S decreases the asset value by turning valuable liquid hydrocarbons into significantly cheaper gas (Goldstein and Aizenshtat, 1994; Machel, 2001).

The criteria for TSR to occur in hydrocarbon reservoirs are: (1) an adequate supply of dissolved sulfate (primarily from anhydrite), (2) organic compounds (the reactants) and (3) relatively high reservoir temperatures (greater than about 100-140 °C) in order to initiate this reaction. For H_2S to accumulate, the reservoir must be relatively free of reactive iron, or else H_2S will be scavenged to form iron sulfide (pyrite) (Machel, 2001). In cases where all of the above criteria are met in a reservoir containing or sealed by layers of anhydrite ($CaSO_4$), then the abundance of H_2S in this reservoir may be an indication of TSR. However, one should be cautious as the high concentration of H_2S could result from the thermal decomposition of organic sulfur compounds in oil or source rock kerogen. One way to confirm the origin of H_2S, in this case, is by using

sulfur isotopes. Since H_2S is generated by high-temperature reduction of anhydrite sulfur during TSR, thus the $\delta^{34}S$ of H_2S would have values closer to that of the anhydrite (positive values). In contrast, organic sulfur generated from hydrocarbon source rocks normally has very negative $\delta^{34}S$ values. Also, the presence of sulfur-rich solid residues (pyrobitumens), containing a large proportion of insoluble organic matter and admixed elemental sulfur, may confirm the occurrence of TSR. These pyrobitumens show enrichment and depletion in the $\delta^{34}S$ and $\delta^{13}C$, respectively (Machel, 2001).

1.2.2.5 Gas Deasphalting

Deasphalting is a physical-chemical alteration process in which asphaltenes precipitate from heavy to medium oils through the dissolution into an oil of gas or light hydrocarbons (> C_6). Deasphalting is triggered by external gas injection, as a result of secondary migration or by secondary alteration processes (e.g., thermal cracking) occurring in the oil bearing formation (Tissot and Welte, 1978).

Influx of gas into the reservoir disturbs the equilibrium conditions and leads to chemical changes in oil composition. As a result of this injection, the average molecular weight of the petroleum drops, light oil forms and asphaltene is provided with a reasonable environment for precipitation (Blanc and Connan, 1994; Roger et al., 1974; Tissot and Welte, 1978). However, according to Wilhelms and Larter (1994), the gas injection results in asphaltenes precipitation only if the host reservoir contains oil unsaturated with regard to gas. Also, it occurs in reservoirs with a separate gas cap that undergoes burial. Precipitation of asphaltenes can lead to issues such as plugging the pores since it can be present as extreme viscosity bitumen (tar mats) within the porous media.

A mixture of NSOs, aromatics and asphaltenes can be observed in the composition of deasphalted solid reservoir bitumens (Rogers et al., 1974). Tar mats can be clearly identified as obvious zones that: (1) usually reside close to discontinuities such as water/oil contact, (2) have a higher concentration of asphaltene with respect to oil leg (20-60 wt% of C_{15}^{+} compounds). Tar mats formed by gas deasphalting contain solvent-soluble asphaltene

material as opposed to weakly soluble reservoir pyrobitumens formed by in-reservoir crude oil maturation (Wilhelms and Larter, 1994).

1.2.2.6 Gravitational Segregation

Gravitational segregation is one of the physical post-accumulation processes that may influence the composition of thick oil columns and results in the formation of heavy oils and tar mats. Gravitational segregation comes into play in pools with large vertical extent and small temperature gradient. As a result of this phenomenon oil molecules move by diffusion attempting to reach equilibrium between their chemical and gravitational potential. Thus, heavier asphaltene components tend to accumulate and settle at the bottom of the pool while lighter components (higher gas in solution) reside at shallower depths. Consequently, API gravity and gas oil ratio (GOR) decrease progressively with depth in these columns (Blanc and Connan, 1994; Tissot and Welte, 1978).

However, the presence of permeability barriers within reservoirs as well as the effect of adsorption processes on clay minerals led Wilhelms & Larter (1994) to conclude that asphaltene precipitation from static oil columns could be induced by gravitational segregation but accumulation of these asphaltenes would be on the barriers within the oil column rather than the base of it. They also stated that although concentration of asphaltene precursor entities (APEs) near the base of oil columns is possible through the diffusion of APE's in solution along the chemical and gravitational potential gradients, this concentration mechanism cannot account for the large accumulation of asphaltenes at the bottom of thick oil columns (>80 m).

1.2.2.7 Other Processes

Other chemical and physical post-expulsion processes, which are believed to be of less importance to account for viscous oil and tar mat accumulations, include:

Inspissation & Oxidation (abiogenic chemical oxidation)

Inspissation is a term used to describe the "drying-up or thickening of an oil" as it loses its gases

and lighter constituents through vaporization. The process initiates as the oil comes into contact with atmosphere. Vaporization starts with gases and light compounds and moving towards the heavier fractions; however, heavy residues hardly become affected by vaporization.

Oxidation of oil as an alteration process can lead to production of oil with heavier contents. This is not considered as very prominent process since it only affects oil deposits at the earth's surface (eg Trinidad tar lake). It can also happen at the subsurface below the "aeration zone" (0-220 m), where oxygen is available either dissolved in waters or in a chemically bound state. The oxidized oil is heavier in its initial state since light components and gas constituents have been removed already through inspissation. In general this process yields very heavy tarry oil possibly depleted in paraffins and enriched in polycyclic compounds (Milner et al., 1977). Several studies and experiments have concluded that inspissation and atmospheric oxidation is responsible for decreasing API gravities of oils by few degrees (~2°) (Milner et al., 1977). Overall the process is not globally very significant for reservoired fluids though of course ultimately surface oxidation is the fate of all eroded oil reservoirs.

Secondary Migration and Adsorption on Clay Mineral Effects

It has been stated that secondary migration of whole oil might lead to composition changes in petroleum (Hodgson and Baker, 1959). Their suggestion was based on the idea that during hydrocarbon migration, high polar asphaltic fractions and heavy metal complexes (Ni and V) have a high tendency to be adsorbed to the rock pores and surface of clay minerals, whereas the lighter non-polar fractions will pass through. Consequently, it is expected that asphaltene, resins and trace metal content gradient will decrease along the axis of oil migration. In other words, heavier oils will accumulate downdip (deeper) and lighter fraction will accumulate in shallower reservoirs. This trend is the opposite to that of maturation. Integrating geochemistry and geology, i.e. chemistry analysis of oil fractions, basin structure, migration pathways) is required to confirm if secondary migration effects are a dominant factor in generating heavy oil and tar mats deposit.

Although the tendency of polar asphaltic fractions and heavy metal complexes (Ni and V) to adsorb onto mineral surfaces has been reported in a number of studies (Hodgson and Baker, 1959 and others), Wilhelms and Larter (1994) tend to disregard the asphaltene adsorption onto clay

surfaces as an important triggering mechanism for tar mat formation. This conclusion is based on the fact that if heavy oils and tar mats form through the adsorption process onto clay minerals, then these heavy highly viscous deposits should be restricted to and present in all clay-rich or shaley sequences.

In-reservoir Pressure Reduction During Uplift

Reduction in pressure and temperature caused by reservoir uplift can lead to asphaltene precipitation and tar mat formation as several studies reported the precipitation of asphaltenes close to the wellbore where the pressure is reduced during production (Haskett and Tartera, 1965 and others). However, Wilhelms and Larter (1994), through case studies on tar mats at the Ula and Oseberg fields, argued that pressure reduction cannot be considered as the major process in tar mat formation. Their argument was based on the fact that these reservoirs, where tar mats are found, have not experienced any uplift during and following oil filling. Also, tar mats in these reservoirs are found close to the oil-water contact (OWC) which cannot be explained by the asphaltene precipitation caused by pressure reduction. It is difficult for the heavy fraction of oil to selectively settle down to the bottom of the reservoir as particulates through the tortuous pore structure. Diffusive transport in solution must be involved.

Oil mixing

Wilhelms and Larter (1994), through case studies on tar mats in the Ula field, concluded that although in-carrier mixing of two charges with different maturities can cause localized precipitation of asphaltenes, it is not a significant cause of the tar mat formation in the studied area. The complexity in this process lies within the difficulty of mixing large amounts of two oils with different maturities, as the more mature oil may replace the less mature oil without allowing for effective complete mixing (oil displacement).

Chapter Two: MOTIVATIONS AND RESEARCH OBJECTIVE

Although heavy oil production is increasing, many puzzling aspects of the petroleum systematic remain, not least of which is the origin of Saudi heavy oils. Heavy oils, extra heavy oils and tar mats are common in the Middle East, particularly in Saudi Arabia. Several studies in the literature reported the existence of heavy oils and "tar mats", at the base of oil columns in some of Saudi Arabia carbonate reservoirs, discussed the challenges associated with the presence of tar mats on oil production and presented drilling and development solutions from an engineering point of view (e.g., Okasha et al., 1998; Halpern et al., 2004; Akkurt et al., 2009; AlUmran et al., 2005; Al-Shehri et al., 2011; Seifert et al., 2012).

However, the number of published studies that geochemically characterize heavy oil deposits and tar mats in Saudi Arabia and in the Middle East in general as an attempt to understand their origin is limited. For example, Riley et al. (1977), geochemically investigated the origin of a 500 ft. thick tar mat impeding both oil production and water injection in the eastern part of Arab-D limestone formation that is sealed with an anhydrate, Uthmaniyah area (Ghawar field) in Saudi Arabia. They concluded that gas deasphalting of the reservoired Uthmaniyah oil was the main process producing the tar mat. The gas was proposed to have been a more mature later charge expelled from the same source rock as the oil; the later charge then migrated up-dip from the source kitchen to the eastern part of Uthmaniyah and resulted in in-reservoir asphaltene precipitation.

Tobey et al. (1993) conducted another geochemical study on core samples from the same formation (Arab-D, Uthmaniyah area) but studied different wells using an extractability test by organic solvents (naphtha, toluene and either methylene chloride or trichloroethane), and both an elemental and a pyrolysis analysis before and after core extraction to assess the origin and effect of the tar mat presence on the reservoir quality (permeability and porosity). Based on the extractability test, the authors found that the tar is a heterogeneous mixture of both soluble hydrogen-rich components and insoluble hydrogen-deficient components with a sulfur content of 7.5 wt%. They concluded that the hydrogen-rich components were generated by gas deasphalting whereas thermochemical sulfate reduction (TSR) was proposed as a formation mechanisim for the insoluble hydrogen-deficient components.

Additionally, in Oman, Huc et al. (2000) carried out a geochemical study to examine the origin of bitumen which might fill up to 40% of the Barik sandstone reservoirs' porosity in the Fahud Salt Basin. The authors used NMR, elemental analysis and density measurements to characterize the bitumen. The results showed that the bitumen has a relatively high density (1.3–1.4 g/cm^3), a hydrogen deficiency (H/C= 0.65), a highly aromatic character (NMR 75% C_{aro}), and is rich in sulfur (4.2 wt %). This bitumen is also insoluble in organic solvents and has a high "bitumen" reflectance (1.2%). Huc et al. suggested that the bitumen is a low mature pyrobitumen generated from an early oil charge, that was severely biodegraded as a result of a regional uplift that brought the reservoir near the surface (reservoir temperatures <80°C). The heavy oil deposit formed by the severe biodegradation then underwent an extensive heating (140°C) resulted from a subsequent burial of the reservoir to the present day depth (4500 m). This latter burial led to thermal cracking of the oil into light hydrocarbons and insoluble residue (pyrobitumen).

In another study, Carpentier et al. (1998) used both a geophysical (electrical logs) and a geochemical (Rock-Eval and biomarkers) approach to investigate the distribution and origin of a tar mat, ranging from 4 to 23 m thick, existing in the crestal part of the S. Field in Abu Dhabi, UAE. The authors found that the tar mat was systematically positioned at the base of the Thamama B reservoir, just above the Dense Limestone formation (horizontal permeability barrier) and appeared to not be present in the water leg nor related to the present day or paleo-OWCs. They concluded, based on biomarkers, that there was no difference between the tar mat and the above oil leg in terms of oil origin or maturity level. Moreover, they thought that gravitational segregation of the heavier components from the oil leg and subsequent trapping of these components in the low porosity/permeability zone at the base of the reservoir is the likely cause for the tar mat formation.

Furthermore, in Kuwait, Abdul Azim et al. (2006) used geochemical, logging and production data to gain insight into the origin and distribution of tar mats in the giant Upper Zubair sandstone reservoir. The authors identified two distinct tar mats. The first, 100 m thick, was historically detected in the main producing reservoir close to the oil-water contact (OWC) (9345-9446 ft). The other tar mat was found above the historically detected tar zone obstructing production from a well completed recently on the crestal part of structure (9175-9291ft). On the one hand, the historically detected tar mat (9345-9646 ft) was characterized by the presence of

undegraded paraffins, low maturity biomarker signature, and high asphaltene and aromatic hydrocarbon content. The authors suggested that this tar zone was formed by biodegradation of low maturity oil charge that filled the reservoir at the time when the reservoir temperature was around 40-50°C. With subsequent burial, a later more mature charge migrated into the reservoir, and resulted in the precipitation of asphaltenes and subsequently the formation of the tar mat. On the other hand, leakage of light hydrocarbons through the faults was claimed to be the main reason for the formation of the heavy residual bitumen (tar mat) at the crestal area (9175-9291 ft). This latter conclusion was based on the fact that biodegradation cannot explain the areal distribution of tar mats over the field.

Moreover, Kaufman et al. (1998) analyzed oils from the Great Burgan Oil Filed, in Kuwait, to evaluate reservoir compartmentalization using geochemical approach. The oil column is 1,200 ft (365 m) thick extending through Burgan reservoirs (Third Burgan, Fourth Burgan, Mauddud and Wara). The authors observed a large variation in the oils' compositional and physical properties through the column although these oils have similar origin and maturity. For example, oil gravities vary from 39° at the shallowest reservoir to 10° close to the OWC. Moreover, the base of the column has a heavy oil and tar mat. As per a series of geochemical properties (e.g., % sulfur content, *n*-C_{17}/pristane) which correlated strongly to depth, the authors concluded that the Burgan reservoirs have a gravity vs. depth trend. Therefore, gravitational segregation of the heavier molecules was proposed to explain the increase in oil density (decrease in API gravity) with depth and the formation of the tar mat at the base of the column.

A clear understanding of the geological settings as well as heavy oil and natural bitumen formation processes is essential to describing the nature and distribution of heavy oil shows, establishing oil-oil and oil-source correlations, and reliably predicting the quality of petroleum in different zones of a reservoir (e.g., viscosity) (Blanc and Connan, 1994). Viscosity variation in heavy oil fields has a huge impact on oil production (Larter et al., 2008). Understanding the range of viscosity variations in crude oils and controls on these variations is crucial for reservoir characterization, modeling, simulation, reserves calculation and well placement. Reliable oil quality prediction, such as estimates of oil API gravity and viscosity can radically affect the economics of oil field development (Peters and Fowler, 2002). However, while biodegradation has been found to be the main mechanism producing most Albertan Oil Sands (e.g., Evans et al.,

1971; Allan and Creaney, 1991; Larter et al., 2008; Adams, 2008; Fustic, 2011), Venezuelan Orinoco belt heavy oils (e.g, Demaison, 1977; Cassani and Eglinton, 1991) and other biodegraded oil fields (e.g., Koopmans et al., 2002), the origin of the Saudi and Middle Eastern heavy oils is much less clear. Therefore, the objective of this study is to investigate the bulk and molecular composition of heavy oils from the Mid Cretaceous Safaniya sandstone reservoir from well-X in Saudi Arabia to help gain insight into the origin of these heavy oils.

Chapter Three: GEOLOGY

This chapter first begins by reviewing the regional geology of Saudi Arabia including its tectonics and major petroleum systems and then discusses the geological setting of the study area.

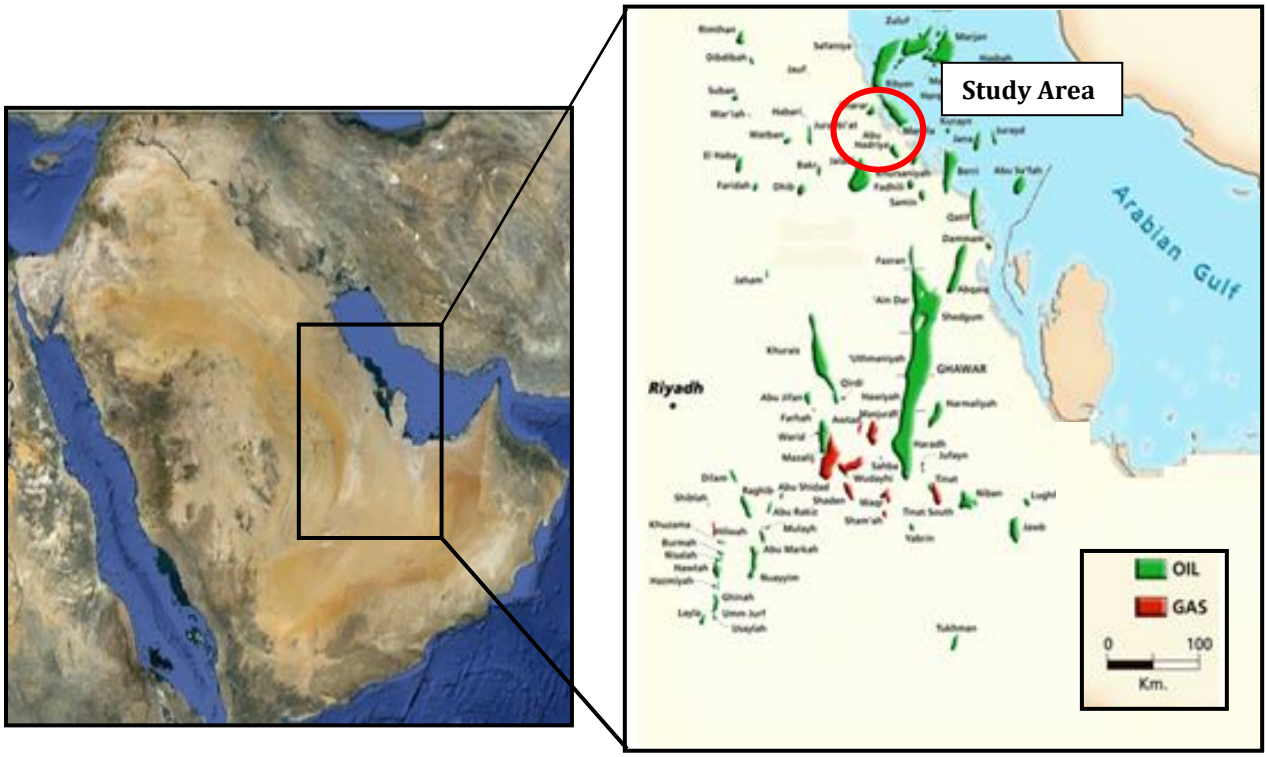

Fig. 3.1 Middle East region map (on the left) showing location of Saudi Arabia and a map on the right showing the X Field within the onshore oil and gas producing area along the west coast of the Arabian Gulf (Modified from Google Map, 2013 and Cantrell et al., 2013 in press).

3.1 Regional Geology of Saudi Arabia

3.1.1 Tectonic Settings

Tectonically, Saudi Arabia is located on the Arabian Plate, occupying more than 70% of the plate. The Arabian plate was originated ~25Ma by rifting Northeast Africa to from the Red Sea and Gulf of Aden. Fig. 3.2 shows that the Arabian Plate is situated in between the Eurasian, Indian and African Plates. The Arabian plate is bordered by the Red Sea Rift to the west, the Aden Gulf to the south, and the Bitlis-Zagros Thrust Belt to the northeast. Over millions of years, the Arabian Plate adjoined with the African and Indian crustal plates have been moving northward and colliding with the Eurasian Plate. The result of this movement is a complex of mountain ranges spanning from the Pyrenees in the west, Alborz and Zagros Mountains in Southern Europe and Iran, to the Himalayas and ranges of Southeast Asia (Hempton, 1987; NASA, 2013).

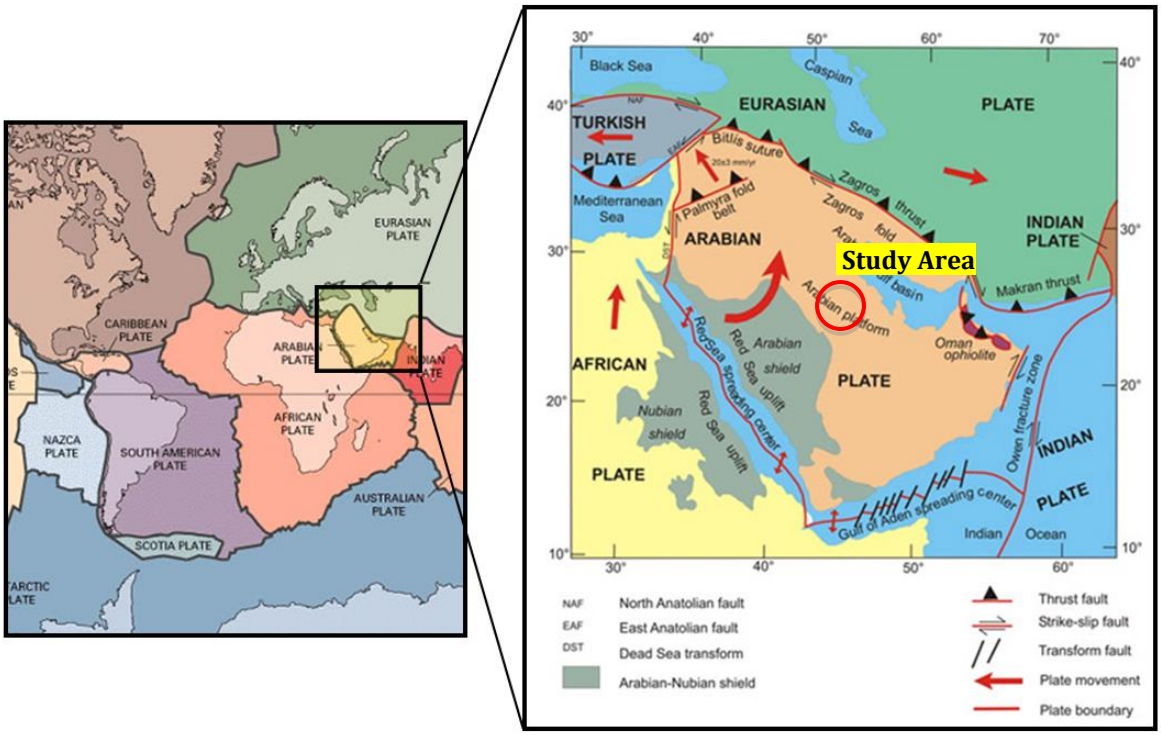

Fig. 3.2 Partial tectonic map on the left shows location of the Arabian Plate and a detailed map on the right displays active tectonic margins surrounding the Arabian Plate (Modified from NASA, 2013 and Saudi Geological Survey, 2013).

There are three types of active tectonic margins that confine the Arabian Plate as summarized by Bilal (2013). These are:

1) A **Convergent margin** of thrust fault zones, spanning from northwest to east of the Arabian Plate, passes along the Anatolian Fault, the Bitlis Suture in Turkey, the Zagros Mountains in Iran and the Makran-Oman (Fig. 3.2). These zones occurred as a result of the Arabian Plate thrusting beneath the Eurasian Plate.
2) A **Divergent margin** is present as an oceanic-rift spreading centre which is comprised of the Red Sea Rift and, the Aden Gulf to the west and south of the Arabian Plate, respectively.
3) A **Transform margin** is present as the Owen-Sheba intra-oceanic transform fault zone and, the Dead Sea transform strike-slip fault zone to the southeast and northwest of the Arabian Plate, respectively.

The description of the tectonic framework of the Arabian Plate has been discussed in Cantrell et al. (2013 in press), Beydoun (1991), and Alsharhan and Nairn (1997). According to these authors, this framework can be subdivided into six tectonic phases that shaped the Arabian Plate geology as follows:

1) Precambrian (800-650 Ma): Formation of the basement as the oldest portion of the Arabian plate.

2) Ordovician-Silurian Glaciation and De-glaciation (460-440 Ma): The Late Ordovician was marked by the expanding of the polar glaciers across Gondwana and most of western parts of Arabia. In the Early Silurian, widespread deposition of the Lower Qusaiba shales of the Qalibah Formation, the source rock of the Paleozoic reservoired Saudi oils, occurred as a result of risen sea level in response to de-glatiation. A hiatus associated with a global sea-level drop occurred in the late stages of Silurian.

3) Late Devonian to the Early Carboniferous (~370-360 Ma): The period was marked by the Hercynian Orogeny structural event that caused the Central Arabian uplift and the Arabian plate to become tilted eastward. The uplifting mechanism exposed Devonian and older rocks to erosion and transformation of the northeast Gondwana margin from a passive to an active margin. The Arabian Plate was also rotated through 90° in an anticlockwise direction.

4) Late Permian through the Jurassic Zagros Rifting (~250Ma): Initiated by fragmentation of the Arabian-Gondwana/Iranian-Laurasia super continent and eventually rifted, by the Early Triassic, along the Zagros line to form the Neo-Tethys Sea (eastern margin of the Arabian Plate). During the Jurassic, the Arabian plate was relatively tectonically stable and was located at the Equator enabling the development of a wide shallow shelf on the western passive margin of the Neo-Tethys on which carbonates accumulated over the shelf and inner platform. As a result of the rising sea level and tectonic differentiation, intra-shelf depressions such as the Arabian, Gotnia, and the South Rub 'al Khali Basins were formed and hence most of the Arabian Gulf petroleum source-reservoir-seal rocks were deposited during the Jurassic and Cretaceous.

5) Middle to Late Cretaceous (~100-60 Ma): Closure of the Neo-Tethys began, and the "Hercynian" structures were rejuvenated and started forming the major eastern Arabian petroleum traps (e.g., the Ghawar anticline, Figure. 3.1 & 3.3).

6) Tertiary (~35 Ma) Zagros Orogen: Marked by initiation of the Zagros Orogeny due to compression between Arabia and Asia. The Arabian plate converged and subducted beneath Iran and caused the Arabian plate to tilt slightly to the northwest to form a series of anticlines and thrusts in the Zagros Mountains. The Arabian Gulf foreland basin, which lies beneath the western edge of the Zagros thrust, was created as a result of this collision.

The Saudi Geological Survey (2013) indicates that the oldest portion of the Arabian Plate in Saudi Arabia is Precambrian crystalline continental crust as a basement with a thickness and age of 40-45 km and 870-550 million years old, respectively. The Precambrian basement includes volcanic, sedimentary, and calc-alkaline intrusive rock terranes creating strongly deformed complex geological structures in the region. During orogenic events occurring in the early Proterozoic (780-650 Ma), the Precambrian terranes converged and resulted in deformation, metamorphism, and uplift, culminating in the Nabitah Orogeny, and intruded by plutonic rocks during a subsequent 100 million-year period of orogenic collapse, extension, exhumation, and strike-slip faulting.

A younger rock sequence unconformably overlays the Precambrian basement. This sequence includes Cambrian to Pleistocene aged sedimentary rocks, surficial Cenozoic flood basalts, Paleogene-Holocene intra-continental and, current oceanic basins along the Red Sea and the Gulf

of Aden. The oceanic basins were formed during the last stage when the Arabian and Africa Plates started to separate at about 25 million years ago. During this period, western and southern margins of the Arabian Plate were uplifted and partly covered by sub-aerial flood basalt which formed the Red Sea Escarpment. The northern and northeastern margins were also sutured, resulted in formation of the Zagros Fold and the Thrust Belt.

Figure 3.3 below shows a simplified geological cross section across Saudi Arabia and Qatar from the Arabian Shield to the Arabian-Persian Gulf. The figure clearly demonstrates horst-graben blocks, present as a dominant structure in the Precambrian basement which was formed as a result of the Hercynian Orogeny during the Carboniferous. This Hercynian Orogeny had significantly brought about changes in basin geometry, basement uplifts, and regional uplift around the Arabian Shield, as reflected by gently eastward dipping sedimentary sequences in the cross section. The Hercynian Orogeny also caused basement structure reactivated and formed major north-south-trending, basement-involved horst blocks in central and eastern Saudi Arabia. These reactivated basement-involved structures were later sites of extensive erosion and structural trap formation that were favorable for petroleum accumulation (Pollastro, 2003).

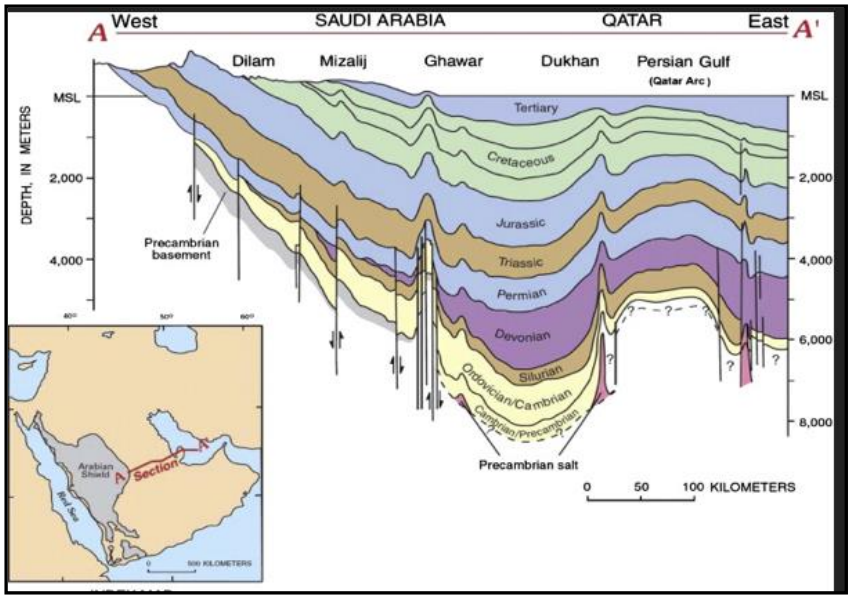

Fig. 3.3 Simplified west-east geological cross-section extending from central part of the Arabian Shield to the Arabian Gulf with line section shown in the index map (Modified from Alsharhan and Nairn, 1997 and Pollastro, 2003).

In relation to the prolific oil and gas fields of Saudi Arabia which are mainly distributed within eastern and northeastern margin of the Arabian Plate (Figure 3.1). Beydoun (1991), Alsharhan and Nairn (1997) and Pollastro (2003) pointed out that huge amounts of hydrocarbons contained in the region are related to: (1) the margin's long and stable-tectonic history with extensive depositional platform in the region along a pre-Mesozoic passive margin of Gondwana; (2) the subsequent tectonic events that formed multiple intra-platform basins followed by extensive source rock deposition within the basins; and (3) the multiple tectonic compression and extension stages which resulted in a favourable structural trapping and stratigraphic framework that was prior to or concurrent with hydrocarbon generation and migration events.

3.1.2 Petroleum Systems in Saudi Arabia

Saudi Arabia covers a large part of the Arabian Basin which is the primary producer of oil and gas in Saudi Arabia (Figure 3.4). The basement structures beneath the Arabian Basin have substantially controlled sediment deposition and subsequent structural growth of the basin.

Two main petroleum systems account for the petroleum generation and accumulation in Saudi Arabia's prolific region covering east-central Arabian Peninsula and Arabian Gulf. Hydrocarbon generated from these petroleum systems have largely contributed to oil and gas production in the world's largest fields in Saudi Arabia notably Ghawar and Safaniya Fields (Figure 3.4)(Pollastro, 2003). The systems are grouped into the Paleozoic petroleum system and the Mesozoic petroleum system (reflecting the age of the source and reservoirs) based on the distinct timing of their formation that relates to the tectonic evolution of the Arabian Plate. The timing was particularly marked by the Paleo-Tethys closure and the merging of Pangea, followed by subsequent breakup of Pangea and opening of the Neo-Tethys during the Late Triassic to Early Jurassic (Cantrell et al., 2013 in press).

These two major petroleum systems have been discussed in many publications and some of them are Cantrell et al. (2013 in press), Pollastro (2003), and Alsharhan and Nairn (1997). This following section briefly describes characteristics of key elements of the petroleum systems which include source rocks, reservoir rocks, seal rocks, and mechanisms of hydrocarbon trapping

and migration. Geochemistry of the source rocks is also briefly outlined. Key elements of these petroleum systems are summarized in Figure 3.5 and Table 3.1.

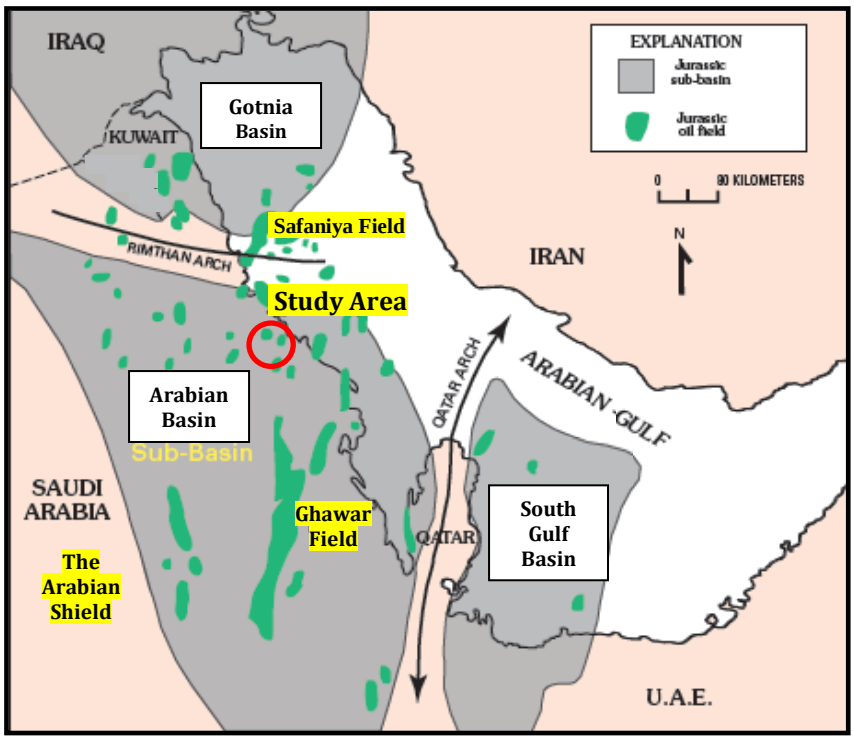

Fig. 3.4 A map showing distribution of Jurassic petroleum source rocks accumulated in Gotnia, Arabian and Southern Arabian Gulf Basins (modified from Alsharhan and Kendall, 1986).

3.1.2.1 The Paleozoic Petroleum System

The Paleozoic petroleum system geographically covers an area south and south west of the Greater Ghawar Field Province and extends into the western flank of the Qatar Arch Province and the southeasternmost parts of the Widyan Province (Pollastro, 2003).

The system is associated with a main source rock of Early Silurian organic-rich Qusaiba Member of the Qalibah Formation (Mahmoud et al., 1992). Deposition of the Qalibah Formation is related to glaciation termination at the end of Ordovician followed by transgression during Early Silurian that led to deposition of organic matter on the continental shelf of northern Gondwana (Jones and Stump, 1999).

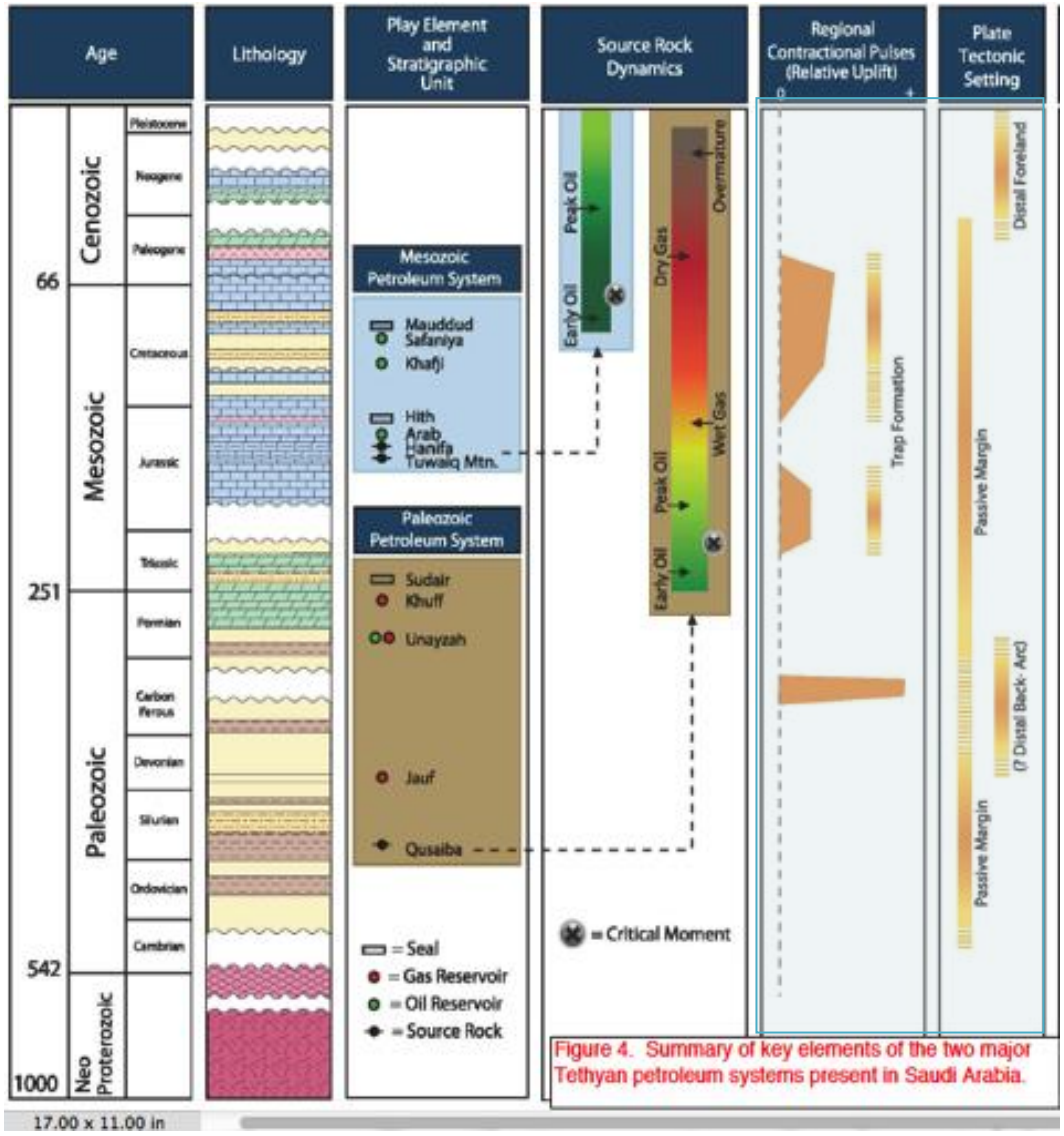

Fig. 3.5 A summary of key element characteristics of the two main petroleum systems in Saudi Arabia (after Cantrell et al., 2013 in press).

According to Abu-Ali et al. (1991), the Early Silurian Qusaiba Shale Member, also known as basal hot shale due to high gamma ray interval, is characterized by dark-gray to black micro-laminated, euxinic shale containing as much as 20 weight percent total organic carbon (TOC). Organic materials contained in the shale are mainly oil-prone Type II (amorphous marine algae) kerogens. The Paleozoic-sourced oils have API gravities range from 40° to 53° with less than 0.1 weight percent sulfur content (Table 3.1).

Table 3.1 A Summary of Key Element Characteristics of the Two Main Petroleum Systems in Saudi Arabia. (modified from Alsharhan and Nairn, 1997; Cantrell et al., 2013 in press).

	Paleozoic System	Mesozoic System
Main Source Rocks	Lower Silurian Qusaiba Hotshale	lower Tuwaiq Mountain Formation Hanifa Formation
Main Reservoirs	Devonian Sandstones of the Jauf Formation Permo-Carbonifereous Siliciclastics Unayzah Group Permo-Triassic carbonates of the Khuff Formation	The Upper Kimmeridgian- Lower Tithonian Carbonates of Arab Formation The Middle Cretaceous Safaniya and Khafji reservoirs
Secondary Reservoirs	Ordovician Clastic Sarah and Sandstone Qasim Formations	Shu'aiba, Dharuma and Hanifa Formations
Ultimate Regional Seal of the System	Sudair shales	Evaporites of the Hith Formation Shales and Tight Carbonates of the Mauddud Formation
Source Rock Charge Time	210 Ma (Late Triassic)	100 Ma (Late Cretaceous)
Source Rock Type	Type II Kerogen	Type II Kerogen
Source Rock Thickness	6 to 75 m	Tuwaiq Mountain 150 m, Hanifa 30 m
TOC	Average 5%, Maximum 20%	Average 3.5%, Maximum 14.3%
API	40° to 53°	30° to 45°
Sulfur Content	> 0.1 %	up to 3.5%
$\delta^{13}C$ (V-PDB)	-29.8	(-26.5 to -27.7)

The Paleozoic petroleum system is associated with three main sandstone-dominated reservoirs including the Devonian Jauf Formation, the Unayzah Group, and the Khuff Formation. Depositional setting of the reservoirs is estuarine-tidal environments that inter-tongue with barrier bar and foreshore marine sandstones. Secondary sandstone reservoirs in this petroleum system include the Ordovician Sarah and Qasim Formations that are associated with shallow marine and glacial to peri-glacial depositional environments, respectively (Cantrell et al., 2013 in press).

The Paleozoic petroleum system has several regional seal rocks. The Lower Silurian Qusaiba "hot shale seals the Pre-Qusaiba reservoirs while a shaley D3B stratigraphic zone widely seals

the Jauf reservoir. The major seal rock of the Unayzah reservoirs is the basal Khuff Formation comprising transgressive shales and carbonates (Pollastro, 2003). The trapping mechanisms in the Paleozoic petroleum system are primarily formed by structural settings associated with basement block faulting, wrench faulting, and tectonic salt movement and deformation Stratigraphic traps are locally provided by low porosity siltstones and rarely carbonate mudstones for the Jauf, Unayzah, and Khuff reservoirs (Cantrell et al., 2013 in press).

According to Cantrell et al. (2013 in press), the Qusaiba source rock started expulsion at maturity of 0.7% (vitrinite reflectance equivalent) that occurred at 210 Ma (Triassic). It was followed by peak oil and peak gas expulsion occurred at about 152 Ma (Early Jurassic) and 140 Ma (Mid Jurassic), respectively (Figure 3.6). The figure also demonstrates that hydrocarbon expulsion from the Silurian Qusaiba Shale noticeably post-dates the phase of mid-Carboniferous trap formation in eastern and central Saudi Arabia. The migration of petroleum is concluded to be vertical movement to the reservoirs above and below the source rock layer. A present day maturity map for the Qusaiba "hot shale" is shown in Figure 3.6 below.

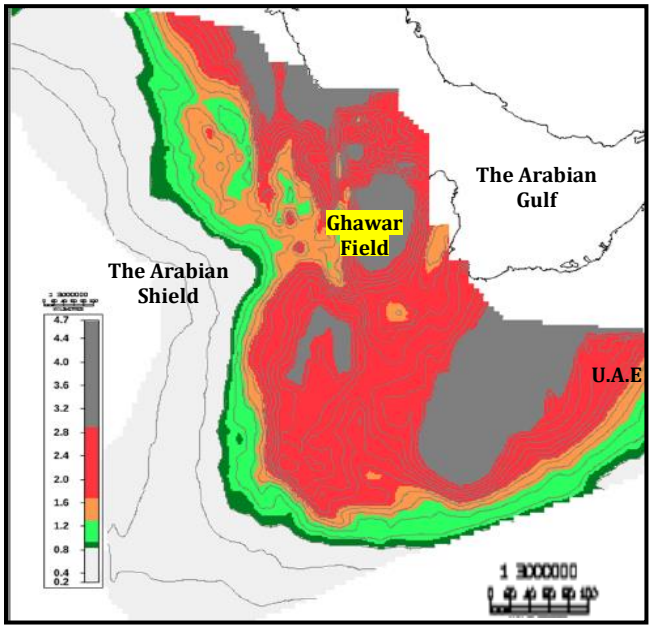

Fig. 3.6 Present-day maturity map of the Silurian Qusaiba hot shale source rock, Saudi Arabia (Modified from Cantrell et al., 2013 in press).

3.1.2.2 The Mesozoic Petroleum System

The Mesozoic petroleum system (Jurassic and Cretaceous) geographically covers all of the Greater Ghawar Province, the Widyan Province and a region covering Qatar northward to the east coast of Arabian Gulf (Pollastro, 2003).

The system is generally associated with two main source rocks of the Jurassic Hanifa and Tuwaiq Mountain Formations, and reservoir rocks with ages ranging from Lower Jurassic to Upper Cretaceous. The Jurassic Hanifa and Tuwaiq Mountain Formations are laminated, organic-rich lime mudstone with widespread distribution, deposited during the late Jurassic. Based on geochemical data, these source rocks are considered to be excellent type II, oil-prone source rock with an average TOC content of about 3.5% and a maximum TOC of about 14.3% (Cantrell et al., 2013 in press). Oils produced from the Jurassic reservoirs in the Arabian Basin have medium API gravities (30-45°) and high sulfur (up to 3.5%) (Table 3.1). These characteristics are typical for oils from a marine, carbonate anoxic setting (Sinninghe Damsté et al., 1988).

The Mesozoic petroleum system has three main reservoir rocks including the Upper Jurassic Arab Formation and the Middle Cretaceous Safaniya and Khafji Formations. The most prolific oil-producing interval is the Upper Kimmeridgian to Lower Tithonian Arab Formation that internally comprises four upward-shoaling carbonate and anhydrite cycles (Powers et al., 1966). (Cantrell et al., 2013 in press). The Middle Cretaceous Safaniya and Khafji Formation reservoirs are typically coarse-grained, poorly consolidated sandstones of deltaic depositional setting (Ayers et al., 1982).

The typical seal rock in the Mesozoic petroleum system that separates the Jurassic oils from mixing with the Cretaceous oils is evaporites. Evaporites of the Hith Formation are the main major regional seal with a thickness reaching up to 287 m in some areas, such as the Abqaiq Field. However, Alsharhan and Kendall (1994) reported that this seal is not well developed along the eastern and northeastern part of Saudi Arabia, including the study area, allowing Jurassic oils to mix with Cretaceous oils and hence the production of Cretaceous oils with a Jurassic origin is limited to the eastern and northeastern part of Saudi Arabia. Occurrence of this anhydrite is probably due to restriction across the platform during a slow sea level rise after widespread exposure of the Arabian shelf. Other seal rocks include fine-grained, impermeable carbonate

rocks or shales that cap carbonate reservoirs of the Hanifa, Tuwaiq Mountain and Dhruma formations. Intra-formational shales and tight carbonates of Mauddud Formation perfectly seal the reservoirs within the Khafji and Safaniya Formations (Alsharhan and Nairn, 1997).

A basin modeling study suggests that the Jurassic source rocks began oil expulsion during the Late Cretaceous. Figure 3.5 shows that the Jurassic Hanifa source rock was in the oil window which led to oil migration during the Late Cretaceous. On the other hand, the Tuwaiq Mountain source rock reached early-stage maturity for oil generation at about 100 Ma and continued to attain its peak oil expulsion in the deeply buried areas at Early Tertiary time, approximately during a period of 65-54 Ma (Cantrell et al., 2013 in press). Hydrocarbons generated then began to accumulate in an extensive gentle fold structures around the region. Extensive vertical migration of oils from a more limited number of very organic-rich source intervals is suggested from a large number of reservoir data (e.g., pressure) (Ayers et al., 1982).

Figure 3.7 illustrates the thermal maturity map of the Jurassic Hanifa source rock. The maturity of the source rock increases eastward, however it approaches the gas window in the low basinal area east of the Ghawar field.

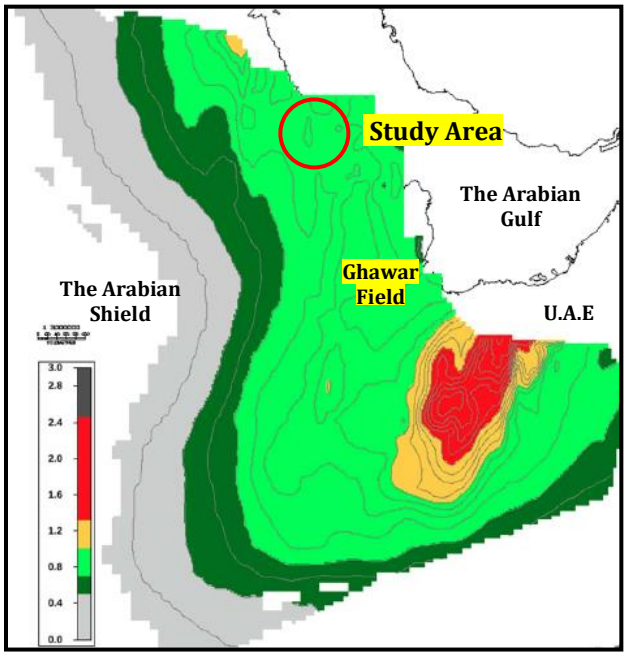

Fig. 3.7 Base Hanifa thermal maturity map based on modeled vitrinite reflrectance values (Modified from Cantrell et al., 2013 in press).

At present, the Hanifa and Tuwaiq Mountain source rocks east of the Ghawar structure have passed through the oil window, whereas the source rocks in the center of the Arabian Basin are still in the oil generation window. In the western part of the Arabian Basin, the source rocks are either immature or are just starting to enter the oil window (Cantrell et al., 2013 in press).

3.2 Study Area

3.2.1 Location and Field Structure

As mentioned in the previous section, the study area is part of the onshore X-Field, located on the west coast of the Arabian Gulf in northeastern Saudi Arabia (Fig. 3.1). The X field is sited in primarily uninhabited barren desert with topography ranging from 13 meter to 50 meter above sea level. Morphology of the field area generally occurs as low hills rising above the gently rolling terrain of loose sand anchored by shrub and bushes. The hills are made up by Neogene sandy limestone to sandstone (Miles, 1961).

Structurally, the study area regionally lies on an anticlinal-dome structure with major axis trending in a NE-SW direction. Dip of the structure has angle varying from about 4° on the northern nose to about 9° on the southwestern flank (Alsharhan and Nairn, 1997).

3.2.2 Stratigraphy of the Mid Cretaceous Safaniya member

The studied well in the X field penetrated a 3373-3484 feet (1028-1062 m) interval of the Mid Cretaceous Safaniya Member of the Wasia Formation. In this study area, the Wasia Formation is underlain by the Shu'aiba Formation and unconformably overlain by Aruma Formation (Figure 3.8). The Wasia Formation (Albian-Turonian), primarily consists of limestone, sandstone and shale that are deposited in a fluvial dominated delta and near shore environments in central, eastern, and northeastern Saudi Arabia (Powers et al., 1966). Figure 3.8 shows that the Wasia Formation comprises 7 members in a sequence from bottom to top notably Khafji (sandstone), Safaniya (sandstone), Mauddud (limestone), Wara (limestone), Ahmadi (limestone), Rumaila (limestone) and Mishrif (limestone) (Alsharhan and Nain, 1997).

The Safaniya Member is one of the important hydrocarbon reservoirs of the mid-Cretaceous Wasia Formation in the northeastern part of the Arabian Peninsula. Stratigraphically, the Safaniya Member is part of a gently eastward dipping sedimentary sequence of Cambrian to Recent age resting on the Arabian Platform to the east of the Arabian Shield (Alsharhan and Nain, 1997).

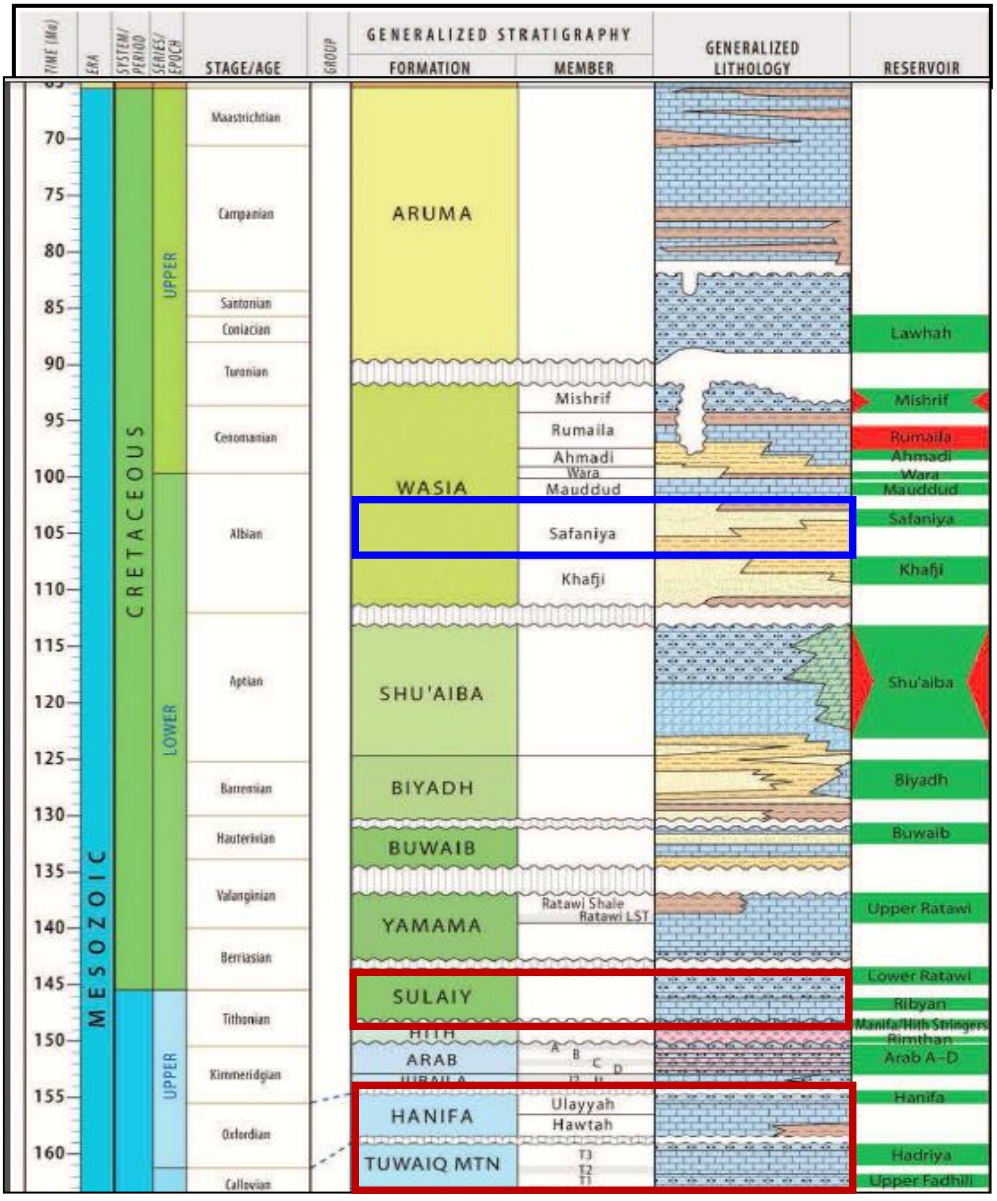

Fig. 3.8 A Stratigraphic section and generalized lithologies for the Cretaceous petroleum system in Central and Eastern Saudi Arabia. The studied reservoir and possible source rocks are highlighted in blue and red, respectively (Modified from Cantrell et al., 2013 in press).

Cagatay et al. (1995) point out that the Safaniya Member near the northeast coast of Saudi Arabia has a thickness of about 110 m consisting mainly of sandstones, locally interbedded with minor portions of shale and limestone. The Safaniya Member in this area consists of three sandstone-dominated lithofacies, including clean quartz sandstone, laminated argillaceous sandstone, and carbonate-cemented sandstone. The litho-facies of the Safaniya Member particularly within the region of the northeastern Saudi Arabia and the northwestern Arabian Gulf are generally associated with a delta front and delta plain with fluvial and distributary channels depositional setting.

3.2.3 Tectonic Evolution of the Safaniya Reservoir (Burial History)

A burial history model of the Safaniya reservoir as interpreted from the well study is displayed in Figure 3.9. The figure shows a current bottom hole temperature that reaches 55°C (± 2°C) at a depth of 3700 ft. The model also suggests that the maximum paleo-temperature the SFNY reservoir was subjected to is 76°C (± 2°C) at a depth of 5700 ft. This is in agreement with the result of a study by Cagatay et al. (1996) that was conducted on a well adjacent to the well studied here. Their study well has a bottom hole temperature of 74°C at a depth of 5628 ft.

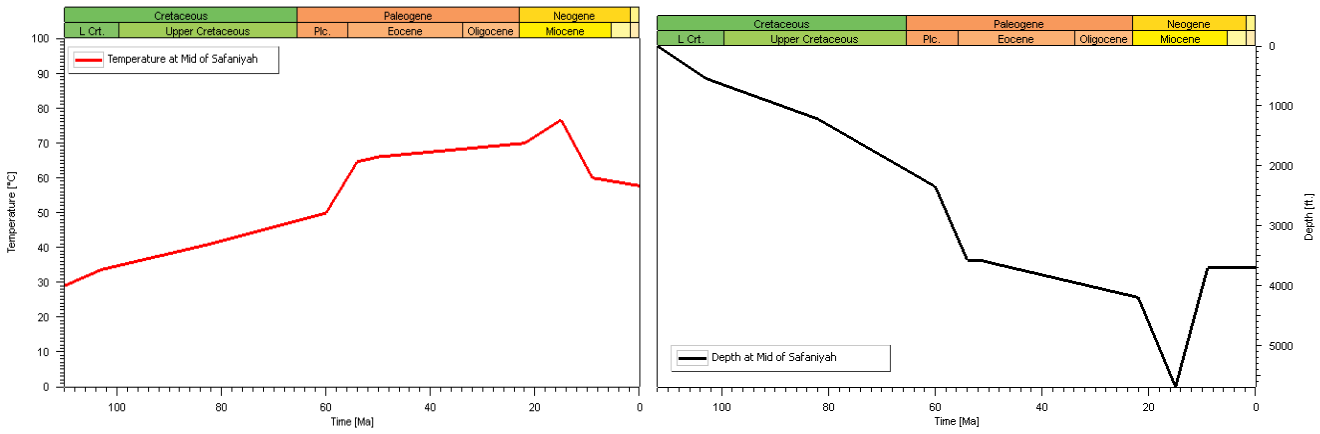

Fig. 3.9 Burial history diagram of the Safaniya Member of the studied well.

In this study, the model suggests that deposition of the Safaniya Member was followed by burial until the end of the Turonian. Subsequently, regional tectonic events such as compression that

occurred along eastern part of the Zagros belt during the Campanian caused uplift and sub-aerial erosion of 70-m thick upper part of the Wasia Formation. The eroded units included the whole Mishrif Member and most of the Rumaila Member. As a result, the pre-Aruma unconformity formed. Impact of the regional tectonic events during this time, structural traps for hydrocarbon accumulations started to form (Ayres et al., 1982). Burial stage resumed and deposited the Aruma Formation at the end of the Campanian until the end of the Middle Eocene. In between Middle Eocene to Miocene, there was a hiatus of depositional event due to structural growth and non-deposition in the area. The last major event in the burial history of the area was Plio-Pleistocene Zagros orogeny which then resulted in folding with NW-SE trends and uplift in the Arabian Gulf area.

3.2.4 Reservoir Quality

Reservoir data available from the study well include core porosity and permeability data. Table 3.2 lists the data with respect to depths where the data was collected. A series of logs including gamma ray, neutron-density porosities is also available as shown in Figure 3.10.

Table 3.2 Porosity (%) and Permeability (mD) Data of Cores from the Studied Safaniya Reservoir.

Core #	Depth (ft)	Porosity (%)	Permeability (mD)
1	3373.4	22.8	14.07
2	3374.5	31.7	657.77
3	3377.6	32.4	-
4	3378.4	33.1	2380
5	3380.6	-	-
6	3382.3	32.6	-
7	3476.3	33.5	-
8	3477.3	33.3	8930
9	3478.6	32	8240
10	3479.8	31.1	7000
11	3480.7	30.4	8680
12	3481.4	31.4	7320
13	3482.5	33	9720.48
14	3483.5	31.1	9550
15	3484.2	32.1	7840

The table shows both core porosity and permeability data collected from an interval depth of 3373.4 to 3484.2 ft. The porosity data range from 22.8% to 33.5% with an average of 31.5%. On the other hand, permeability data in the table 3.2 show a relatively wide range values from 14.07 to 9720.48 mD with an average permeability of 6393.8 mD.

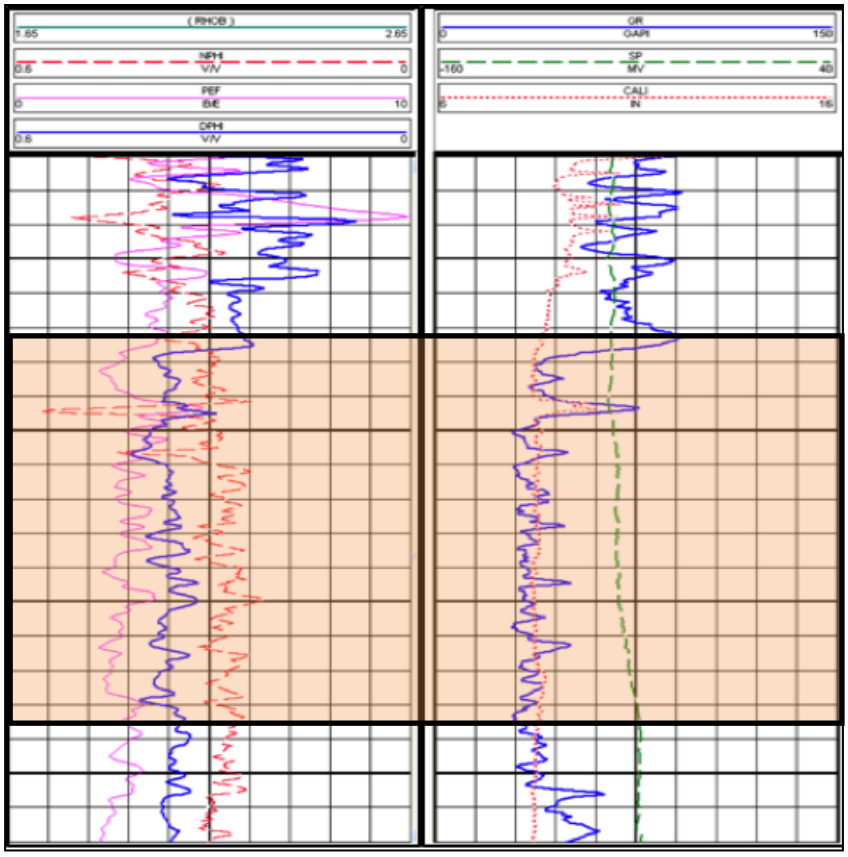

Fig. 3.10 Lithology and porosity from Gamma ray log (right), and neutron and density porosity log (left), respectively. The studied reservoir interval is highlighted.

In general, both porosity and permeability data suggest a good reservoir condition within this section from the well studied. Except condition at 3373.4 ft which gives the lowest porosity and permeability values of 22.8% and 14.07mD, respectively. Less porous and less permeable

conditions at this depth are due to the presence of a thin clay/shaly clay bed that is marked by appearance of a high gamma ray kick from 30 API to 75 API at 3375ft (Fig. 3.10). In particular, neutron and density porosity logs, and core porosity and permeability data show slight different trends in between shallower and deeper sections of the reservoir. The core porosity and permeability data at deeper sections in between 3477.3ft and 3484.2ft are high with average values of 32% and 8410 mD, respectively compared to the shallower section. Furthermore, a shift of gamma ray trend line is shown in Fig 3.10, from 30 API at deeper section (3477.3ft and 3484.2ft) to 75 API at shallower section (above 3375ft). These may suggest slightly different lithology units in vertical extent that compose the Safaniya Member in the section of the studied well. The deeper section is likely to be sandstone dominated unit while the shallower section is interpreted to be interbedded of sandstone and clay/shale unit.

In conclusion, the core and log derived porosity data, and core permeability data suggest that the deeper section of the Safaniya Member at the interval depth of 3410-3484 ft have good reservoir quality as reflected by high porosity and permeability, with lithology dominated by sandstone units. The shallower section with interval depth of 3373-3382 ft is made up by interbedded sandstone and clay/shale units that have less porous and less permeable reservoir units.

3.2.5 Hydrocarbon Sources and Migration

No oil-to-source rock correlations are available for the Mid Cretaceous Safaniya oils from the studied area. However, possible source rocks for these oils were inferred from the literature. As mentioned earlier, production from the Cretaceous reservoirs is limited to the northern and northeastern oil fields in Saudi Arabia. Aryes et al. (1982) have concluded that the Mid Cretaceous (Hauterivian-Turonian) oils were generated either from the Jurassic (Callovian-Oxfordian) Tuwaiq Mountain /Hanifa source rocks or locally from the Cretaceous (Berriasian-Valanginlan) sediments of the Sulaiy Formation.

The Mid Cretaceous reservoired oils have very similar geochemical and physical characteristics to the Jurassic oils. Therefore, the Cretaceous oils were suggested by Aryes et al. to be early charges from the Jurassic Carbonate Tuwaiq Mountain /Hanifa source rocks or the equivalent Jurassic source rock in the Gotnia Basin, north of Saudi Arabia (Iraq). This early charge has been

proposed to have vertically migrated and filled the Cretaceous reservoirs in the northern and northeastern oil fields of Saudi Arabia as the Jurassic regional seal (Hith Anhydrite) is rather poorly developed or missing in this region.

According to Aryes et al. (1982), the only sediment within the Cretaceous sequence that is adequately organic rich (TOC > 2%) and may have acted locally as a source rock, is the basal Cretaceous Sulaiy Formation. The Sulaiy sediments are composed of limestone, calcarenite and calcarenitic limestone deposited in a shallow marine setting and contain sulfur-rich, amorphous kerogen. The Sulaiy was suggested to have contributed to the Cretaceous oil accumulations in the northernmost part of the Gulf and in southeast Iraq.

Furthermore, the Albian Kazhdumi source rock, present in the Khuzestan subbasin in Iran and the northernmost Gulf, could potentially have fed the Mid Cretaceous reservoirs (Areys et al., 1982). The Kazhdumi source rock is made up of shales and cherts with Type-II kerogen and total organic contents of about 10% (Ala, 1982). However, the geochemical data of the studied Safaniya oils, as will be discussed in chapter five, indicate origin from carbonate source rock and hence eliminating the possibility of Kazhdumi shales as source rock for these oils.

Chapter Four: MATERIALS AND METHODS

The study involved the analysis of produced oil and reservoir core-extracted oil samples across the Mid Cretaceous Safaniya sandstone reservoir (Wasia Formation section) from well-X in Saudi Arabia. The bulk compositions of all samples (extracts and produced oil) were obtained by TLC- FID Iatroscan (section 4.1). The core samples were solvent-extracted, as described in section 4.2, and then analyzed by Gas Chromatography Mass Spectrometry (GC-MS) using full scan mode. All samples (extracts and produced oil) were then separated into fractions (saturated hydrocarbons, aromatic hydrocarbons and polars) based on polarity. Only saturated and aromatic hydrocarbon fractions were analyzed for molecular compositions by GC-MS. Based on the chemical composition of the samples, only twelve samples representing different depths were chosen for stable carbon and sulfur isotopic analysis. The total sulfur content (%S) was also determined for the selected samples.

4.1 Samples Screening (TLC-FID Iatroscan)

The gross composition of the samples was determined using the Thin-Layer Chromatography-Flame Ionization Detection Iatroscan system (FID-TLC Iatroscan) using a modification of the method described by Karlsen and Larter (1991). The process in brief included crushing, dissolving and sonicating 500 mg of the core sample in 5 ml dichloromethane in a sealed vial. Then, a precise volume of the mixture was applied directly by a syringe onto the base of Iatroscan chromatographic rods (10 rods per rack). The Chromarods-S III used in this procedure are quartz rods with a thin layer of silica gel (mean diameter 60Å, average particle size 5µm). The Chromarods were then developed in solvents of increasing polarity (*n-hexane*, toluene/ *n-hexane* (1:1) and DCM/methanol (93:7) to separate hydrocarbons from resin/asphaltenes. Following the rods development, the Chromarods were scanned using an IATROSCAN MK-6S instrument with flame ionization detector and electronic integrator at a scan speed of 60 sec to ensure full ionization of bitumen. Hydrogen was used as the carrier gas at a constant flow rate of 160 ml/min. The concentration (wt %) of the saturated hydrocarbon, aromatic hydrocarbon, resin and asphaltene fractions were calculated and calibrated against a standard tar sand bitumen from Alberta using Peak Simple software. For quality control purposes, analytical blanks were run

prior to sample addition and triplicate runs were carried out for each sample on different rods to ensure reproducibility of the results.

4.2 Extraction and Fractions Separation

Prior to the GCMS and stable isotope analysis, the core samples were extracted with dichloromethane CH_2Cl_2 (DCM). Then, all samples (core extracts and produced oil) were passed through a column of anhydrous (sodium sulfate, Na_2SO_4) to remove any traces of water. Before the separation process, internal standards were added to the samples for quantitation purposes. For molecular compositions, samples were transferred in DCM to a Florisil Solid-Phase Extraction (SPE) column (500 mg of SPE) for deasphalting. The maltenes were fractionated from the Florisil column with 5 ml *n*-hexane and 3 ml DCM, and further separated into hydrocarbon and non-hydrocarbon fractions by 5 ml *n*-hexane and 5 ml DCM, respectively using an Isolute C18 nonendcapped (NEC) column (500 mg sorbent mass)(modified from Bennett and Larter, 2000 and Bennett et al., 2002). The hydrocarbons were then separated into saturated, and aromatic fractions using liquid chromatography on a silica-gel column. A modification of Bastow's proposed method for liquid chromatography was used (Bastow et al., 2007). First, 20 mg of the hydrocarbon fraction was introduced in *n*-hexane to a glass column dry packed with 0.6 g of high-purity grade silica gel (60A particle size 0.063-0.200mm; 70-230 mesh). The saturated hydrocarbon fraction was eluted by 2 ml of *n*-pentane, using small aliquots (40 x 50 µl) at first, allowing each of the aliquots of solvent to run down to the silica gel. After the saturated hydrocarbons elution, the aromatic fraction was eluted by 2 ml of methylene chloride. Finally, the thiophene compounds were eluted from the liquid chromatography column into the aromatic fraction by 2 ml iso-propyl alcohol (IPA).

4.3 Characterization Methods

4.3.1 GC-MS Analysis of the Saturated and Aromatic Hydrocarbon Fractions

GC-MS analysis of the saturated and aromatic hydrocarbon fractions of extracts and produced oil was performed on an Agilent 6890N Series II gas chromatograph (GC) interfaced to an Agilent

5973 Mass Selective Detector (MSD) operating in electron impact mode. The samples were injected into the GC inlet in split/splitless mode. Chromatography was accomplished on an HP-5MS 30 m x 0.25 mm x 0.25 μm capillary column using helium as the carrier gas at a constant flow rate of 1.5 ml/min and temperature programming from 40° (hold time 5 min) to 325°C (hold time 15 min) at 4°C/min. Analysis was carried out using 70 eV ionization potential. GC/MS data were acquired in single ion monitoring (SIM) mode with 50 – 100 msec dwell times for ions of interest. Cycle time was approximately 0.7s.

The following ions were monitored: m/z 85 (normal alkanes); m/z 97 (cyclohexanes); m/z 177 (25-norhopanes); m/z 191 (tricyclic and pentacyclic terpanes); m/z 217 and m/z 218 (steranes) for the saturated hydrocarbons, and for the aromatic hydrocarbons m/z 91 (alkylbenzene); 128 (naphthalene); m/z 142 (C_1-naphthalenes); m/z 154 (Biphenyl); m/z 156 (C_2-naphthalenes); m/z 168 (C_1-Biphenyl + Dibenzofuran); m/z 170 (C_3-naphthalenes); m/z 178 (phenanthrene); m/z 184 (C_4-naphthalenes and dibenzothiophene); m/z 192 (C_1-phenanthrenes); m/z 198 (C_5-naphthalenes and C_1-dibenzothiophenes); m/z 206 (C_2-phenanthrenes); m/z 212 (C_2-dibenzothiophenes); m/z 231 (triaromatic steroid hydrocarbons); m/z 253 (monoaromatic steroid hydrocarbons) (Peters et al., 2005; Huang et al., 2003).

The NOTS standard was prepared by mixing individual standard stock solutions, (1,1-binaphthyl, squalane, d8-naphthalene, d10-phenanthrene, d4-cholestane, d16-adamantane, d30-phenyldodacane and d32-Pentadecane in 25 ml mixture of *n*-hexane/toluene (24:1). 5 μl of the NOTS was added to each sample before the SPE separation step. After analysis on the GC-MS, compound peak areas were integrated using the Agilent MSD Productivity ChemStation (RTE integrator). Compound ratios were then calculated directly from peak areas by comparing integrated peak areas with the related internal standard peak area e.g. steranes versus d-4 cholestane (internal standard), assuming a relative response factor (RRF) of one between the two (modified from Bennett et al., 2002). Absolute concentrations of different compounds were calculated according to the following formula:

$$\text{Absolute concentration} = (\text{peak area}_{\text{compound}} / \text{peak area}_{\text{related internal standard}}) \text{ X } (\text{weight}_{\text{related internal standard (μg)}} / \text{weight}_{\text{sample (mg)}}) \text{ x } 1000$$

The list of identified compounds by GC-MS, sample chromatograms and molecular structures are

shown in Appendix 1. The molecular concentrations measured in the investigated samples are shown in Appendix 2.

4.3.2 Stable Carbon Isotope Ratios Measurements

Carbon isotope measurements were performed on selected whole-oil extracts. A100 µg of sample was weighed into small tin cup, packed down and then flushed into the system with Helium Gas. Carbon dioxide from the packed whole oils was prepared by combustion at 1020 ^{o}C and transferred to the sample inlet of a Continuous Flow-Elemental Analysis-Isotope Ratio Mass Spectrometry (CF-EA-IRMS), by a Costech 4010 elemental analyzer interfaced to a Finnigan MAT Delta+XL mass spectrometer. The Carbon isotope ratios are determined by comparing the respective sample peak areas to reference gas peak inlet through the open split. The $\delta^{13}C$ values are the deviation of $^{13}C/^{12}C$ ratio in the samples from the standard and are reported in per mil notation relative to the V-PDB (Vienna Pee Dee Belemnite) as shown below:

$$\delta^{13}C=[(^{13}C/^{12}C)_{sample}/(^{13}C/^{12}C)_{V\text{-}PDB} - 1] \times 1000$$

Carbon isotope ratios were calibrated, during and after each set of samples, using reference material and corrected for systematic drift and to internal laboratory standards of known isotopic composition. The following reference materials were used:

Standard	$\delta^{13}C$ ‰
USGS 24	-16.0 ± 0.1
IAEA-CH-6	-10.4 ± 0.2
IAEA-CH-7	-31.8 ± 0.2
NBS 22	-30.03 ± 0.2
USGS 40	-26.39 ± 0.2
USGS 41	37.63 ± 0.2

The accuracy and precision of the UofC Isotope lab standards for $\delta^{13}C_{organic}$ are around ± 0.2 ‰. (ISL-UofC).

4.3.3 Sulfur Isotope Ratios Measurements

Total sulfur of selected samples was extracted via Parr bombing and converted into barium sulfate ($BaSO_4$) prior to the sulfur isotope analysis (modified from John Morris Scientific). In this procedure, 0.12 g of the rock extract sample was combusted with oxygen in a sealed Parr 1108 Combustion Bomb vessel under 35 atmosphere oxygen pressure. To aid the combustion, few drops of sulfur-free diluent (alcohol) were added to the sample. After 15 minutes, all hydrocarbons were oxidized to carbon dioxide and water by reaction, and all sulfur compounds were converted to sulfuric acid. The vessel with all parts of the interior was washed with sufficient amounts of distilled water. The washings including the sulfuric acid were collected in a beaker and heated on a hot plate. Then, it was acidified with a few drops of a concentrated hydrochloric acid. Following that, a 10 ml of 10% barium chloride solution was then added gradually to the washings to precipitate the sulfate as barium sulfate ($BaSO_4$). Consequently, the $BaSO_4$ precipitate was collected by filtering the solution through a Nitrocellulose filter membrane (0.45μm) and was then washed with warm water until free from chlorides. Finally, the filter membrane with the precipitate were left to dry completely then weighed to determine the exact weight of the $BaSO_4$ precipitate. The total sulfur was then calculated gravimetrically according to the following formula:

$$\%S = 32/233\ (\text{weight}_{BaSO4\ (g)} / \text{weight}_{sample\ (g)}) \times 100$$

$BaSO_4$ samples were weighed into small tin cups, packed down and then flushed into the system with Helium Gas. Sulfur dioxide (SO_2) from the packed $BaSO_4$ was prepared by combustion at 1050 ^{o}C and transferred to the sample inlet of Continuous Flow-Isotope Ratio Mass Spectrometry (CF-EA-IRMS), using a Carlo Erba NA 1500 elemental analyzer interfaced to a VG PRISM II mass spectrometer. To assist the combustion process, niobium pentoxide was added to all $BaSO_4$ samples and standards.

During each sample run, the sulfur isotope ratios were determined by comparing the respective sample peak areas to the reference gas peak inlet from the DI reference bellows of the mass spectrometer. The ratios are reported in per mil notation relative to the V-CDT (Vienna -Canyon Diablo Troilite). $\delta^{34}S$ values are calculated as shown below:

$$\delta^{34}S=[(^{34}S/^{32}S)_{sample}/(^{34}S/^{32}S)_{V\text{-}CDT} - 1] \times 1000$$

Sulfur isotope ratios were calibrated, during and after each set of samples, using reference material and corrected for systematic drift and to internal laboratory standards of known isotopic composition. The following reference materials were used:

Standard	$\delta^{34}S$ ‰
NBS 127	21.1 ± 0.4
IAEA S05	0.5 ± 0.2
IAEA S06	-34.1 ± 0.2
IAEA S1	-0.3
IAEA S2	22.7 ± 0.2
IAEA S3	-32.6 ± 0.2

The accuracy and precision of the UofC Isotope lab standards for $\delta^{34}S$ are around ± 0.3‰. (ISL-UofC; Grassineau et al., 2001).

Chapter Five: RESULTS AND DISCUSSION

This section discusses the study results and provides an interpretation of the findings for the research question, specifically "what processes led to the occurrence of heavy oils from the Mid Cretaceous SFNY reservoir in the X-Field, Saudi Arabia?".

5.1 General Geochemical Characterization

5.1.1 Physical Properties and Bulk Composition

Table 5.1 depicts the gross physical and geochemical data for the rock extracts and produced oil obtained from the Mid Cretaceous Safaniya (SFNY) reservoir. The physical properties of the samples show no significant variation with all being low in API gravity (13.2°-15.7°) and high in sulfur (6.2- 8.7%). High sulfur values are typical of petroleum from a marine carbonate source rock deposited in an anoxic setting. Most of the sulfur in crude oils results from early diagenetic reactions between the deposited organic matter (OM) and aqueous sulfide species (Sinninghe Damsté et al., 1988). Hydrogen sulfide and polysulfides are generated in excess in the marine environment by sulfate-reducing bacteria under highly reducing conditions. However, the high sulfur values may also infer early-generated products from oil-prone, sulfur-rich kerogens (Type IS or IIS) (Tissot & Welte, 1978; Lewan et al., 1998), or petroleum altered by biodegradation (Head et al., 2003; Wenger & Isaksen, 2002; Larter et al., 2006b) or thermochemical sulfate reduction (Zhang et al., 2007).

The data also show no pronounced variation in the samples' geochemical properties. All of the samples from the SFNY reservoir are low in saturated hydrocarbons (13.8% average, n=21) yet rich in aromatic hydrocarbons (47.1% average, n=21) and polar compounds (resins and asphaltenes (39.2% average, n=21)) with saturate/aromatic ratios significantly below 1. Such physical and geochemical characteristics are typically attributed either to low maturity non-degraded oils containing a high proportion of heavy and naphtheno-aromatic compounds, or to biodegraded oils that may have partially or completely lost their n-alkanes (Milner et al., 1977). Generally, similarities in the bulk physical properties and geochemical composition within the sample set suggest similar source facies and maturity.

Table 5.1 Bulk Physical and Geochemical Data for Rock Extracts and Produced Oil From the SFNY Reservoir (Wasia Formation).

Sample #	Sample Type	Depth (ft)	Bitumen Content (wt%)	API° *	Sulfur (%)	Saturates (wt%)	Aromatics (wt%)	Resins (wt%)	Asphaltenes (wt%)	Sat/aro
1	Rock Extract	3373.1	2.8	14.7	-	15.8	42.0	16.9	25.3	0.4
2	Rock Extract	3375.5	13.4	14.3	7.3	14.0	49.7	11.9	24.5	0.3
3	Rock Extract	3377.6	11.5	15.2	-	16.0	42.7	13.4	27.9	0.4
4	Rock Extract	3380.3	14.1	15.4	-	13.7	46.3	13.0	27.0	0.3
5	Rock Extract	3382.2	13.1	15.4	7.4	12.8	46.7	11.9	28.7	0.3
6	Rock Extract	3385.1	10.8	15.1	-	15.1	43.8	14.5	26.6	0.3
7	Rock Extract	3389.8	9.2	15.6	-	14.9	46.4	13.3	25.4	0.3
8	Rock Extract	3392.8	11.3	15.2	6.8	15.3	43.5	12.4	28.9	0.4
9	Rock Extract	3433.4	10.5	15.2	7.9	14.2	49.6	12.6	23.6	0.3
10	Rock Extract	3435.7	15.7	14.7	-	13.3	52.4	11.3	23.1	0.3
11	Rock Extract	3437.5	10.2	14.5	-	15.6	39.8	16.4	28.3	0.4
12	Rock Extract	3440.5	14.7	14.3	7.5	15.0	41.6	15.1	28.4	0.4
13	Rock Extract	3466.2	13.8	15.1	8.1	12.8	52.9	11.0	23.3	0.2
14	Rock Extract	3469.9	12.6	14.6	-	13.0	40.2	13.5	33.3	0.3
15	Rock Extract	3471.2	6.8	14.8	-	13.3	55.6	11.6	19.5	0.2
16	Rock Extract	3473.2	4.3	15.2	-	13.7	50.3	10.5	25.5	0.3
17	Rock Extract	3479.3	1.7	15.2	-	10.9	47.2	12.9	29.0	0.2
18	Rock Extract	3480.2	1.3	15.6	7.9	9.7	50.0	11.1	29.1	0.2
19	Rock Extract	3482.9	1.8	15.3	8.3	12.3	51.2	10.6	25.9	0.2
20	Rock Extract	3484.1	2.1	15.7	8.1	11.0	43.9	11.7	33.5	0.2
21	Produced Oil	3370-3470	-	13.2	6.2	16.6	53.3	8.2	21.9	0.3

* API: apparent API gravities determined by POPI (Pyrolytic Oil-Productivity Index) involving pyrolysis of crude oils or stained reservoir rock (usually diluted with solvents). API is computed from hydrocarbon yields at various temperature regions on the pyrogram and by comparison with data acquired on actual produced oils (Jones et al., 2004). Sat/aro: saturated hydrocarbons/aromatic hydrocarbons.

Figure 5.1 portrays a plot of the bitumen content of the studied rock extracts vs. reservoir depth. The samples have bitumen content ranging from 2.1 to 15.7 wt %. The plot shows that there is a sharp decrease in the bitumen content of the samples at a depth of 3473' and downward. The bitumen saturation obtained from the samples at this depth and downward is less than 5 weight percent. This decrease in the bitumen content is due to low oil, high-water saturation zone as interpreted from the resistivity log (Figure 5.1). Also, the sample at the shallowest part of the reservoir (3373 ft) shows low bitumen content (2.8 wt%). Based on gamma ray log, this depth was characterized, in chapter two - section 3.2.4, by the presence of a low porosity/permeability thin shaly clay bed which explains the low oil saturation at this depth.

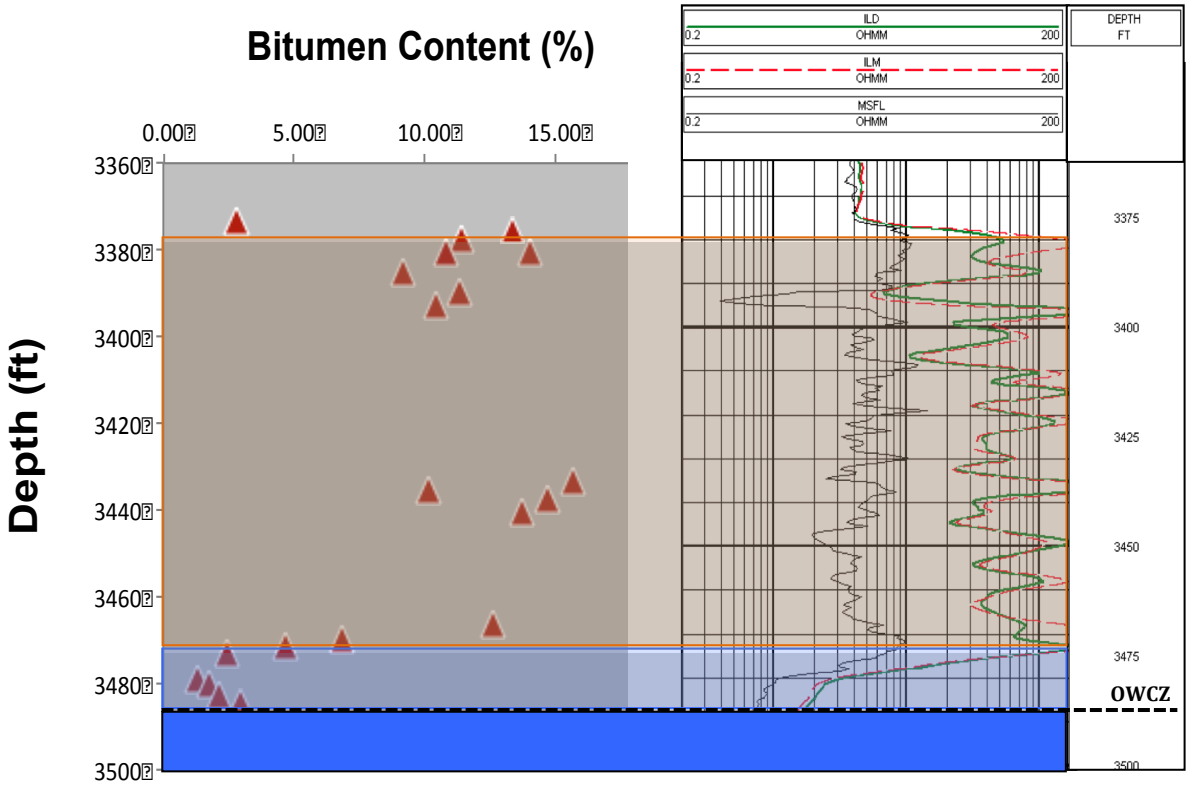

Fig. 5.1 Plot of the bitumen content (extract yield) for the analyzed extracts versus reservoir depth (left); the resistivity log of the SFNY reservoir (right), showing low oil saturation towards the oil-water zone.

5.1.2 Saturated Hydrocarbon Parameters

Saturated hydrocarbons are commonly employed for diverse applications, e.g., oil-oil and oil-source rock correlations, source maturity assessment, determination of source rock lithology and post accumulation alteration processes (e.g., Peters et al., 2005; George et al., 2002; Ten Haven et al., 1987). Saturated hydrocarbon parameters used to characterize the studied samples are shown in table 5.2.

Table 5.2 Saturated Hydrocarbon Parameters for the Analyzed Samples Calculated from GC-MS (*m/z* 85).

Sample #	Sample Type	Depth (ft)	Pr/Ph	Pr/*n*-C_{17}	Ph/*n*-C_{18}	CPI
1	Rock Extract	3373.1	0.39	0.19	0.55	0.94
2	Rock Extract	3375.5	0.37	0.19	0.55	0.89
3	Rock Extract	3377.6	0.35	0.19	0.57	0.89
4	Rock Extract	3380.3	0.36	0.19	0.57	0.91
5	Rock Extract	3382.2	0.38	0.19	0.55	0.89
6	Rock Extract	3385.1	0.35	0.19	0.58	0.90
7	Rock Extract	3389.8	0.40	0.20	0.55	0.90
8	Rock Extract	3392.8	0.37	0.20	0.58	0.91
9	Rock Extract	3433.4	0.35	0.20	0.58	0.91
10	Rock Extract	3435.7	0.36	0.20	0.58	0.93
11	Rock Extract	3437.5	0.37	0.20	0.58	0.92
12	Rock Extract	3440.5	0.37	0.20	0.57	0.91
12-R	Rock Extract	3440.5	0.37	0.20	0.59	0.92
13	Rock Extract	3466.2	0.35	0.19	0.58	0.90
14	Rock Extract	3469.9	0.38	0.20	0.57	0.90
15	Rock Extract	3471.2	0.39	0.20	0.55	0.90
16	Rock Extract	3473.2	0.41	0.20	0.54	0.92
17	Rock Extract	3479.3	0.37	0.20	0.57	0.91
18	Rock Extract	3480.2	0.37	0.20	0.57	0.92
19	Rock Extract	3482.9	0.40	0.20	0.55	0.91
20	Rock Extract	3484.1	0.37	0.20	0.57	0.91
21	Produced Oil	3370-3470	0.56	0.22	0.46	0.93
21-R	Produced Oil	3370-3470	0.55	0.22	0.46	0.93

Pr/Ph: Pristane/Phytane,(Didyk et al., 1978); **Pr/*n*-C_{17}:**Pristane/ C_{17} normal alkane; **Ph/*n*-C_{18}:**Phytane/ C_{18} normal alkane, (Peters et al., 2000; Connan & Cassou, 1980); **CPI**: Carbon Preference Index $=[(C_{25}+C_{27}+C_{29}+C_{31}+C_{33})/(C_{26}+C_{28}+C_{30}+C_{32}+C_{34}) + (C_{25}+C_{27}+C_{29}+C_{31}+C_{33})/(C_{26}+C_{28}+C_{30}+C_{32}+C_{34})]/2$, (Bray & Evans,1961). Duplicate analyses are indicated by the sample # followed by the letter suffix R.

The lithology of source rock and redox condition during deposition of organic matter can be assessed by the **acyclic isoprenoid alkanes**, pristane (Pr) and phytane (Ph). The source of these compounds is phytol, a derivative from the side chain of chlorophylls, (Powell & McKirdy, 1973; Peters & Moldowan, 1993). Under oxidizing conditions a decarboxylation reaction takes place to form Pr, leading to Pr/Ph ratios greater than one, whereas Ph is predominantly formed under reducing conditions leading to values less than unity (Figure. 5.2) (Didyk et al., 1978). Also, Peters and Moldowan (1993) pointed out that Pr/Ph ratios ≤ 1 are commonly observed for carbonate-sourced oils. All of the studied samples are characterized by pristane/phytane (Pr/Ph) ratios less than 1.0 (Table 5.2), which indicate the same origin for all samples from a carbonate source rock deposited in anoxic conditions. However, caution should be taken when using this parameter for the following reasons: (1) most of Pr is generated from thermal degradation of kerogen (Larter et al., 1979); (2) chlorophyll side chain is not the only source for Pr and Ph. Goossens et al. (1984) and Ten Haven et al. (1987) argued that Ph can be sourced from archaeal membranes and that zooplankton and tocopherol (Vitamin E) could also be precursors for Pr. Moreover, Methyltrimethyltridecylchromans (MTTCs), derived during diagenesis, have been also proven by Li et al. (1995) in some cases to act as originators for Pr.

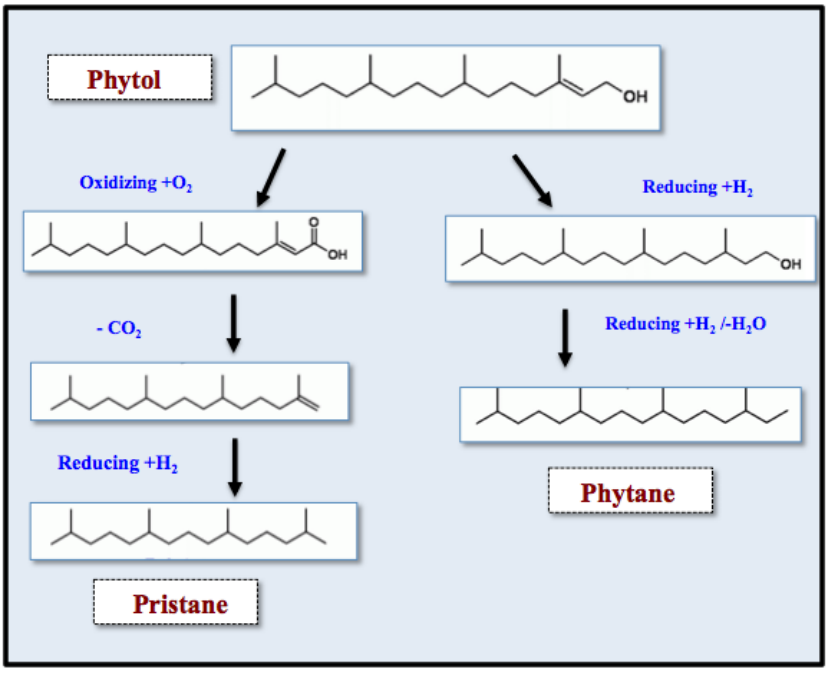

Fig. 5.2 A summary of the diagenetic transformation of phytol to pristane and phytane (Modified from Didyk et al., 1978).

Figure 5.3 shows a cross plot of **phytane/*n*-C_{18} versus pristane/*n*-C_{17}** for the studied petroleum samples from SFNY reservoir. This plot is commonly used to infer source anoxicity and organic matter type (e.g., Peters et al., 2000; Connan & Cassou, 1980). No differences in these two ratios were observed for the sample set across the reservoir supporting the notion of petroleums derived from a single major source rock facies (Table 5.2 & Figure 5.3). The samples plot in a field typical for marine algal Type-II organic matter deposited under a reducing regime. Moreover, Waples (1985) stated that these ratios are also useful in assessing thermal maturation of crude oils and bitumen from sedimentary rocks. According to Waples (1985), *n*-alkanes are generated faster than isoprenoids with increasing thermal stress leading to lower Ph/*n*-C_{18} and Pr/*n*-C_{17} ratios. The plot shows that the studied samples are uniform in thermal maturity. Connan et al. (1980) concluded that moderate levels of biological degradation may be mirrored by higher relative concentration of the iosprenoids Pr and Ph relative to the *n*-alkanes. No increase in both the Ph/*n*-C_{18} and Pr/*n*-C_{17} ratios was observed for the sample set.

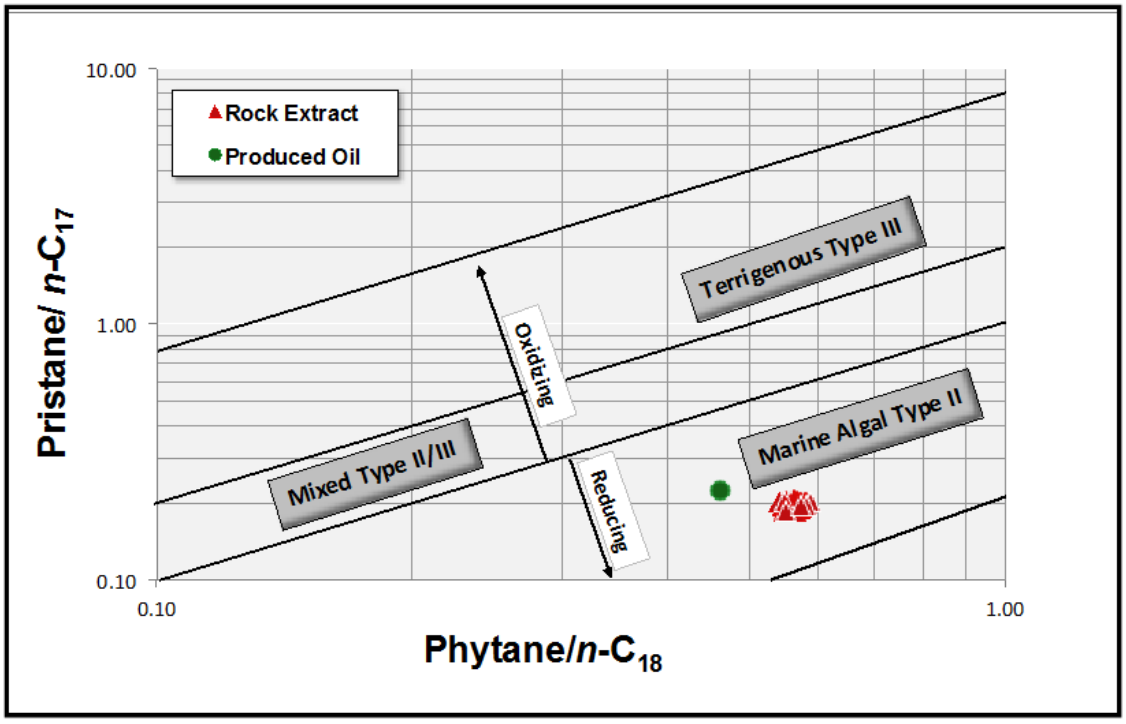

Fig. 5.3 Pristane/*n*-C_{17} versus phytane/*n*-C_{18} for rock extracts and oil from the SFNY reservoir used to describe organic matter type and source rock depositional environment. The plot indicates similar source rock organic facies (marine algal Type-II organic matter) and anoxic depositional environment for all samples. Interpretive fields and labels are adopted from Peters et al. (2000).

One of the parameters used to assess the source facies is the **short- vs. long-chain *n*-alkanes** derived from aquatic algal/microbial and terrestrial plant sources, respectively. The n-alkane distribution for all samples is dominated by *n*-C_{17} (Fig. 5.4), signifying a marine source for the n-alkanes (Sinninghe Damsté et al., 2002). The **Carbon Preference Index (CPI)** represents the ratio of long chain *n*-alkanes with an odd carbon number to long chain *n*-alkanes with an even number (Bray & Evans, 1961; Peters et al., 2005). The ratio is calculated as follows:

$$\mathbf{CPI = [(C_{25}+C_{27}+C_{29}+C_{31}+C_{33})/(C_{26}+C_{28}+C_{30}+C_{32}+C_{34})}$$
$$\mathbf{+ (C_{25}+C_{27}+C_{29}+C_{31}+C_{33})/(C_{26}+C_{28}+C_{30}+C_{32}+C_{34})]/2}$$

According to Peters et al. (2005), oils and extracts with significantly higher (odd preference) or lower (even preference) CPI values than 1.0 indicate low maturity whereas CPI values of 1.0 may result from thermal maturation but do not prove it. However, Tissot and Welte (1978) reported that CPI values less than 1.0 is unusual and indicate predominance of marine carbonate input or hypersaline environment. The studied sample set shows no even or odd carbon preference with CPI values below 1 (CPI average 0.91, n=23) pointing to a carbonate source rock and anoxic depositional setting (Table 5.2 & Figure 5.4).

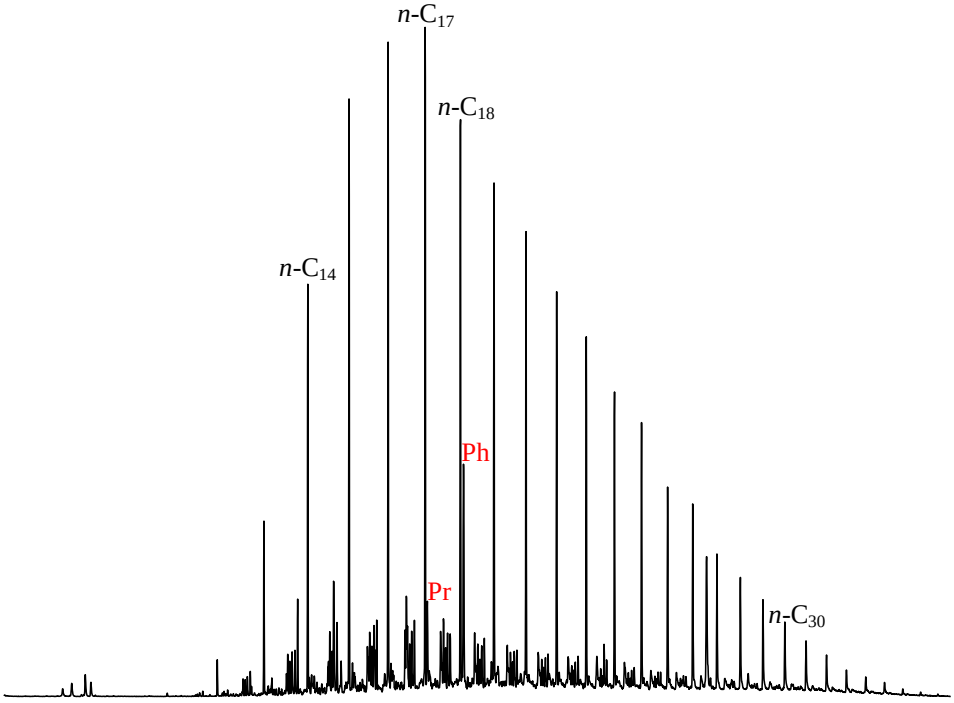

Fig. 5.4 Partial mass chromatogram (*m/z* 85) of the saturated hydrocarbon fraction showing the distribution of the *n*-alkanes for the studied samples from SFNY reservoir. No odd or even carbon preference is witnessed in the *n*-alkanes distribution supporting the anoxic marine depositional setting.

5.1.3 Triterpane and Sterane Biomarker Parameters

Biomarkers (including steranes and hopanes) are geochemical molecular fossils with structures related to biochemicals from once living organisms and found in sedimentary rocks, oils and rock extracts. As such, they provide very useful information on the age and depositional environment of the source rock and the maturity of the crude oils, and also serve as an oil-oil and oil-source correlation tool (Peters & Moldowan, 1993).

5.1.3.1 Facies Assessment

As shown from the previous section 5.1.2, all the studied samples from the SFNY reservoir originate from the same source rock facies. Thus, it is expected that their overall distribution of source related biomarkers would be quite similar. Selected triterpane and sterane biomarker parameters are listed in Tables 5.3 and 5.4, respectively. Partial mass chromatograms (*m/z* 191 & 217) and definition of the geochemical parameters are depicted in Appendix 1.

Hopanes and **tricyclic terpanes** are most likely originating from bacteriohopanetetrol, a cell wall rigidifier in prokaryotic microorganisms (heterotrophic bacteria and also phototrophic cyanobacteria) (Peters & Moldowan, 1993). This group of biomarkers can be easily detected in a saturated hydrocarbon fraction by the molecular fragmentogram at *m/z* 191. Figure 5.5 shows typical terpane distribution (*m/z* 191) of hydrocarbons from the SFNY reservoir. All partial mass chromatograms of the investigated samples show a predominance of the C_{29} 17α(H), 21β(H)-hopane over the C_{30} 17α(H), 21β(H)-hopane (1.03 average, n=23), which is typical for carbonate or marly source rocks deposited under anoxic conditions (Peters et al., 2005). This finding is supported by the high Homohopane Index (HHI) ratio for the samples (0.14 average, n=23). The HHI is commonly used as an indicator of redox conditions in marine sediments (Ourisson et al., 1984). Usually, HHI values $\geq$ 0.10 are recognized for strongly reducing (low Eh) marine conditions during source rock deposition (Peters & Moldowan, 1993). According to Huang and Pearson (1999), oils generated from sulphur-rich source rocks under anoxic conditions mostly exhibit elevated C_{35} hopanes. Sinninghe Damsté et al. (1995) regarded that sulfurization reactions during diagenesis under anoxic marine settings selectively preserve the intact biologically-derived C_{35} bacteriohopane skeleton resulting in the abundance of C_{35} homohopanes and hence in higher HHI values (Figure 5.5 & Table 5.3).

Table 5.3 Hopane and Tricyclic Terpane Source Parameters Calculated from GC-MS (*m/z* 191) for the Analyzed Samples.

		Hopanes			Tricyclic Terpanes			
Sample #	Sample Type	C29/C30 H	C31R/C30 H	HHI	C22/C21 TT	C24/C23 TT	C26/C25 TT	C24 Tet/C26 TT
1	Rock Extract	0.99	0.37	0.14	1.43	0.23	0.47	0.84
2	Rock Extract	1.04	0.37	0.14	1.42	0.26	0.49	0.83
3	Rock Extract	1.02	0.38	0.14	1.49	0.26	0.46	0.84
4	Rock Extract	1.02	0.38	0.14	1.43	0.26	0.38	0.86
5	Rock Extract	1.04	0.41	0.14	1.43	0.25	0.42	0.85
6	Rock Extract	1.06	0.38	0.13	1.33	0.30	0.46	0.84
7	Rock Extract	1.07	0.39	0.13	1.44	0.22	0.35	0.86
8	Rock Extract	1.01	0.39	0.14	1.49	0.23	0.36	0.86
9	Rock Extract	1.05	0.41	0.14	1.51	0.23	0.38	0.86
10	Rock Extract	1.01	0.37	0.14	1.51	0.23	0.40	0.85
11	Rock Extract	1.01	0.37	0.14	1.50	0.25	0.42	0.85
12	Rock Extract	1.01	0.37	0.14	1.50	0.24	0.38	0.86
12-R	Rock Extract	1.00	0.36	0.14	1.46	0.25	0.39	0.87
13	Rock Extract	1.06	0.36	0.14	1.52	0.24	0.39	0.86
14	Rock Extract	1.07	0.38	0.13	1.59	0.24	0.40	0.87
15	Rock Extract	1.01	0.39	0.14	1.52	0.23	0.40	0.86
16	Rock Extract	1.02	0.39	0.14	1.48	0.23	0.40	0.86
17	Rock Extract	1.01	0.39	0.13	1.47	0.24	0.42	0.85
18	Rock Extract	1.01	0.39	0.13	1.45	0.22	0.35	0.87
19	Rock Extract	1.04	0.40	0.13	1.55	0.21	0.37	0.89
20	Rock Extract	1.02	0.39	0.13	1.56	0.24	0.34	0.87
21	Produced Oil-SFNY	1.01	0.39	0.13	1.33	0.22	0.36	0.86
21-R	Produced Oil-SFNY	1.01	0.39	0.13	1.39	0.23	0.35	0.86

$C_{29}H/C_{30}H$: 30-norhopane/C_{30} hopane; **$C_{31}R/C_{30}H$: C**31 homohopane 22R/C_{30} hopane, (Peters et al., 2005); **HHI**: homohopane index= ($C_{35}\alpha\beta$ homohopane S+R)/(ΣC_{31}-$C_{35}\alpha\beta$ homohopanes S+R), (Ourisson et al., 1984); **C_{22}/C_{21}TT:** C_{22} tricyclic terpane/ C_{21} tricyclic terpane; **C_{24}/C_{23}TT:** C_{24} tricyclic terpane/ C_{23} tricyclic terpane; **C_{26}/C_{25}TT:** C_{26} tricyclic terpane/ C_{25} tricyclic terpane; **C_{24} Tet/C_{26}TT:** C_{24} tetracyclic terpane/ C_{26} tricyclic terpane, (Peters & Moldowan, 1993; Peters et al., 2005). Duplicate analyses are indicated by the sample # followed by the letter suffix R.

The carbonate or marl source indicated, is also in agreement with other parameters based on **tricyclic terpane compounds**. The C_{24}/C_{23} tricyclics ratio as a function of the C_{22}/C_{21} tricyclic ratio is useful to differentiate between a shale and carbonate source. High C_{22}/C_{21} and low C_{24}/C_{23} tricyclic terpane ratios indicate a predominantly carbonate source rock depositional environment (Peters et al., 2005). Very high C_{22}/C_{21} tricyclic trepane ratios (1.47 average, n=23) and low C_{24}/C_{23} tricyclic terpane (0.24 average, n=23) were observed for the studied samples. Also, the C_{26}/C_{25} tricyclic terpane and $C_{31}(22R)/C_{30}$ hopane ratios effectively distinguish petroleums from a marine and lacustrine environment. Unlike lacustrine oils, oils from marine source rocks usually have C_{26}/C_{25} tricyclic terpane ratios less than 1 and $C_{31}R/C_{30}$ hopane greater

than 0.25. The investigated samples are characterized by low C_{26}/C_{25} tricyclic terpane (0.40 average, n=23) and relatively high $C_{31}R/C_{30}$ hopane (0.38 average, n=23), typifying a marine carbonate source. Moreover, the samples show abundant C_{24} tetracyclic terpanes compared to C_{26} tricyclic terpanes which confirms the restricted marine carbonate source rock settings (Figure 5.5 & Table 5.3) (Peters & Moldowan, 1993).

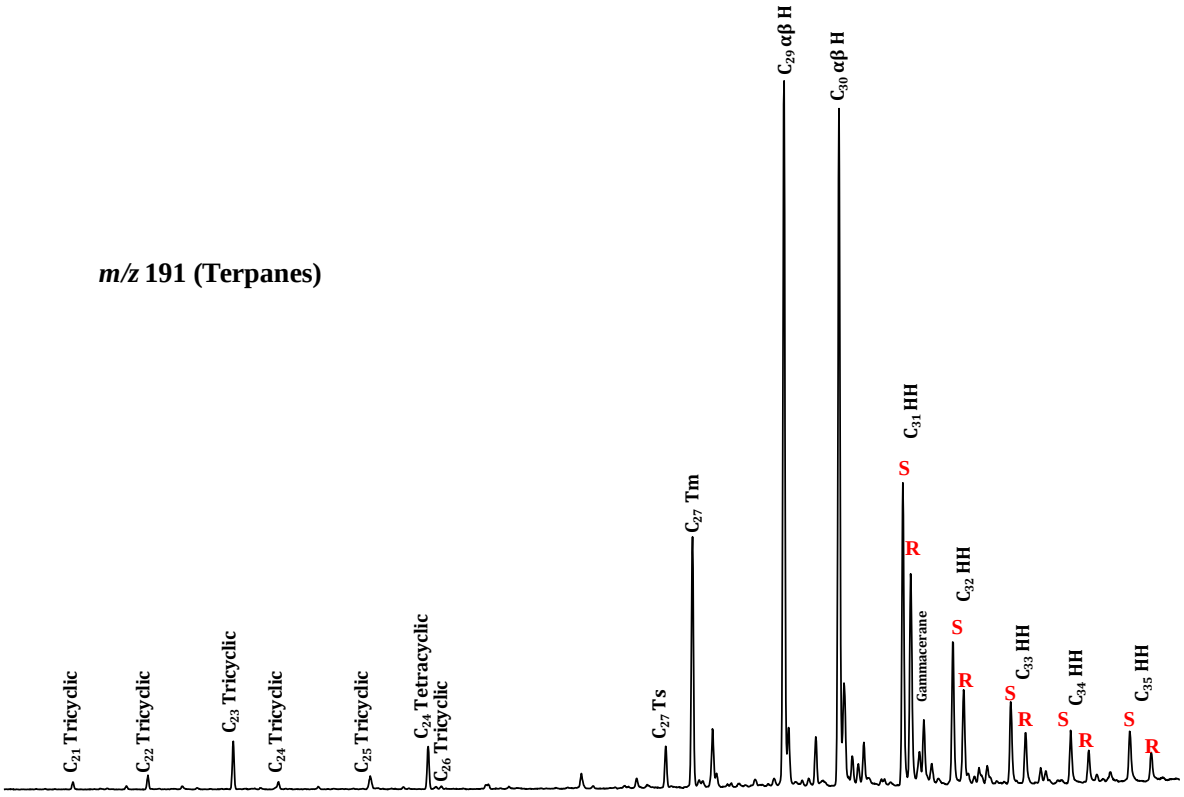

Fig. 5.5 Partial mass chromatograms (*m/z* 191) showing the distribution of tricyclic terpanes and hopanes for the studied samples from SFNY reservoir. Important peaks are indicated. H: 17α(H), 21β(H)-hopane; HH: homohopanes.

Steranes and diasteranes are another important class of biomarkers which can be used to assess the lithology of source rock, nature of source depositional environment and maturity. This class of compounds is believed to derive from sterols, which are important components of the membrane and hormone in eukaryotic organisms (Mackenzie et al., 1982). Diasteranes are the rearranged products from sterol precursors during diagenesis. Steranes and diasteranes are detected using *m/z* 217 mass chromatograms (Peters et al., 2005).

The **C_{27}, C_{28}, and C_{29} ααα- 20R (5α, 14α, 17α (H)-steranes)** are among the parameters used in assessing paleoenvironment and source of sedimentary organic matter (e.g., Peters & Moldowan, 1993). The distribution of these biological configurations for the studied samples is displayed on a classical ternary diagram (Figure 5.6). The studied samples contain high concentrations of ααα C_{29} -R steranes (50.4% average, n=23) (Table 5.4). Huang and Meinshein (1979) originally interpreted the high concentrations of C_{29} (24-ethylcholestanes) in oils compared to C_{27} (cholestanes) and C_{28} (methylcholestanes)-steranes as an origin from terrestrial source. However, the previously investigated source parameters in this study show no evidence for land plant input to the source rock. Several studies (e.g., Peters & Moldowan, 1993; Rullkötter et al., 1986; Peters et al., 2005; Wang et al., 2008) later reported the abundance of C_{29} steranes in crude oils derived from carbonate source rocks with no or only little higher plant input. Furthermore, Peters et al. (2005) stated that this diagram is better used as an oil-oil and oil-source correlation tool due to some ambiguity and broad overlaps of different depositional environments in steranes ternary diagram. Therefore, similarities in the C_{27}, C_{28}, and C_{29} (ααα-R steranes) distribution within the investigated sample set is interpreted as indicating an origin from a single source facies with a uniform composition of organic matter and hence a similar depositional environment.

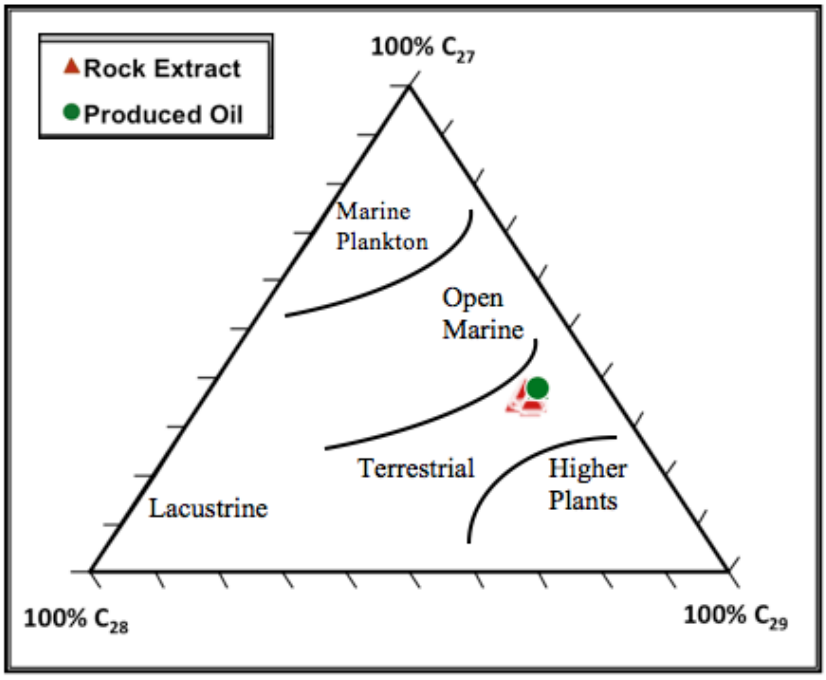

Fig. 5.6 Ternary diagram showing the distribution of ααα-20R steranes for the studied samples from SFNY reservoir. Fields are adopted from Huang and Meinshein (1979).

Table 5.4 Steranes and Diasteranes Source Parameters Calculated from GC-MS (*m/z* 217) for the Analyzed Samples from SFNY Reservoir.

		Steranes (ααα-R)			Diasteranes	
Sample #	Sample Type	C27%	C28%	C29%	C27-C29DIAR	C27 DIAR
1	Rock Extract	35.34	15.63	49.03	0.14	0.05
2	Rock Extract	36.53	12.68	50.79	0.13	0.05
3	Rock Extract	36.38	13.73	49.89	0.13	0.04
4	Rock Extract	36.42	13.27	50.31	0.12	0.06
5	Rock Extract	36.52	13.35	50.14	0.13	0.05
6	Rock Extract	37.60	13.55	48.86	0.13	0.05
7	Rock Extract	37.61	13.17	49.21	0.13	0.05
8	Rock Extract	36.10	12.33	51.56	0.12	0.04
9	Rock Extract	36.64	12.92	50.44	0.13	0.04
10	Rock Extract	38.22	12.87	48.92	0.12	0.05
11	Rock Extract	37.53	13.51	48.95	0.12	0.05
12	Rock Extract	37.64	11.76	50.60	0.13	0.05
12-R	Rock Extract	38.32	11.68	50.00	0.12	0.04
13	Rock Extract	37.85	12.80	49.35	0.13	0.05
14	Rock Extract	37.32	11.81	50.87	0.13	0.04
15	Rock Extract	35.71	12.55	51.74	0.12	0.04
16	Rock Extract	35.33	12.83	51.83	0.13	0.05
17	Rock Extract	35.35	12.47	52.17	0.12	0.05
18	Rock Extract	35.77	12.93	51.31	0.12	0.04
19	Rock Extract	36.09	14.22	49.69	0.13	0.04
20	Rock Extract	35.93	12.82	51.25	0.13	0.04
21	Produced Oil	36.51	12.47	51.01	0.12	0.05
21-R	Produced Oil	37.40	11.97	50.63	0.12	0.05

C_{27}%: C_{27} ααα-20R sterane/(ΣC_{27}-C_{29}ααα-20R) steranes; **C_{28}%:** C_{28} ααα-20R sterane/(ΣC_{27}-C_{29}ααα-20R) steranes; **C_{29}%:** C_{29} ααα-20R sterane/(ΣC_{27}-C_{29}ααα-20R) steranes, (Peters & Moldowan, 1993); **C_{27}/C_{29} DIAR:** C_{27}/C_{29} diasterane ratio = ΣC_{27}-C_{29} diasteranes/ (ΣC_{27}-C_{29} diasteranes + ΣC_{27}-C_{29} regular steranes); **C_{27} DIAR:** C_{27} diasterane ratio = C_{27} diasteranes/ (C_{27} diasteranes +C_{27} regular steranes), (Rubinstein et al., 1975; Peters & Moldowan, 1993). Duplicate analyses are indicated by the sample # followed by the letter suffix R.

The steranes and diasteranes (*m/z* 217) distribution of the SFNY samples further supports the carbonate rich lithology of the source rock (Figure 5.7). Acidic sites on clastic rocks stimulate the conversion of steranes to diasteranes. Thus, the **diasterane ratio (DIAR)** defined as the ratio of C_{27}-C_{29} diasteranes over C_{27}-C_{29} regular steranes and is normally used to discriminate petroleum from clastic versus those from carbonate rocks (Rubinstein et al., 1975; Peters & Moldowan, 1993). High DIAR indicates a clay rich source rock whereas lower ratios are typical for anoxic carbonate rich source rock. The concentration of diasteranes is low in all of the investigated

samples (0.13 average, n=23)(Table 5.4), reflecting an anoxic, clay-poor, carbonate source rock lithology. However, low DIAR in petroleum can also result from low thermal maturity (Peters et al., 1990). At low thermal stresses, the conversion of steranes to diasteranes might not be completed leading to low DIAR ratio.

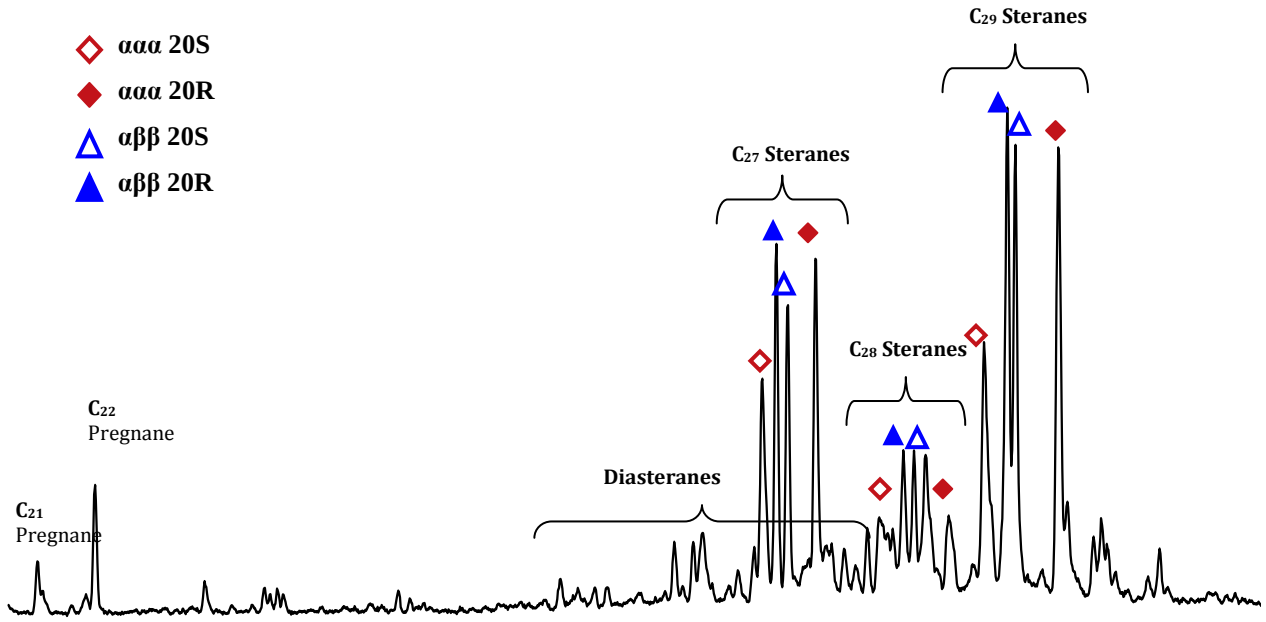

Fig. 5.7 Partial mass chromatograms (*m/z* 217) showing the distribution of steranes and diasteranes for the studied samples from the SFNY reservoir. Important peaks are indicated.

Figure 5.8 illustrates a plot of pristane/(pristane+phytane) vs diasteranes/(diasteranes + regular steranes) for the analyzed samples from SFNY reservoir. According to Peters et al. (2005), there is a positive correlation between Pr/(Pr+Ph) and C_{27} diasteranes/(diasteranes+steranes) governed by the depositional environments. Pr/(Pr+Ph) increases with source clay content, as measured by increasing diasteranes, which parallels oxidative strength (Eh) of the water column during deposition of the source rocks. The studied samples are low in both Pr/(Pr+Ph) and diasteranes/(diasteranes + regular steranes) ratios (0.05 average, n=23) (Table 5.4), confirming the oils likely generation from a carbonate source rock deposited under dominantly anoxic environmental conditions .

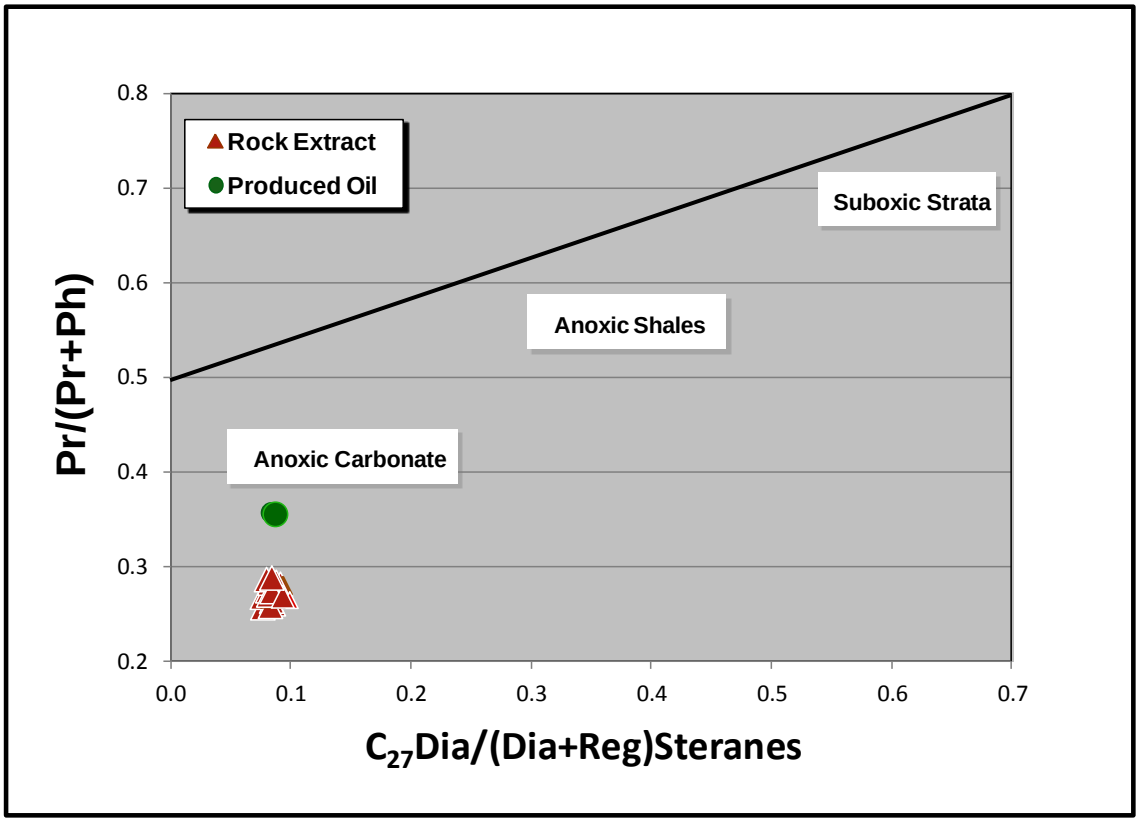

Fig. 5.8 Cross plot of Pristane/(Pristane+Phytane) vs C_{27} diasteranes/ (diasteranes+regular steranes) ratios of the analyzed extracts and oil, reflecting marine source signature and reducing settings.

5.1.3.2 Source Maturity Assessment from Reservoired Oils

Since petroleum accumulation in any reservoir is comprised of a mixture of early and more progressively mature charge filling the trap over geological time scales, the notion of the concept of a single oil maturity is somewhat illusory and it is expected that different petroleum components will reflect the stage of thermal maturity that they were generated at. Hence, biomarkers are useful in assessing maturity at the early to mid oil window as they are dominant in oil fractions expelled within this range. While, the light and aromatic hydrocarbon parameters become more abundant in advanced stages of thermal maturity and thus are more reliable in assessing the overall maturity of the bulk oil along with the biomarkers (Wilhelms & Larter, 2004).

Some parameters based on tricyclic terpanes, hopanes and steranes classes are useful to assess the relative maturity of source rocks and oils (Moldowan et al., 1992; Peters & Moldowan, 1993;

Rullkötter et al.,1984; Seifert & Moldowan, 1986). The maturity assessment using biomarker compounds is based on the fact that biological precursor molecules respond differently in different ranges of thermal maturity and transform into more thermodynamically stable geochemical fossils. Calculated common maturity parameters are listed in Table 5.5. Overall, the studied samples from the SFNY reservoir show fairly uniform values in all maturity parameters indicating a thermally homogenized mixture.

The **terpane** distribution patterns (*m/z* 191, Figure 5.5) and the tricyclic/17α(H), 21β(H)-hopane ratio of the studied samples (Table 5.5) show a dominance of pentacyclic terpanes (hopanes) over tri- and tetracyclic terpanes. This dominance suggests that the samples are mostly generated at early stages of maturation as organic matter cannot degrade pentacyclic terpanes to generate lighter ones under low thermal stress levels, resulting in low tricyclic terpanes relative to hopanes (Peters et al., 1990). Also, low tricyclic/hopane ratios indicate an origin from source rocks deposited under marine conditions (Peters et al., 2005). This is in agreement with the previously investigated source parameters in this study.

Another commonly used thermal maturity parameter is the **Ts/(Ts+Tm) ratio** which is believed to be both maturity- and source-dependent (Peters & Moldowan, 1993). C_{27}Ts (18α(H)-22,29,30-trisnorneohopane) is thermally more stable than C_{27}Tm (17α(H)-22,29,30-trisnorhopane) and hence the ratio of C_{27} Ts/(Ts+Tm) terpanes increases with thermal maturity. The same is valid for the ratio **C_{29}Ts/(C_{29}Ts + C_{29}H) [**C_{29}Ts (18α(H)-30-norneohopane) /(C_{29}Ts + C_{29}H (17α(H), 21β(H)-30-norhopane)]. Although these two parameters are source dependent, they can be used to assess thermal maturity when dealing with petroleums from a common source facies (Peters et al., 2005). The studied samples are characterized by low C_{27} Ts/(Ts+Tm) and C_{29}Ts /(C_{29}Ts+C_{29} Hopane) ratios (0.15 and 0.06 average, n=23, respectively). These ratios along with the vitrinite reflectance (Rc), calculated from an empirical calibration for marine source rocks based on Ts/(Ts+Tm) (not published), shows that the investigated samples belong to a source rock that started expulsion at very early stage of maturation (~0.42 %Rc). The Rc formula for Ts/(Ts+Tm) is not calibrated for Saudi oils and the indicate maturity is thus notional but it is clear the oil maturities are low.

Table 5.5 Steranes and Terpanes Maturity Parameters Calculated from *m/z* 217 and 191, Respectively for the Analyzed Samples.

	Tricyclic Terpanes & Hopanes					Steranes		
Sample #	TT/H	22S/(22S+22R)	C29 Ts/(C29 Ts+C29 H	Ts/(Ts+Tm)	Rc	20S/(20S+20R)	ββ/(αα+ββ)	(C21+C22)/(C27-C29)
1	0.05	0.58	0.06	0.17	0.42	0.47	0.49	0.08
2	0.06	0.59	0.06	0.16	0.41	0.47	0.49	0.08
3	0.06	0.58	0.06	0.15	0.40	0.48	0.49	0.08
4	0.05	0.58	0.06	0.16	0.41	0.49	0.49	0.08
5	0.05	0.58	0.06	0.15	0.40	0.48	0.49	0.09
6	0.06	0.58	0.06	0.15	0.41	0.48	0.50	0.09
7	0.05	0.58	0.06	0.15	0.40	0.48	0.49	0.09
8	0.05	0.58	0.06	0.15	0.40	0.46	0.49	0.08
9	0.05	0.57	0.06	0.15	0.40	0.46	0.49	0.08
10	0.05	0.58	0.07	0.15	0.40	0.47	0.50	0.08
11	0.05	0.60	0.06	0.15	0.40	0.46	0.50	0.08
12	0.05	0.59	0.06	0.16	0.42	0.44	0.49	0.08
12-R	0.05	0.58	0.06	0.15	0.40	0.45	0.50	0.08
13	0.05	0.58	0.06	0.15	0.40	0.46	0.50	0.08
14	0.05	0.59	0.06	0.15	0.40	0.47	0.50	0.08
15	0.05	0.58	0.06	0.15	0.40	0.45	0.49	0.08
16	0.05	0.58	0.06	0.15	0.40	0.46	0.49	0.08
17	0.05	0.58	0.06	0.15	0.40	0.46	0.49	0.08
18	0.05	0.58	0.06	0.15	0.40	0.45	0.49	0.08
19	0.05	0.58	0.05	0.15	0.40	0.49	0.51	0.08
20	0.05	0.58	0.06	0.15	0.40	0.46	0.49	0.08
21	0.05	0.58	0.06	0.15	0.40	0.46	0.49	0.08
21-R	0.05	0.58	0.06	0.15	0.40	0.46	0.49	0.08

TT/H: tricyclic terpane/ hopane = C_{21}-C_{29} tricyclic terpane/C_{29}-C_{33} hopane, (Peters et al., 2005)**; 22S/(22S+22R):** C_{31} 22S/ C_{31} (22S+22R) homohopane, (Seifert & Moldowan, 1978; Peters et al., 2005); **C_{29}Ts/(C_{29}Ts + C_{29}H):** C_{29}18α(H)-30-norneohopane)/(C_{29} 18α(H)-30-norneohopane + C_{29} 17α(H),21β(H) hopane), (Peters & Moldowan, 1993; Peters et al., 2005); **Ts/(Ts+Tm)=** C_{27} 17α-22,29,30-trisnorhopane / (C_{27} 17α-22,29,30-trisnorhopane+ C_{27} 18α-22,29,30trisnorneohopane), (Peters & Moldowan, 1993; Seifert and Moldowan, 1978); **%Rc:** vitrinite reflectance calculated from Ts/(Ts+Tm) =1.08* (Ts/Ts+Tm)+0.24, (Bennett, not published); **20S/(20S+20R)=** C_{29} ααα 20S/(20S +20R) steranes, (Seifert & Moldowan, 1978); **(ββ/ ββ+αα):** C_{29} (ββ/ ββ+αα) steranes, (Seifert & Moldowan, 1986); **(C_{21} + C_{22})/(C_{27}-C_{29}):** **(**C_{21}+C_{22}) short chain steranes/(ΣC_{27}-C_{29}) long chain steranes, (Wingert & Pomerantz, 1986). Duplicate analyses are indicated by the sample # followed by the letter suffix R

Although the **diasterane ratio (DIAR) is commonly used to evaluate the clay content in a**

source rock, Rullkötter et al. (1984) found that the steranes rearrange to form the more thermodynamically stable diasteranes at high levels of thermal maturity, leading to a higher abundance of diasteranes. According to Rullkötter et al., the transformation of steranes to diasteranes occurs through stimulation by the clay minerals or possibly by hydrogen-exchange reactions that are enhanced by water. The DIAR ratio, as shown earlier in Table 5.4, further supports the early expulsion of the studied samples. Additionally, the relative abundance of short chain steranes C_{21} and C_{22} confirms the low thermal maturity of the sample set. Usually, the low abundance of C_{21} and C_{22} steranes relative to C_{27}-C_{29} steranes is typical of oil generated at low thermal maturities (Wingert & Pomerantz, 1986).

The maturity parameters **[C_{31} αβ 22S/(22S+22R)] homohopane and [C_{29} ααα sterane 20 S/(20S +20R)] sterane** have high specificity for immature and early oil generation because isomerization at the C-22 in the (C_{31}- C_{35} 17α(H), 21β(H)-homohopanes) and at the C-20 in the (5α, 14α, 17α (H)-steranes) occurs preceding other biomarker thermal reactions (Seifert & Moldowan, 1978). Unlike the previously investigated maturity parameters in this study, these two ratios for the sample set are at or near equilibrium values 0.58 and 0.47, respectively (Table 5.5), signifying a main phase of oil generation. This is common for most oils and these parameters are actually of little value in real applications. The **C_{29} (ββ/ ββ+αα) steranes** ratio for the samples range between (0.49-0.51) however suggest source maturities near peak oil generation. The (ββ/ ββ+αα) ratio increases from near-zero values to 0.7 with increasing thermal maturity due to isomerization at C-14 and C-17 in the C_{29} 20S and 20R regular steranes. (Seifert & Moldowan, 1986).

There are two explanations for the inconsistency in these maturity biomarker parameters. The first is that the enrichment of the 22S homohopanes and 20S sterane relative to their biological configurations (R), and the abundance of ββ sterane epimers might not be a result of catagenesis but rather a result from sulfuration reactions at the early diagenetic stage as noted by Moldowan et al. (1992) and Ten Haven et al. (1986). A fully isomerized homohopanes in immature sulfur-rich carbonate rocks from the Adriatic Basin were detected by Moldowan et al. (1992). The release of sulfurized hopanoids from the kerogen at early stage of maturation was proposed to be the main reason for the enrichment of the 22S/(22S+22R) in these low mature oils rather than thermal isomerization. The origin of the studied SFNY samples from sulfur rich kerogen (Type-IIS) with sulfur content as high as 8% could be the reason for these samples to appear to be

mature in some hopane and sterane biomarker maturity parameters. The other and the more plausible explanation, as mentioned earlier under this section, is that all petroleum accumulations represent a mixture of oils generated at different stages of maturity and therefore different maturity tracers would reflect different degrees of thermal maturation based on the stage that they were generated at (Wilhelms & Larter, 2004).

5.1.4 Aromatic Hydrocarbon Parameters

Aromatic hydrocarbons are proven to be useful for an interpretation of the source rock lithology, depositional environment as well as maturity (Hughes et al., 1995).

5.1.4.1 Facies Assessment

Dibenzothiophenes are sulfur-containing compounds in the aromatic "hydrocarbon" fraction, which can provide important information about the organic matter source. A plot of dibenzothiophene/phenanthrene (DBT/Phen) versus pristane/phytane (Pr/Ph) is illustrated in Figure 5.9. In this classic diagram (Hughes et al., 1995), DBT/Phen acts as a proxy for kerogen and oil sulfur content, representing the availability of reduced sulfur for incorporation into the organic matter, whereas pristane/phytane acts as a proxy for the redox potential of the depositional environment. All samples have low Pr/Ph ratios (< 1.0) and high DBT/Phen ranging from 0.8 to 2.2, indicating an anoxic depositional environment and an iron-deficient source rock such as a marine carbonate and marl, as classified by Hughes et al. (1995). However, with increasing reservoir depth, there is a decrease in the oil DBT/Phen ratio. The decrease in the DBT absolute concentration (from 41 to 13 μg) relative to a constant absolute concentration of Phen with depth could be a result of a later charge mixing only with the oils at the top of the reservoir (Stainforth, 2004) or it could be a result of an alteration process (e.g., water-washing)(Palmer, 1993).

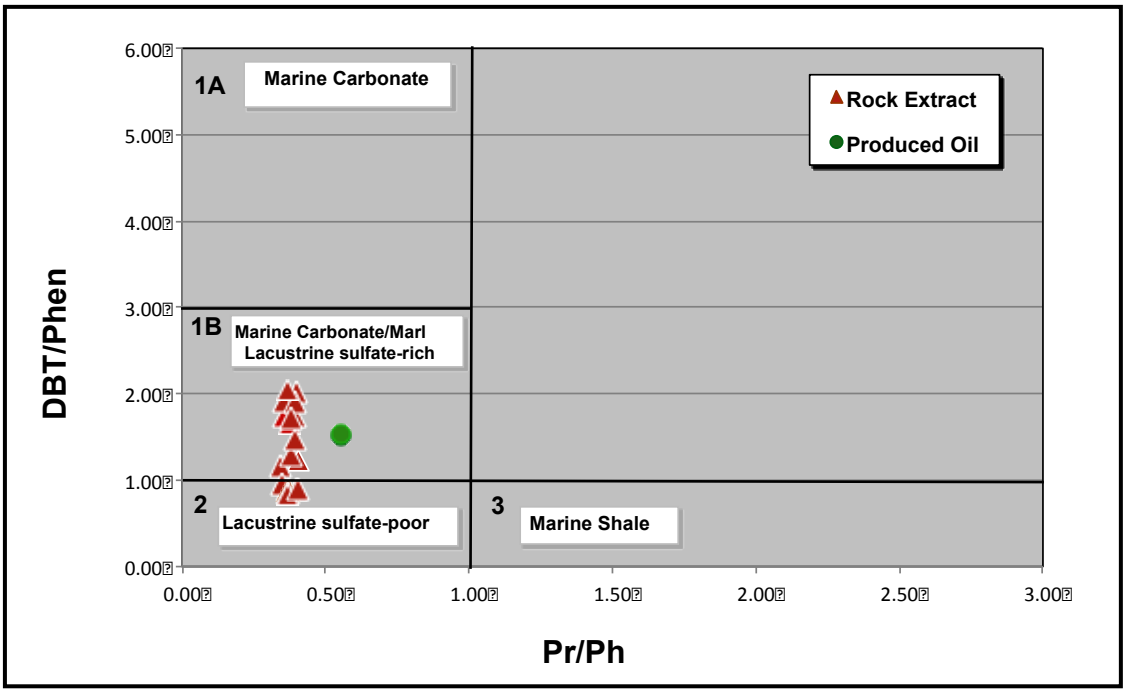

Fig. 5.9 Plot of dibenzothiophene/phenanthrene (DBT/Phen) versus pristane/phytrane ratios of the analyzed extracts and oil, reflecting mixed lithology source rocks (marine carbonate and marl) and reducing settings. Fields are adopted from Hughes et al. (1995): 1A: Marine Carbonate; 1B: Marine Carbonate, Marine Marl and Lacustrine Sulfate-rich; 2: Lacustrine Sulfate-Poor; 3: Marine Shale and Other Lacustrine source rocks.

5.1.4.2 Maturity Assessment

Alkylaromatic hydrocarbon homologues and isomers with different thermodynamic stability were used to assess the thermal maturity of the studied oil samples. Calculated maturity parameters are listed in Table 5.6 and partial mass chromatograms (m/z 178, 184, 192, 198, 231& 253) are depicted in Appendix 1. Generally, the investigated samples have uniform maturities as reflected by the calculated maturity parameters (Table 5.6).

Ratios of **mono- and triaromatic steroid hydrocarbons** are usually considered as typical maturity indices. With elevated degrees of thermal stress, C-ring monoaromatic steroid hydrocarbons tend to aromatise and are transformed to ABC-ring triaromatic steroids through the loss of a methyl group at the A/B ring junction (Fig. 5.10). This process leads to a decrease in the ratio of monoaromatic steroid (MA) to triaromatic steroid (TA) hydrocarbons (TA/MA+TA)

(Mackenzie, 1984; Peters et al., 2005). The analyzed samples from SFNY reservoir have low TA/(MA+TA) ratios (average 0.21, n=23) (Table 5.6), indicating low thermal maturity. Moreover, the low maturity level of the sample set is also supported by the low ratios of **short side-chain C_{21}-triaromatic steroid hydrocarbons to long side-chain C_{28}-triaromatic** components [TA (I)/ TA (I+II) steroids] (average 0.13, n=23). Increased thermal maturity degrades the long side-chain to short side-chain TA steroids (Fig. 5.11), increasing the components [TA (I)/ TA (I+II) steroids] ratio (Beach et al., 1989).

Table 5.6 Aromatic Hydrocarbon Maturity Parameters Calculated from GC-MS Mass Chromatograms (*m/z* 178, 192, 231& 253) for the Analyzed Samples.

			Aromatic Hydrocarbons					
Sample #	Sample Type	Depth (ft)	TA/(TA+MA)	TA I/(I+II)	MPI	%Rc	MPR1	MPR2
1	Rock Extract	3373.1	0.20	0.13	0.71	0.83	0.56	0.68
2	Rock Extract	3375.5	0.20	0.12	0.70	0.82	0.63	0.67
3	Rock Extract	3377.6	0.21	0.11	0.70	0.82	0.63	0.71
4	Rock Extract	3380.3	0.21	0.12	0.68	0.81	0.61	0.63
5	Rock Extract	3382.2	0.21	0.12	0.72	0.83	0.61	0.72
6	Rock Extract	3385.1	0.22	0.13	0.68	0.81	0.59	0.66
7	Rock Extract	3389.8	0.21	0.13	0.68	0.81	0.63	0.69
8	Rock Extract	3392.8	0.21	0.11	0.69	0.82	0.61	0.70
9	Rock Extract	3433.4	0.19	0.13	0.69	0.81	0.59	0.71
10	Rock Extract	3435.7	0.19	0.13	0.70	0.82	0.63	0.70
11	Rock Extract	3437.5	0.19	0.13	0.73	0.84	0.61	0.72
12	Rock Extract	3440.5	0.20	0.14	0.68	0.81	0.60	0.66
12-R	Rock Extract	3440.5	0.20	0.14	0.72	0.83	0.58	0.68
13	Rock Extract	3466.2	0.19	0.13	0.66	0.80	0.56	0.63
14	Rock Extract	3469.9	0.19	0.13	0.70	0.82	0.54	0.65
15	Rock Extract	3471.2	0.21	0.12	0.69	0.82	0.59	0.66
16	Rock Extract	3473.2	0.21	0.11	0.69	0.82	0.54	0.66
17	Rock Extract	3479.3	0.20	0.12	0.67	0.80	0.56	0.66
18	Rock Extract	3480.2	0.20	0.13	0.70	0.82	0.55	0.64
19	Rock Extract	3482.9	0.19	0.12	0.69	0.82	0.59	0.65
20	Rock Extract	3484.1	0.20	0.12	0.63	0.78	0.58	0.63
21	Produced Oil	3370-3470	0.20	0.13	1.01	1.00	0.49	0.83
21-R	Produced Oil	3370-3470	0.18	0.15	1.00	1.00	0.48	0.82

TA/(TA+MA)= C_{26}-C_{28} triaromatic steroids/(C_{27}-C_{29} monoaromatic steroids + C_{26}-C_{28} triaromatic steroids), (Mackenzie et al., 1984; Peters et al.,2005); **TA(I)/(I+II)**: short-side chain triaromatic steroid hydrocarbo /(short-side chain triaromatic steroid hydrocarbon + long-side chain triaromatic steroid hydrocarbon), (Beach et al., 1989); **MPI-1:** methylphenanthrene Index = 1.5* [2-+3-methylphenanthrene]/[phenanthrene + 1- + 9- methyl phenanthrene]; **%Rc:** vitrinite reflectance calculated from MPI-1= 0.6*MPI+0.4; **MPR-1=** 1-methylphenanthrene/phenanthrene**; MPR-2=** 2-methylphenanthrene/phenanthrene, (Radke & Welte, 1983). Duplicate analyses are indicated by the sample # followed by the letter suffix R.

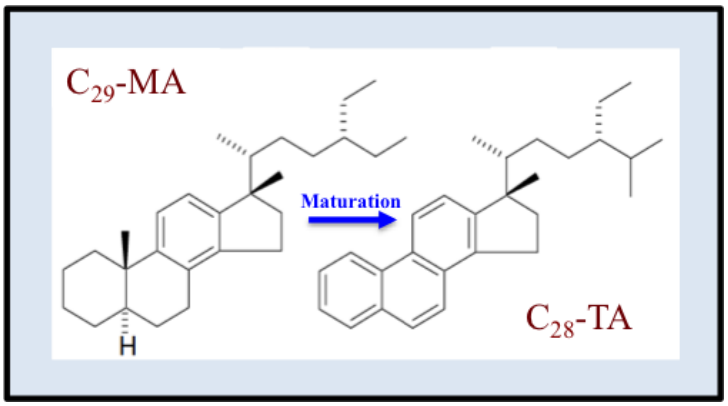

Fig. 5.10 Transformation of the C_{29} -monoaromatic (MA) steroids to C_{28} -triaromatic steroids (TA) with increasing maturity (after Peters et al., 2005).

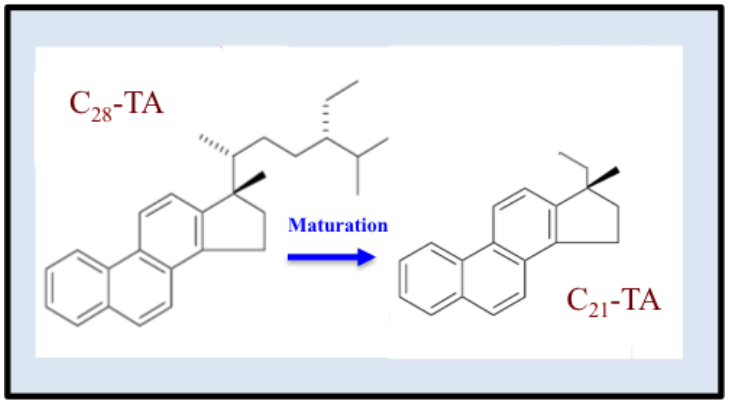

Fig. 5.11 Transformation of the long side-chain C_{28} -triaromatic steroids to short side-chain C_{21} -triaromatic steroids with increasing maturity (after Peters et al., 2005).

Another widely used measure of thermal maturity based on aromatic hydrocarbons employs changes in the relative distribution of alkylated homologues of phenanthrene compounds (e.g., Radke & Welte, 1983). With progressive maturation, the alkylphenanthrenes are transformed to the more thermally stable β-type isomers (Radke & Welte, 1983). The distribution of methylphenanthrenes in the source is controlled by the thermal maturity in the

approximate range of 0.6 % - 1.7 % vitrinite reflectance. No pronounced maturity trends were observed in the oils from assessment of the methylphenanthrene index (MPI), MPR1 (1-methylphenanthrene/phenanthrene) and MPR2 (2-methylphenanthrene/phenanthrene) ratios for all of the investigated samples (Table 5.6), indicating a thermally homogenized oil mixture throughout the reservoir. These compounds are more reliable in assessing the overall thermal maturity of an oil mixture than biomarkers as the aromatic hydrocarbons are generated in abundance in the more mature fractions of the oil (Wilhelms & Larter, 2004). The vitrinite reflectance of the studied samples is calculated according to the formula %Rc= 0.6*MPI+0.4, based on the methylphenanthrene Index (MPI-1). When calibrated, Radke and Welte (1983) found a positive linear correlation between the MPI-1 and the vitrinite reflectance of shales and coals within the oil window (0.65-1.35 % Rc). As expected, vitrinite reflectance values estimated from the (MPI-1) of the studied oil samples signify a mature oil mixture (0.84 % Rc).

5.1.5 Stable Carbon Isotopes

The stable carbon isotopic composition of selected whole-oil extracts from the SFNY reservoir is shown in Table 5.7. The carbon isotopic composition of a crude oil primarily depends on the $\boldsymbol{\delta}^{13}C$ signature of the source (kerogen) from which it is derived. Hence, stable carbon isotopic composition of oils and source rocks is a useful tool for oil–oil and oil–source rock correlation studies (Fuex, 1977; Sofer, 1984; Chung et al., 1992). Isotopic differences among a group of genetically related oils may indicate variations in the thermal maturity and/or organic facies of the source rock (Fuex, 1977). Biodegradation usually has only little or no effect on the carbon isotopic composition of oils that share a common source (Kennicutt & Mahlon, 1988; Sun et al., 2005). All of the studied samples have $\boldsymbol{\delta}^{13}C$ values of -27.6 per mil on average, which is typical for Saudi Jurassic oils (Carrigan et al., 1995); they also have an almost identical carbon isotopic signature, which indicates that they share the same biological source with no large variation in thermal maturity.

Table 5.7 Carbon Isotopic Compositions of the Whole Extracted Oil of the Studied Samples from the SFNY Reservoir.

Sample #	Sample Type	Depth (ft)	$\delta^{13}C$
2	Rock Extract	3375.5	-27.7
5	Rock Extract	3382.2	-27.6
8	Rock Extract	3392.8	-27.6
9	Rock Extract	3433.4	-27.6
12	Rock Extract	3440.5	-27.6
13	Rock Extract	3466.2	-27.7
15	Rock Extract	3471.2	-27.6
18	Rock Extract	3480.2	-27.6
19	Rock Extract	3482.9	-27.7
20	Rock Extract	3484.1	-27.6
21	Produced Oil	CHT (3370-3470')	-27.7

5.1.6 Conclusions

The investigated sulfur-rich heavy oils from the SFNY reservoir (Wasia Formation) are primarily derived from source rocks exposed to the early oil window stage of petroleum generation. The low thermal maturity is the main control on the occurrence of these heavy oils. However, the more reliable aromatic hydrocarbons (MPI) indicate that the SFNY trap has received a relatively more mature charge resulting in an oil mixture with a vitrinite reflectance of up to 0.84 % Rc. Distributions of n-alkanes, saturated and aromatic hydrocarbons of these oils indicate that they are derived from a single source rock facies (marine algal Type IIS) deposited under anoxic conditions.

Although the studied samples have a common origin and are very uniform in their physical properties, and their gross and molecular compositions, they exhibit dramatic compositional gradients in some of the low molecular weight aromatic compound classes with increasing depth (e.g., DBT, Figure 5.9). A different or later charge of relatively higher maturity petroleum or/and post-generative alteration processes (e.g., biodegradation, water-washing) might have influenced the composition of the SFNY heavy oils resulting in these gradients.

5.2 Assessment of Petroleum Column Compositional Gradient-Inducing Processes

Figures 5.12, 5.13, 5.14 and 5.15 illustrate the component absolute concentration (μg/g or ppm) profiles of the different polycyclic aromatic hydrocarbon families (PAHs) for the studied oils. There is a clear depletion in the low molecular weight (LMW) aromatic hydrocarbons (C_{14-} range) with increasing depth in the reservoir. The absolute concentrations of these compounds are listed in Appendix 2. This section examines possible processes that might have led to these compositional gradient profiles.

5.2.1 Petroleum Charging and Compartmentalization

England et al. (1987) argued that most of the compositional heterogeneities witnessed in oil reservoirs are caused by insufficient vertical mixing of the trapped petroleums with the evolving oil charges during filling, rather than necessarily caused by alteration processes. Stainforth (2004) stated that single reservoirs are normally charged with petroleum downward from the top, as later petroleums are more mature, more gas charged, and thus less dense. Therefore, one possibility for the observed compositional gradient in the LMW aromatic compounds across the SFNY reservoir is that the oils at the top of the reservoir have mixed with a different petroleum charge, or a later, relatively more mature charge from the same source rock. However, according to Stainforth (2004), the gradients caused by later charges are evident mainly in the overall physical properties (API gravity, Gas-Oil Ratios GOR, bubble point etc) and gross compositions, rather than in a definite class of compounds. The studied samples exhibit fairly uniform trends in the physical and bulk chemical compositions throughout the reservoir, while gradients only appear in the low molecular weight (LMW) aromatic hydrocarbon compounds. Also, if a more mature charge had enriched the oils at the top of the reservoir in the LMW aromatic hydrocarbon compounds, it is expected that these oils would also be enriched in the saturated hydrocarbon compounds with comparable molecular weight, however this is not the case. Furthermore, it is apparent that the oils in the SFNY reservoir are generally well-mixed throughout the reservoir as reflected by the uniform source and maturity parameters. This homogenization is also supported by the absence of obvious vertical fluid flow barriers that retard inter compartmental fluid communication (gamma ray log chapter three, section 3.2.4), and by the high porosity and permeability of the reservoir.

Thus, the gradient profiles observed in the LMW aromatic hydrocarbon families of the SFNY oils are likely not a result of filling history and/or compartmentalization.

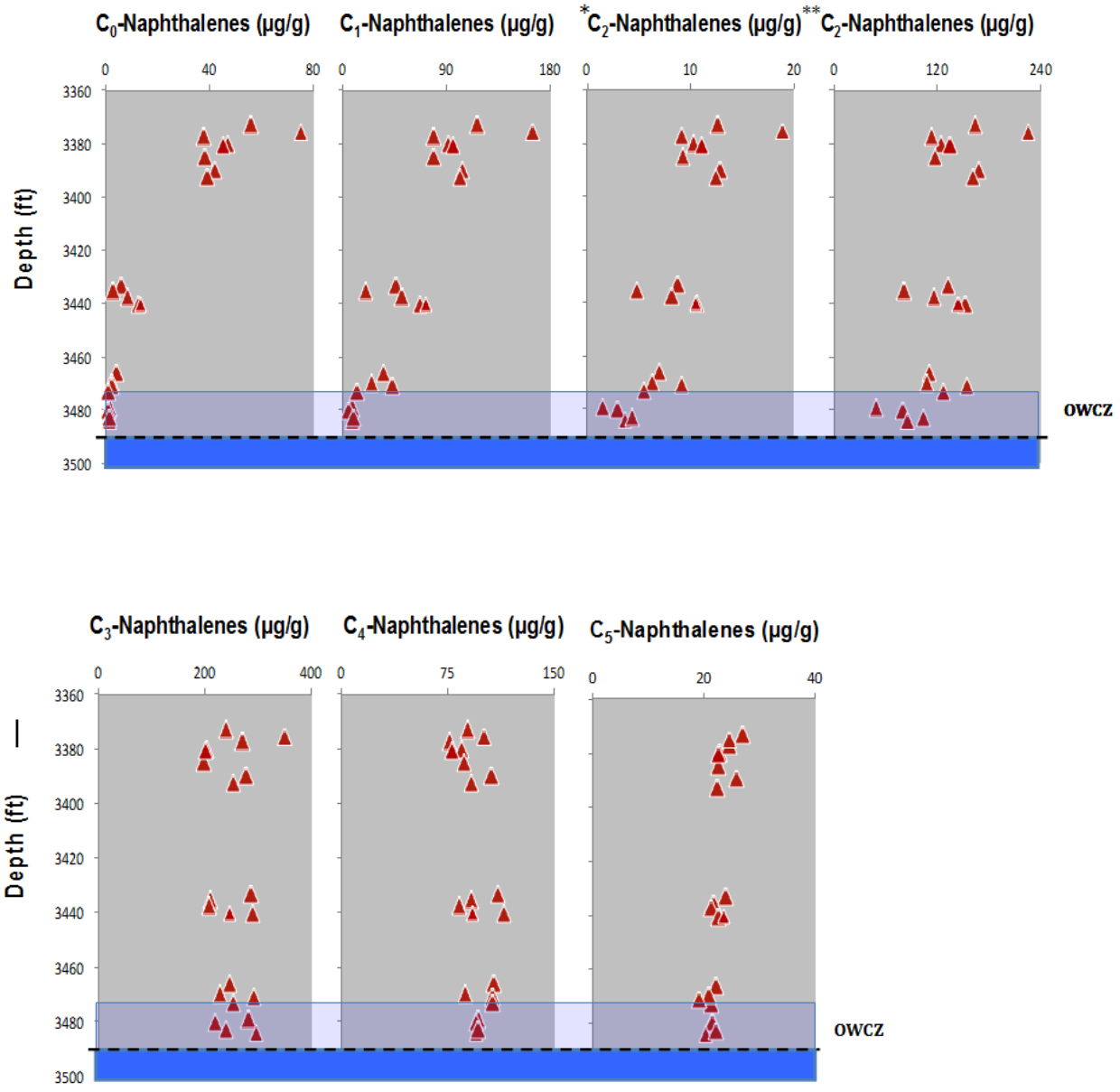

Fig. 5.12 Plots of absolute concentration profiles of naphthalene and alkylated naphthalenes for the studied samples from the SFNY reservoir. C_0, C_1, C_2, C_3, C_4, C_5 prefixes denote the number of alkyl carbons attached to the aromatic ring. * C_2: Methylnaphthalenes, ** C_2: Ethylnaphthalenes. The oil–water contact zone (OWCZ) is defined from the resistivity log.

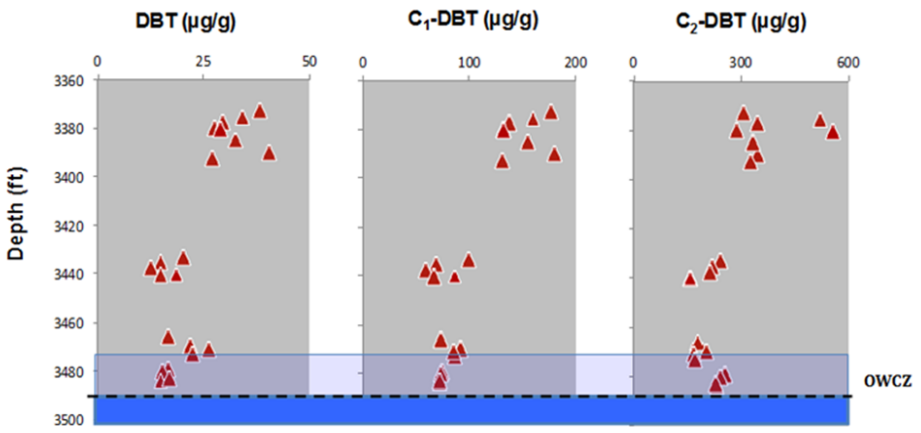

Fig. 5.13 Plots of absolute concentration profiles of dibenzothiophene and alkylated dibenzothiophenes for the studied samples from the SFNY reservoir. C_1, C_2 prefixes denote the number of alkyl carbons attached to the aromatic ring. The oil–water contact zone (OWCZ) is defined from the resistivity log.

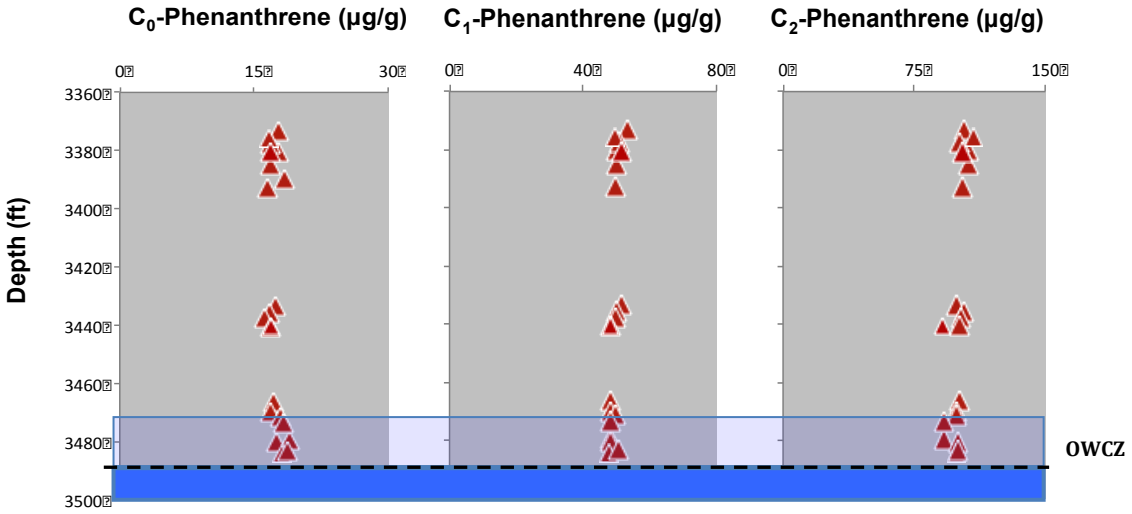

Fig. 5.14 Plots of absolute concentration profiles of phenanthrene and alkylated phenanthrenes for the studied samples from the SFNY reservoir. C_0, C_1, C_2 prefixes denote the number of alkyl carbons attached to the aromatic ring. The oil–water contact zone (OWCZ) is defined from the resistivity log.

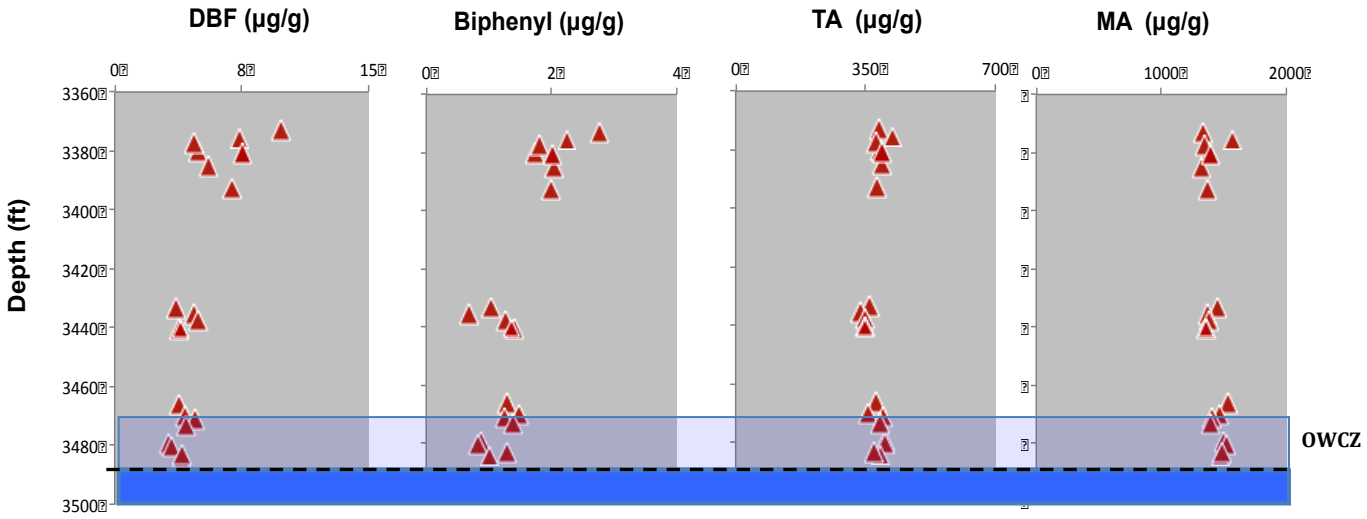

Fig. 5.15 Plots of absolute concentration profiles of dibenzofuran (DBF), biphenyl (BP), triaromatic steroids (TA) and monoaromatic steroids (MA) for the studied samples from the SFNY reservoir. The oil–water contact zone (OWCZ) is defined from the resistivity log.

5.2.2 Biodegradation

Biodegradation is one of the common processes that may generate compositional gradients in a single continuous reservoir (Larter et al., 2003) or compartmentalized reservoirs (Fustic et al., 2011). Usually the normal alkanes are the most rapidly removed by microorganisms. Therefore, the partial or complete depletion of the n-alkanes (*n*-paraffins) relative to branched and cyclic ones in addition to other features such as high density, sulfur, NSO and asphaltene content is known as the most important indicator of oil biodegradation. The order of decreasing degradation rate of compound classes often follows this sequence: n-alkanes > alkylcyclohexanes > alkylbenzenes > isoprenoid alkanes > monoaromatic hydrocarbons > polycyclic aromatic hydrocarbons and sulfur-aromatic compounds > bicyclic sesquiterpanes > steranes > hopanes > diasteranes > pregnanes (Connan, 1984; Peters & Moldowan 1993).

Figure 5.16 represent a typical gas chromatogram of the whole rock extracted oils and a partial mass chromatogram (m/z 97) of the saturated hydrocarbon fraction displaying the alkylcyclohexanes distribution of the studied oils from the SFNY reservoir. Both the gas chromatogram and partial mass chromatogram (m/z 97) show that the samples have lost some of

their n-alkanes and alkylcyclohexanes in the light range (> *n*-C_{15}), respectively. This loss could result from slight biodegradation (PM 1, level 1 on Peters & Moldowan scale of biodegradation). However, it should be noted that the studied reservoir was cored in April, 2008 and hence the loss of the lighter range of *n*-alkanes and alkylcyclohexanes might not be caused by biodegradation but rather by evaporation due to long-term sample storage and/or sample handling.

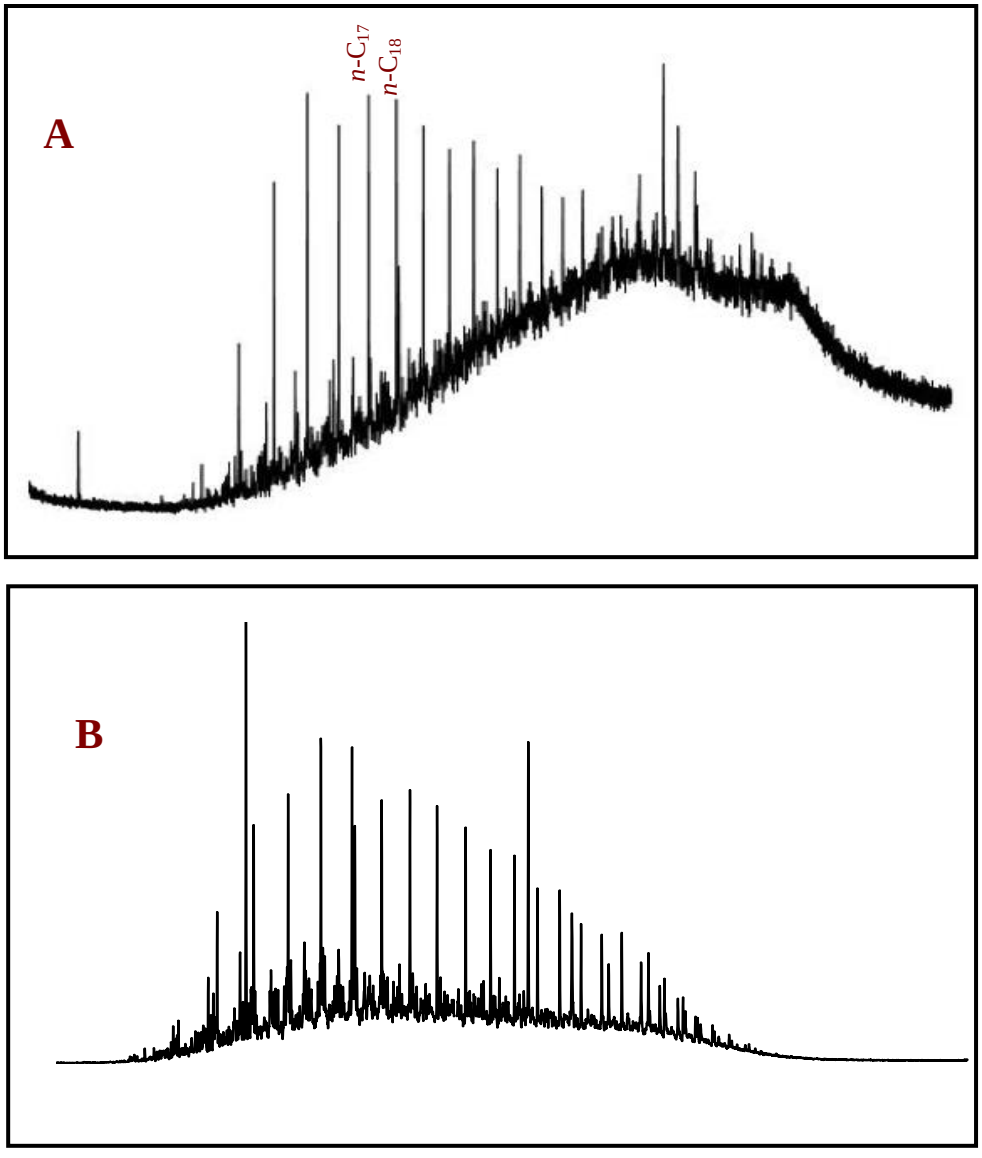

Figure 5.16 Gas chromatogram of the whole rock extract from the SFNY reservoir (A) and partial mass chromatogram (*m/z* 97) of the saturated hydrocarbon fraction showing the distribution of alkylcyclohexanes for the studied samples from the SFNY reservoir (B).

Also, the gas chromatograms of the whole rock extracted oils are characterized by a large unresolved complex mixture (UCM) or hump which is usually regarded to either low thermal maturity or severe biodegradation. In this case study, the hump is deemed to be due to the low maturity of the oils as there is no evidence for severe biodegradation. Figure 5.17 suggests that there is no alteration in the *n*-alkanes, isoprenoids and the more resistant saturated hydrocarbons of the studied samples as reflected by the constant absolute concentrations of these compounds through the oil column.

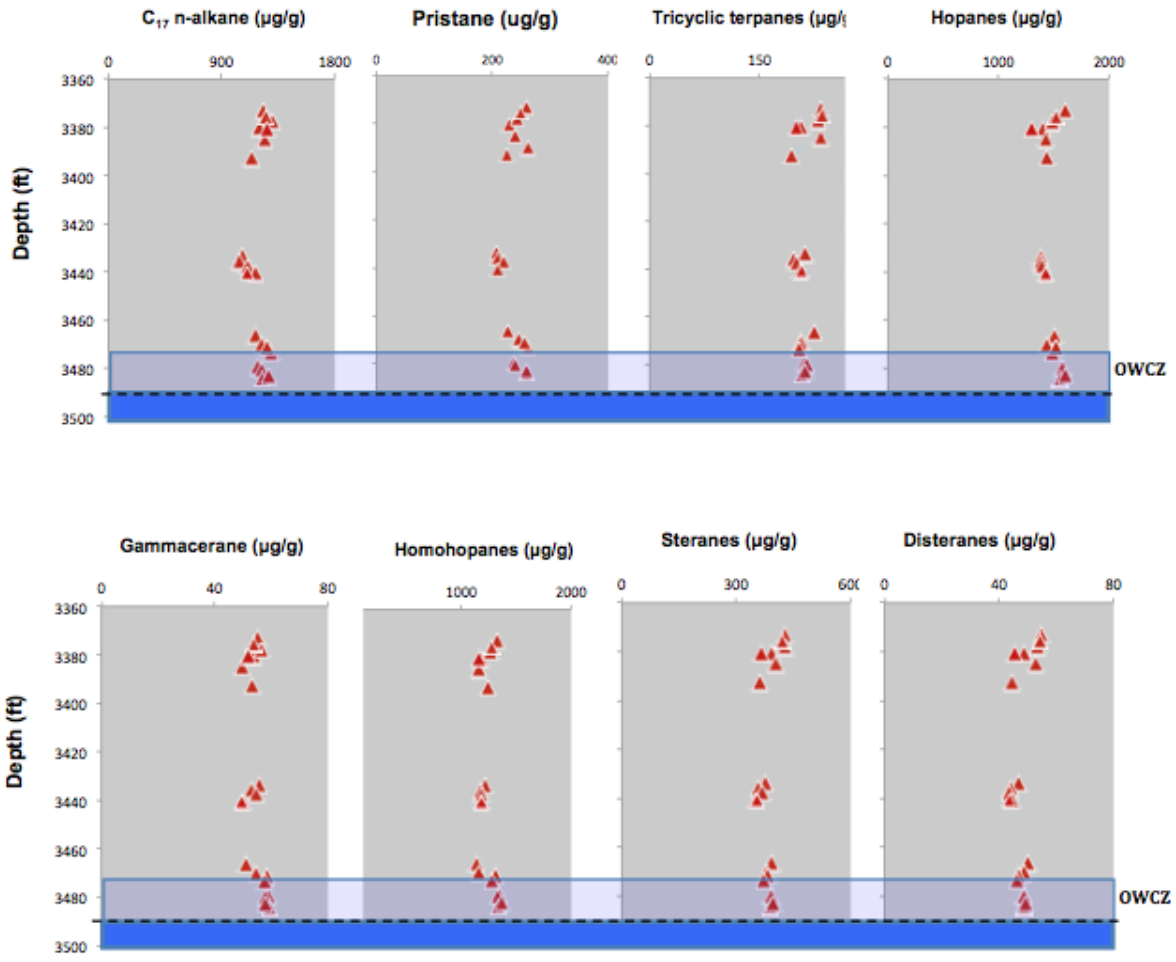

Fig. 5.17 Plots of absolute concentration profiles of the saturated hydrocarbons for the oil samples from SFNY reservoir. The oil–water contact zone (OWCZ) is defined from the resistivity log.

The assumption of no or minimal biodegradation levels for the studied samples (PM 1) is also supported by the absence of 25-norhopanes in the oils (Fig. 5.18), which are demethylated hopane compounds generated only at severe stages of biodegradation in some reservoirs. For example, Bennett et al. (2006) reported the presence of 25-norhopanes in a severely biodegraded Athabasca bitumen column. However, in contrast, no 25-norhopanes were detected by Brooks et al. (1988) in some severely biodegraded Albertan oil sands where regular steranes had been totally destroyed by biodegradation.

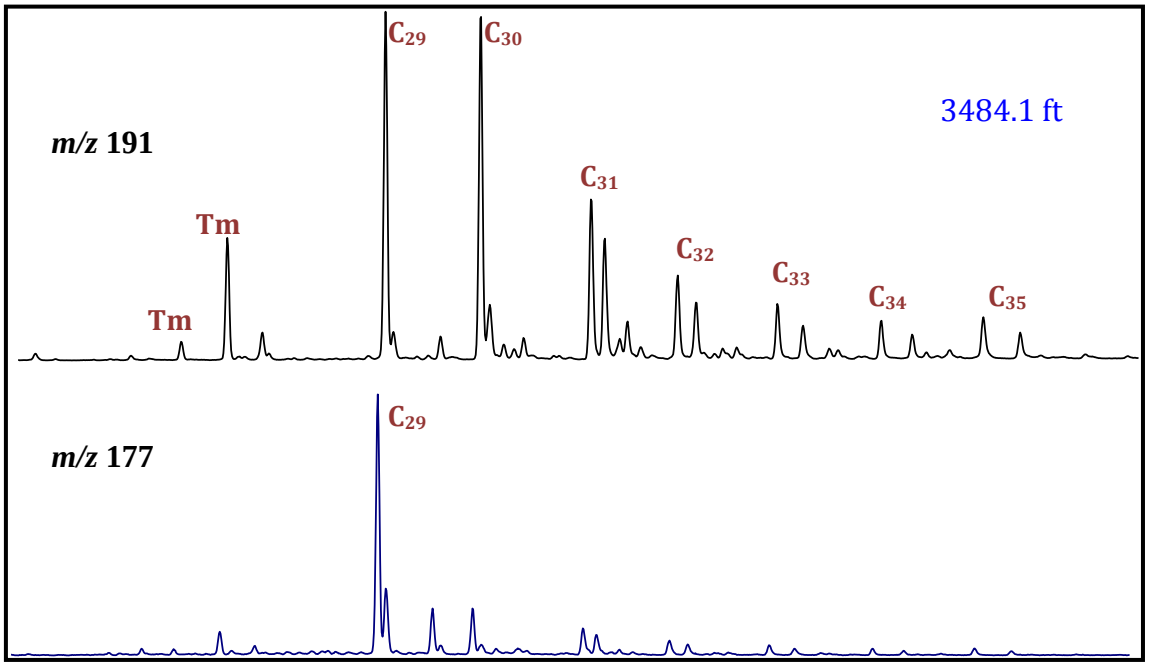

Fig. 5.18 Partial mass chromatograms (*m/z* 191) and (*m/z* 177) of a sample representing the bottom of SFNY reservoir, showing no alteration to the hopane family and no generation of the 25-nor hopanes (demethylated hopanes).

The mono and polycyclic aromatic hydrocarbons are also known to be affected by microbial attack (Connan, 1984; Volkman et al., 1984; Blanc and Connan, 1994; Fisher et al., 1996). Figure 5.19 illustrates the distribution of the mono aromatic long chain alkylbenzenes (LCABs) (*m/z* 91) of three of the studied extracts representing the top (3373.1 ft), middle (3440.5 ft), and bottom (3484.1 ft) of the SFNY reservoir. Figure 5.19 shows that all three samples have some lower molecular weight LCABs (C_8-C_{11}), but that they are severely depleted in the heavier homologues (C_{15+}), when compared to the normal alkylbenzene patterns in a slightly or non-

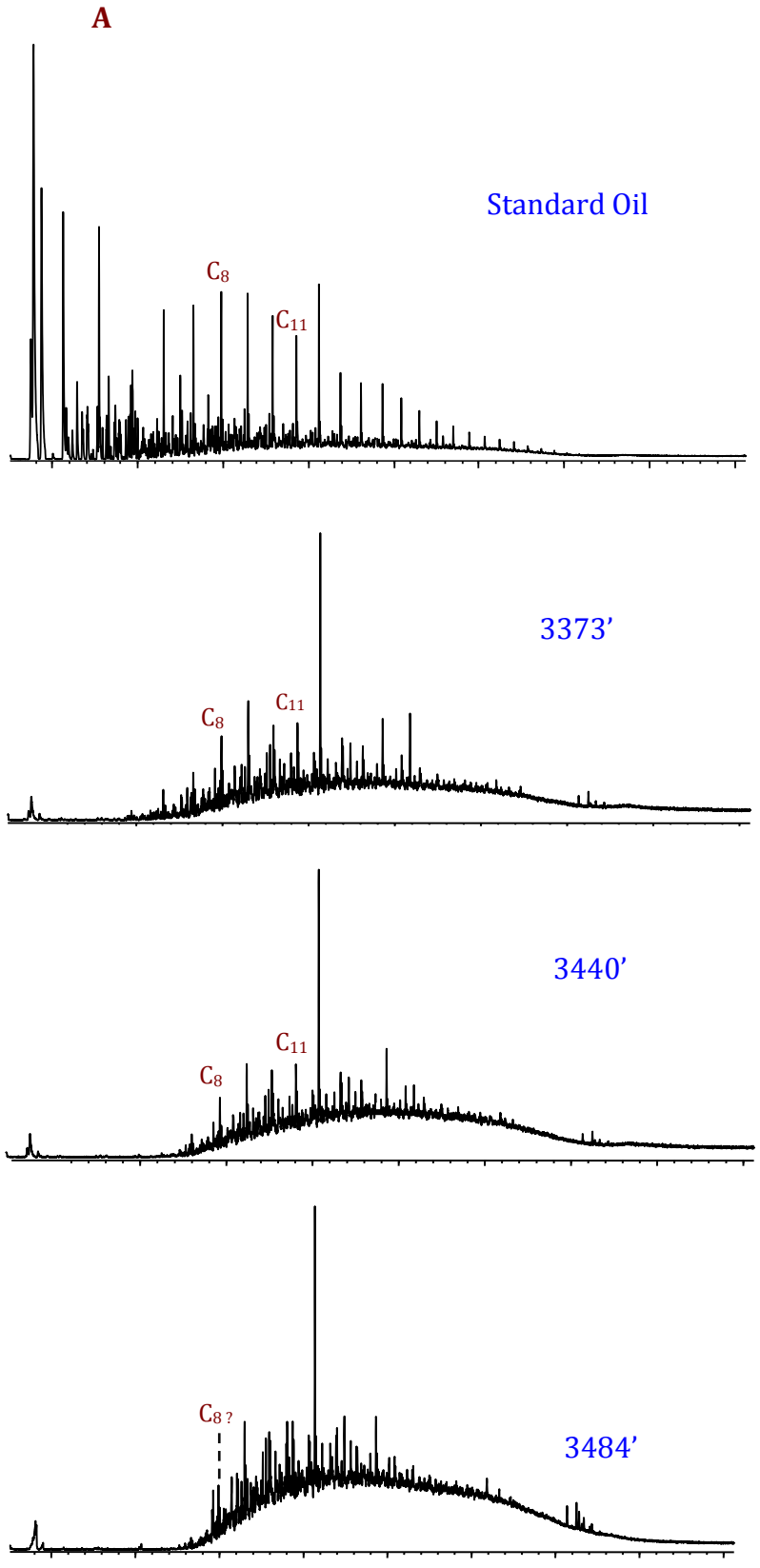

Fig. 5.19 Partial mass chromatograms (*m/z* 91) of the aromatic hydrocarbon fraction showing the alkylbenzenes distribution of the studied samples from the SFNY reservoir (top, middle and bottom) and of a standard oil for comparison (A).

altered standard oil (as shown in figure 5.19 for comparison purposes). The degree of alteration in these compounds slightly increases with increasing reservoir depth, with the most altered sample being at the bottom (3484 ft) and showing a higher hump (UCM), as compared to the other two samples at the top and middle of the reservoir. Although, the low molecular alkylbenzens compounds are sensitive to microbial attack, the severe depletion of these compounds typically occurs close to the point of total destruction of the *n*-alkanes, equivalent to PM 2 on Peters & Moldowan scale of biodegradation (Connan, 1984; Peters et al., 2005). Huang et al. (2004) reported that C_{3+} alkylbenzenes are the first compounds to be depleted before the total removal of *n*-alkanes, but they may persist beyond the total depletion of isoprenoids in the aromatic hydrocarbon fraction, which was not observed in the case study. Hence, the unusual and selective depletion of the higher molecular LCABs, without a similar affect on the comparable molecular weight saturated and aromatic hydrocarbons (C_{15+}), could be explained by incipient biodegradation. Such selective depletion of LCABs while the n- alkanes and isoprenoids are kept intact, were previously reported by Blanc and Connan (1994) in a study on heavy oils from the Pecorade oil field in France. Also, Holba et al. (2004) observed similar effects in a study on the Kuparuk River Field in Alaska, and attributed it to incipient biodegradation.

In classical in-reservoir biodegradation (methanogenic degradation pathway), the depletion in alkylated polycyclic aromatic hydrocarbon compounds occurs only after substantial destruction of n-alkanes and isoprenoids, which is equivalent to degradation level PM 2-3 on Peters and Moldowan scale of biodegradation (Figure 5.20). For example, Huang et al. (2004) reported that the significant reduction in the concentration of naphthalenes, phenanthrenes and their alkylated homologues in biodegraded oils from the Liaohe basin happens at a degradation level > PM 3 where most of the n-alkanes and isoprenoids are already altered. Nevertheless, the polycyclic aromatic hydrocarbon compounds might be consumed by microorganisms in parallel to the n-alkanes under anaerobic biodegradation by sulfate reducing degradation pathway, as observed by Jones et al. (2008) in lab microcosms. To verify whether the depletion in the LMW polycyclic aromatic hydrocarbon compounds of the studied samples from the SFNY reservoir was a result of biodegradation under sulfate reducing or other electron acceptor mediated biodegradation system, a plot representing the ratio of the microbial reactive to more resistant saturated and aromatic hydrocarbons [Pr/n-C17 vs (4-methyl/3-methyl) biphenyl] is used (Fig 5.21). No pronounced

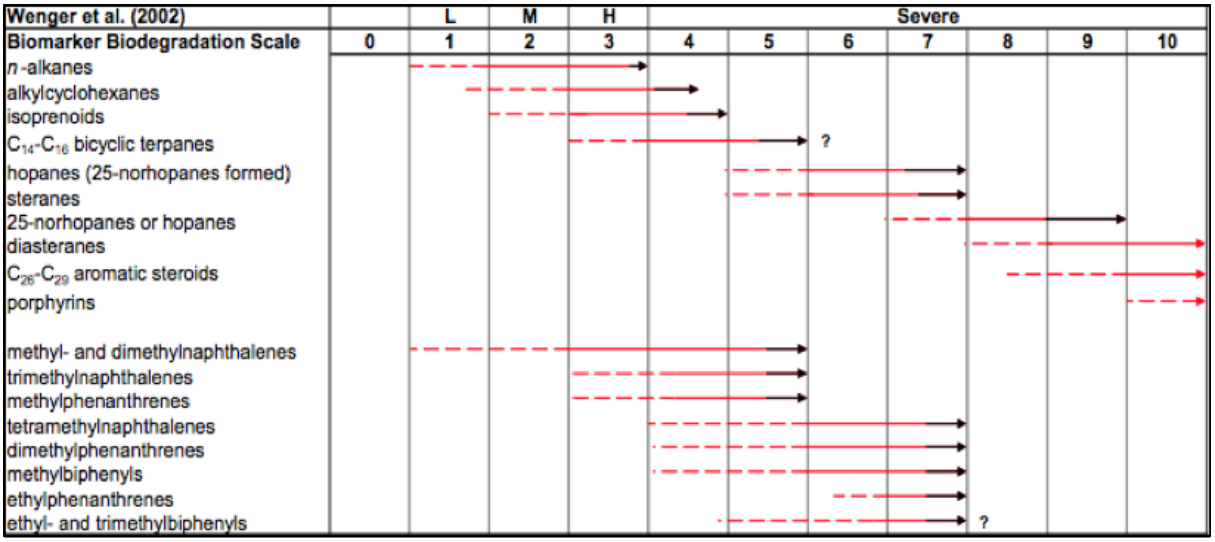

Fig. 5.20 The extent of biodegradation of mature crude oil can be ranked on a scale of 1-10 based on differing resistance of compound classes to microbial attack (from Peters and Moldowan, 1993). Arrows indicate where compound classes are first altered (dashed lines), substantially depleted (solid red), and completely eliminated (black). Sequence of alteration of alkylated polycyclic aromatic hydrocarbons is based on work by Fisher et al. (1996; 1998) Degree of biodegradation from Wenger et al. (2002) reflects changes in oil quality (L, lightly biodegraded; M, moderately biodegraded; H, heavily biodegraded).

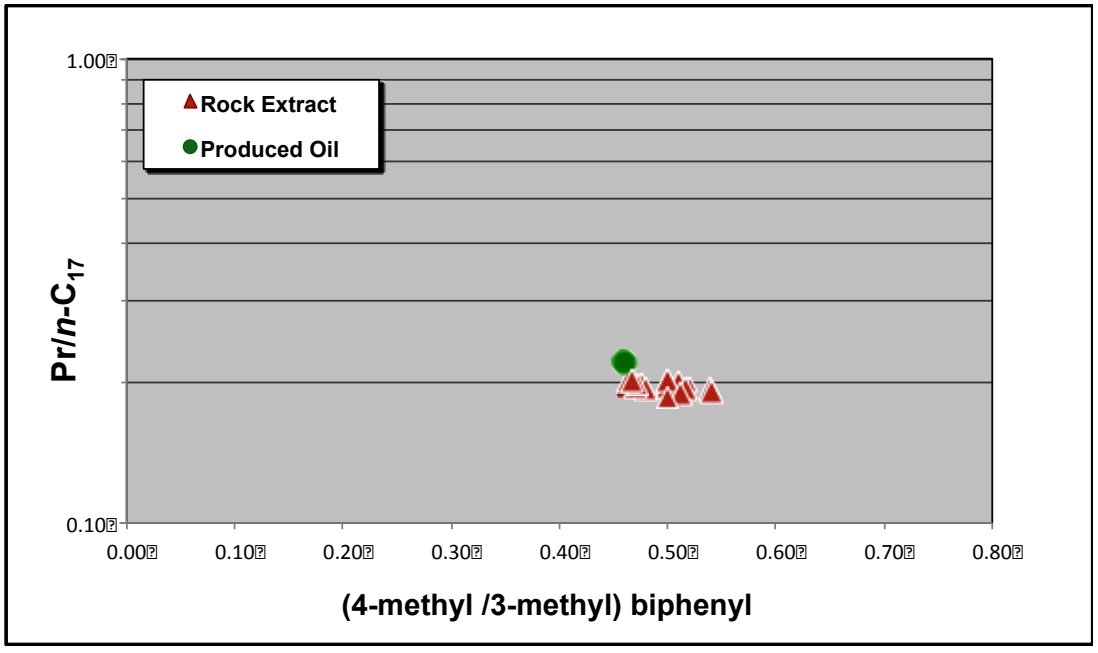

Fig. 5.21 Pristane/*n*-C_{17} versus 4-methyl biphenyl/3-methyl biphenyl for rock extracts and oil from the SFNY reservoir used to infer the degradation pathways under anaerobic conditions (after Jones et al., 2008).

variations were present in these two ratios for all of the samples, suggesting that biodegradation under sulfate reducing conditions as a process responsible for the compositional heterogeneity in the LMW poly cyclic aromatic hydrocarbons of the studied samples seems unlikely. This finding is further supported by the absence of isomeric discrimination in the loss profiles of the LMW alkylnapthalenes, as will be shown in the water washing section (Fig. 5.22).

There is no general agreement on the effect of biodegradation on $\delta^{13}C$ composition of whole oils and whether the $\delta^{13}C$ composition can be used to assess the level of biodegradation. During oil biodegradation, microorganisms preferentially remove the low molecular weight compounds (beginning with *n*-alkanes and moving to the more complex branched, cyclic and naphthenic compounds). Thus, It is expected that the residual oil will be enriched in ^{13}C because microorganisms can more easily break down the ^{12}C-^{12}C bonds as compared to ^{12}C-^{13}C. However, recent study by Marcano (2011) on biodegraded heavy oils from the Alberta Basin (LIoyedminster, Cold Lake, Pease River, Athabasca and Buffalo Head Hills) concluded that, regardless of the severe degrees of biodegradation, such microbial activities do not seem to critically impact the $\delta^{13}C$ composition of whole oils. Also, another study conducted on heavy biodegraded oils from the Laiohe basin (PM 4-8) and Albera basin (PM 3-5) by Algeer (unpublished, 2011) tested whether or not microbial degradation has an influence on the carbon isotopic composition of whole oils. This study similarly showed that the slight enrichment in the heavy isotopes of the studied oils with progressive biodegradation may indicate that this process has a negligible influence on the carbon isotopic composition of the whole oils. Additionally, this thesis study showed that the samples from the SFNY reservoir reflect no variation in their carbon isotopic composition, which indicates the very limited utility of $\delta^{13}C$ composition of the whole oil in verifying the slight degree of biodegradation for this sample set.

Moreover, It was claimed that the increase in the sulfur content in oils is either caused by selective degradation of non-sulfur-containing compounds by microorganisms or the by the incorporation of sulfide to the kerogen shifts the $\delta^{34}S$ to more negative values (Manowitz et al., 1990). However, Marcano (2011) reported that there is a positive correlation between the $\delta^{34}S$ of whole oils and the sulfur content of biodegraded oils with different levels of biodegradation from

the Alberta Basin. She pointed out that the enrichment in the $\delta^{34}S$ of the whole oils is controlled mainly by the source (Type IIS) and level of maturity rather than by biodegradation, as $\delta^{34}S$ of the whole oils did not appear to follow the biodegradation patterns. The $\delta^{34}S$ values of the investigated samples from the SFNY field are listed in Table 5.8. The variations in the $\delta^{34}S$ of the whole oils show no correlation with the sulfur content of the samples and appear to be insignificant (considering the instrument error ± 0.3), thus, insufficient to determine if biodegradation affects the samples' compositions.

Table 5.8 Sulfur Isotopic Compositions of the Whole Extracted Oil of the studied samples from the SFNY reservoir.

Sample #	Sample Type	Depth (ft)	%S	$\delta^{34}S$
2	Rock Extract	3375.5	7.3	-10.8
5	Rock Extract	3382.2	7.4	-11.3
8	Rock Extract	3392.8	6.8	-11.3
9	Rock Extract	3433.4	7.9	-11.6
12	Rock Extract	3440.5	7.5	-11.4
13	Rock Extract	3466.2	8.1	-11.6
18	Rock Extract	3480.2	7.9	-11.5
19	Rock Extract	3482.9	8.3	-11.1
20	Rock Extract	3484.1	8.1	-11.6
21	Produced Oil	CHT (3370-3470')	6.2	-11.5

Although the SFNY reservoir is shallow and the conditions might be suitable for biodegradation to occur, the samples show minimal or no biodegradation. The bottom hole temperature of the SFNY reservoir is 55°C and the water salinity is around 24 g/l. The preservation of the SFNY oils from severe degradation by microbes could be due to a paleo-pasteurization of the reservoir by the deep burial occurred in the Miocene and heating to temperatures as high as 76°C prior to uplift as indicated by the burial history chart of the SFNY reservoir (Figure 3.9, section 3.2.3). The upper temperature limit where microorganisms can survive and degrade hydrocarbons has been reported to be 80°C (Wilhelms et al., 2001a; Larter et al., 2003).

5.2.3 Water washing

The solubility of aromatic hydrocarbons in water is much greater than the saturated hydrocarbons of comparable molecular weight (Kuo, 1994). Several studies reported that water washing effects may result in compositional heterogeneities in petroleum accumulations (Cubitt et al., 1995; Palmer, 1984; Ahsan et al., 1998) Therefore, water washing might potentially be responsible for the observed gradients in the LMW aromatic hydrocarbons of the studied samples from the SFNY reservoir. The most useful parameters in determining whether water washing has occurred are based on the BTEX compounds (benzene, toluene, ethylbenzene and xylene), present in the gasoline range, because of their high solubility in water relative to other hydrocarbon components (Palmer, 1984). No trace of these compounds was detected in the investigated oil and extracts from the SFNY reservoir. The loss of these highly volatile compounds could be due to evaporation during sample extraction procedure or water washing. Lafargue and Barker (1988) thought that the loss of BTEX is commonly associated with water washed oils.

Based on several studies and experiments conducted to assess the effect of water washing on petroleum compositions, the sulfur aromatic compounds (specially dibenzothiophenes) were found to be preferentially removed first by water washing followed by removal of aromatic hydrocarbons. The steranes and terpanes were found to be the least altered by water washing (Palmer, 1984; Lafargue & Barker, 1988). These studies also demonstrated that the effect of water washing decreases with the increasing number of aromatic rings and alkyl substituents. Therefore, it is expected that the low molecular weight monoaromatic ring alkylbenzenes are more susceptible to water washing than the polycyclic aromatic hydrocarbons. However, as shown earlier in the biodegradation section (Fig. 5.19), the alteration in the alkylbenzene homologues is not limited to the low molecular weight alkylbenzenes and hence the effect of incipient biodegradation on alkylbenzenes masks the effect of water washing on these compounds.

It is difficult to distinguish between the effect of water washing and biodegradation as these two possesses occur concurrently in shallow cool reservoirs. However, the proposed diagnostic parameters in the literature to differentiate between the effect of biodegradation on petroleums from those caused by water washing come in favor for the possibility of water washing influencing the LMW polycyclic aromatic hydrocarbons in this study. For example, Eganhouse

and Calder (1976) reported that removal of the ethylnaphthalenes (EN) before dimethylnaphthalenes (DMN) is attributed to water washing, whereas the opposite would indicate biodegradation. The studied samples show a decrease in the EN/DMN with increasing depth (Figure 5.22). Also, Fisher et al. (1998) found in biodegraded oils that bacteria selectively destroy the 1,6-dimethylnaphthalene over the 1,5-dimethylnaphthalene. The DMN homologues (2,6-, 2,7-, 1,3-,1,7-,1,6-, 1,4-, 2,3-, 1,5- and 1,2-) of the studied samples show similar depletion patterns towards the oil-water contact with no selective destruction of any of these homologues on the expense of the others.

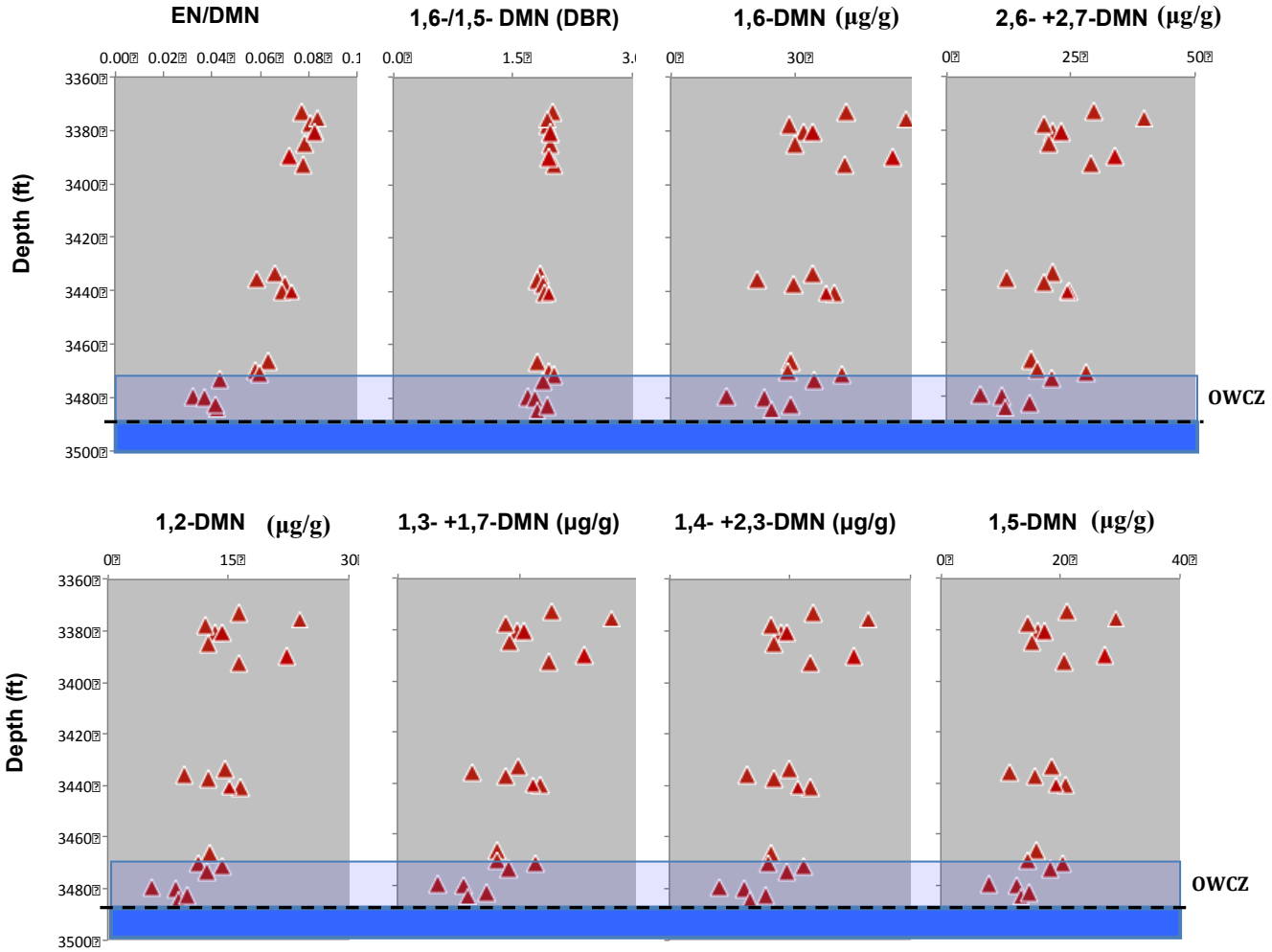

Figure 5.22 Plots of absolute concentration profiles of the dimethylnaphthalene homologues (1,6-, 2,6-+2,7-, 1,2-,1,3-+1,7-, 1,4-+2,3- and 1,5-) for the oil samples from SFNY reservoir. EN/DMN: ethylnaphthalenes/dimethylnaphthalenes; DBR: 1,6-/1,5-dimethylnaphthalenes. The oil–water contact zone (OWCZ) is defined from the resistivity log.

Moreover, Huang et al. (2004) observed an unusual rapid depletion of trimethylnaphthalenes (TMN) over DMN with increasing level of biodegradation in biodegraded oils from the Lengdong field, China. No increase in DMN/TMN witnessed with increasing depth for the studied samples ruling out the effect of biodegradation on the polycyclic aromatic hydrocarbons. It seems unlikely that given the preserved n-alkane profiles and no isomeric variations in the aromatic hydrocarbons that classical biodegradation is causing the gradients in aromatic hydrocarbons. Additionally, Palmer (1984) related the loss in the dibenzothiophene DBT ($C_{12}H_8S$) relative to phenanthrene ($C_{14}H_{10}$) and the methydibenzothiophene MDBT ($C_{13}H_{10}S$) relative to the methylphenanthrene MP ($C_{15}H_{12}$) in a study of Philippine oils to water washing. The studied samples from the SFNY reservoir show decrease in these parameters suggesting that water washing might be a better explanation but I note that most of the geochemical literature is not quantitative but is qualitative in nature and may not be that useful!.

To further investigate the effect of water washing on the LMW polycyclic aromatic compounds of the studied samples and to detect any variation within these compunds across the reservoir, the absolute concentrations of the different polycyclic aromatic hydrocarbon families of the studied samples are plotted vs depth as shown in figures 5.12 to 5.15. The molecular weight, initial and final absolute concentrations, and the degree of solubility (loss percentage) of each class of these compounds are listed in Table 5.9. Figure 5.12 and table 5.9 show that the C_0-C_2 naphthalenes are the lowest in the molecular weight (molecular weight = 128-156 g/mole) and are the most effected compound species among the polycyclic aromatic hydrocarbons. The investigated samples have lost 78-98 % of these compounds with increasing reservoir depth. This decrease in the absolute concentrations of the C_0-C_2 naphthalenes becomes less sharp with increasing molecular weight of the naphthalene group (C_3-C_5 naphthalenes, molecular weight = 170-198 g/mole). The loss in the C_3-C_5 naphthalenes ranges between 30-43%. This is in agreement with the literature that impact of water washing decreases with increasing molecular weight. The biphenyl has a comparable molecular weight (molecular weight = 154 g/mole) to the C_2-naphthalenes (molecular weight = 156 g/mole) and thus is showing almost a similar depletion percentage (71%) in the sample set with increasing depth (Figure 5.15 & Table 5.9).

Furthermore, Price (1976) reported that the heteroatomic feature of some of the aromatic compounds, e.g., dibenzothiophenes (DBT) and dibenzofuran (DBF), could be the reason for

these compounds to be as twice soluble in water as the other aromatic compounds of a similar molecular weight. In this study, the results support this finding as the studied samples have lost 70% of their dibenzothiophene compounds (molecular weight = 184 g/mole) with depth compared to 33% loss in the C_4-napthalenes with a similar molecular weight (molecular weight = 184 g/mole) (Figure 5.13 and Table 5.9). However, the C_0-C_2 dibenzothiophenes in the studied samples show similar degree of depletion regardless to their molecular weight. The depletion of the dibenzofuran analogues the dibezothiophenes as both have the same molecular weight and are heteroatomic compounds (contain atoms other than carbon and hydrogen) (Figure 5.15 & Table 5.9). The C_0-C_2 phenanthrene and, the relatively high molecular weight monoaromatic steroid and triaromatic steroid hydrocarbons appear to be the least affected by water washing (Figure 5.14 & 5.15).

The depletion patterns in the LMW polycyclic aromatic hydrocarbons in this study follow the observations of studies and simulation experiments that researched the effect of waterwashing on petroleum components (Palmer 1984,1993; Kuo, 1994; Lafargue & Barker, 1988) to a certain extent, and thus water washing could possibly explain these gradients. However, generally, the actual solubility of organic hydrocarbon compounds in water is low (Table 5.9), and thus does not fully support the proposed sequence of removal of the aromatic hydrocarbons. For example, the studies (Palmer 1984,1993; Kuo, 1994; Lafargue & Barker, 1988) showed that the DBTs were the first compounds to be removed by water before the other aromatic hydrocarbon compounds, whereas the solubility of the DBT in water (0.21 mg/l) is much lower than the solubility of the other aromatic hydrocarbon compounds (Table 5.9). This contradiction between the water washing patterns reported in the previous studies and the solubility data of the aromatic hydrocarbons (Table 5.9) is also observed in the partition coefficient values of the aromatic hydrocarbon compounds. The partition coefficient is the equilibrium ratio of the concentrations of a solute in a mixture of two immiscible or slightly miscible phases (Sangster, 1997). Since there are no actual oil-water partition coefficient measurements done for the aromatic compounds, the octanol-water partition coefficient (Kow) of these compounds reported in the literature were employed in this study. The octanol-water partition coefficient measures how hydrophobic (water-hating) or hydrophilic (water-loving) a substance is. Compounds with low log Kow exhibit a high tendency to distribute in the water phase whereas high Kow values indicate the preference of a compound to stay in the hydrophobic phase (octanol).

Table 5.9 illustrates the log Kow values of some of the polycyclic aromatic hydrocarbons Montgomery, (2010). The log Kow value of the DBT (4.12) does not reflect that it has the highest tendency to partition in the water phase over the other compounds and hence disagree with the notion that it is the most soluble aromatic hydrocarbon compound. Moreover, while the DBT and DBF compounds have a similar molecular weight (184 g/mole), and show a similar loss percentage in the studied samples, the reported log Kow value of these two compounds does not exhibit that they partition in water in a similar degree (Table 5.9). In contrast, the C_0-naphthalene has the lowest log Kow (3.29) confirming its relatively high solubility in water while the low solubility of C_0-C_2 phenanthrenes in water is confirmed by the relatively high log Kow values (4.57&5.08)(Table 5.9). Although the available log Kow data values show consistency to a certain degree with the molecular weight and loss percentage of some of the aromatic hydrocarbons in the studied samples, the actual solubility of these compounds in water is generally still low and their tendency to stay in the oil phase is high. Therefore, a large volume of water is needed to cause the loss observed in the LMW aromatic hydrocarbon profiles in the studied oils. To get a sense on what volumes of water must interact with the oil to cause these changes, rough estimates based on a simple model proposed by Larter and Aplin (1995) were made using the following equation:

$$\mathbf{C_0 = C_i\,((PV_0)/(PV_0 + 1))^{Vw}}$$

Where P: partition coefficient; Vw: volume of water (m^3); Vo: volume of oil (m^3); C_i: initial compound concentration in petroleum (μg/g); Final Conc C_0: final compound concentration in petroleum (μg/g). The results show that the volumes of water (Vw) needed to result in the loss profiles observed in all of the the LMW polycyclic aromatic hydrocarbons in the studied samples are enormous (Table 5.9). For example, to reduce the itnitial concentration of naphthalene from 75 μg/g to 1 μg/g in the studied oils, around 8511.4 m^3 of water is required. A greater volume is needed to reduce the concentration of DBT from 41μg/g to 13μg/g (27542.3 m^3). Therefore, direct evidence solidifying the interpretation of water washing influencing the LMW polycyclic aromatics in the SFNY petroleum remains elusive as water washing is more effective in shallow petroleum reservoirs that are dynamically flushed with large volumes of fresh meteoric waters. These conditions are met typically in foreland basins. The studied area is part

Table 5.9 The Physical Properties of Different Polycyclic Aromatic Hydrocarbon Families of the Studied Samples from the SFNY Reservoir.

Compound Name	Compound Abbreviation	Molecular Weight (g/mole)	Soluibility in Water (mg/l)	Intial Conc. C_1 (µg/g)	Final Conc C_o (µg/g)	Loss Percentage %	log Kow	Log Vw (m^3)
Naphthalene	C0-N	128	31.40	75	1	98	3.29	3.93
Methylnaphthalene	C1-N	142	25.40	165	6	96	-	-
Ethylnaphthalene	C2-N	156	-	19	2	92	-	-
Dimethylnaphthalene	C2-N	156	8.85	226	50	78	-	-
Trimethylnaphthalene	C3-N	170	-	350	200	43	-	-
Tetramethylnaphthalene	C4-N	184	-	115	77	33	-	-
Pentamethylnaphthalene	C5-N	198	-	27	19	30	-	-
Dibenzofuran	DBF	184	2.86	10	3	68	4.12	4.20
Biphenyl	BP	154	7.50	3	1	71	-	-
Dibenzothiophene	C0-DBT	184	0.21	41	13	69	4.38	4.44
Methyldibenzothiophene	C1-DBT	198	-	181	60	67	-	-
Dimethyldibenzothiophene	C2-DBT	212	-	557	159	71	-	-
Phenanthrene	C0-P	178	0.99	18	16	12	4.57	3.64
Methylphenanthrene	C1-P	192	0.26	53	48	11	5.08	4.08
Dimethylphenanthrene	C2-P	206	-	108	91	16	-	-
Triaromatic Steroids	TA	231	-	421	356	16	-	-
Monoaromatic Steroids	MA	253	-	1566	1391	11	-	-

Solubility data of aromatic compounds (mg/l) determined at 25°C (after May et al., 1978); **Initial Conc C_1**: initial compound concentration in petroleum (µg/g); **Final Conc C_0**: final compound concentration in petroleum (µg/g); **Loss Percentage%= [(**initial compound concentration/ final compound concentration)/ initial compound concentration]*100; **Log Kow**: log octanol-water coefficient, log Kow values were determined at 25°C (after Montgomery, 2010); **log Vw**: volume of water (m^3) calculated from $\mathbf{C_0 = C_i ((PV_o)/(PV_o + 1))^{Vw}}$ **(Larter & Aplin, 1995)** .

of the Arabian intrashelf basin and hence it is difficult to believe that the effect of the SFNY static waters solely could account for the observed gradient profiles across the reservoir.

As the investigated "classical" gradient-inducing processes fully or partially failed to explain the LMW polycyclic aromatic heterogeneities in the SFNY oils, other processes were also believed to have no or minimal influence on the overall composition of the SFNY oils. These processes include: Thermal Cracking Alteration (TCA), Thermochemical Sulfate Reduction (TSR), Gas deasphalting and Gravitational Segregation**.**

The burial history chart of the SFNY reservoir (Chapter 3, section 3.2.3) shows that the maximum paleo-temperature the reservoir was subjected to is 76°C, not high enough to activate neither Thermal Cracking Alteration (TCA) nor Thermochemical Sulfate Reduction (TSR). Moreover, the lithology of SFNY member does not support TSR occurring as it consists mainly of sandstone with some shale and local marly limestone interbeds. No anhydrite or gypsum is available close to the SFNY reservoir to initiate this reaction. Thus, TCA and TSR processes can be ruled out as possible formation mechanisms for the studied heavy oils.

Furthermore, the physical properties and bulk chemical composition data of the SFNY heavy oils (Table 5.1) show that these oils are fairly similar across the reservoir. No manifest increase in the asphaltene content was observed with depth or at the oil-water contact and hence no or minimal effect of gravitational segregation on the studied oils' composition. According to Wilhelms and Larter (1994), the gas influx results in asphaltene precipitation only if the host reservoir contains oil unsaturated with regard to gas. Therefore, examination of gas oil ratio of the SFNY heavy oils is needed before gas deasphalting can be eliminated as an asphaltene precipitation mechanism eventually forming SFNY heavy oils.

5.2.4 Conclusions

The investigated samples from the SFNY reservoir exhibit selective depletion in the high molecular weight alkylbenzenes, this might be an indication of early "incipient" biodegradation. The depletion patterns in the LMW aromatic hydrocarbons in the studied SFNY petroleum follow the observations and conclusions made from studies and experiments on the effect of waterwashing on petroleum to some extent. The depletion patterns along with the absence of isomeric discrimination in the loss profiles of these compounds might suggest water washing as the most likely process resulting in the dramatic gradients displayed in some of the C_{15-} aromatic hydrocarbon fractions (C_0-C_2 naphthalenes, BP, DBF and C_0-C_2 DBT) of the studied SFNY petroleum towards the oil water contact zone (OWCZ). However, the presence of a continuous meteoric water drive is required for effective water washing on petroleum components, usually met in foreland basins. The studied area is part of the Arabian intrashelf basin and thus the SFNY static waters solely cannot fully account for the observed gradient profiles across the reservoir.

Chapter Six: OVERALL CONCLUSIONS AND FUTURE WORK

Heavy oil and natural bitumen accumulations can originate through several mechanisms and processes. They could be either original non-degraded oils generated from kerogen degradation under low thermal stresses or degraded remnants of conventional oils by post-generative alteration processes (e.g., biodegradation, water washing, gas deasphalting). Nevertheless, most of the world's heavy oil and natural bitumen deposits were generated by biodegradation.

The main focus of this study was to gain insight into the origin of heavy oil occurrences in the Middle East and particularly, Saudi Arabia. For this purpose, 21 heavy oil samples (rock extract and produced oil) from the Mid Cretaceous Safaniya sandstone reservoir from well-X in Saudi Arabia were investigated using bulk, molecular and isotopic analysis.

The investigated petroleum set generally shows similar physical and bulk properties, and a similar isotopic signature throughout the reservoir, indicating a common biogenic origin and a comparable level of thermal maturity. Furthermore, these petroleums have close affinity with the biomarker signature of a carbonate Type II-S source that contains mainly algal organic matter as reflected by the high dibenzothiophene/phenanthrene ratios (>1), high C_{35} homohopane, low pristane/phytane (<1) and low diasteranes (0.13). Collectively, these geochemical parameters signify a marine origin for the SFNY oils, and a highly reducing depositional environment of the source rock.

The maturity biomarker parameters (eg., the low TA/(MA+TA), Ts/(Tm+Ts) and C_{29} Ts/(C_{29} Ts+C_{29} H)) of the rock extracts and produced oil from the SFNY reservoir decipher the origin of these heavy oils almost entirely as early generated products from sulfur rich source rock (7.8% S). The high heteroatomic content (mainly sulfur) of kerogen led to the early expulsion of these oils once the source rock was exposed to low thermal stresses (%Rc < 0.5). However, this study in agreement with previous studies (e.g., Wilhelms & Larter) emphasizes the importance of involving different maturity tracers that were generated at different stages of thermal maturity, as all petroleum accumulations represent a mixture of oils with different levels of maturity. The biological biomarkers, in combination with the aromatic hydrocarbon parameters (phenanthrenes and alkylphenanthrenes) of the samples, imply a thermally homogenized mature oil mixture

throughout the SFNY reservoir with vitrinite reflectance of up to 0.84 % Rc.

While no sign of pronounced changes were observed in the C_{15+} saturated and aromatic hydrocarbon fractions of the sample set (except for the alkylbenzenes), the C_{15-} saturated and aromatic hydrocarbon fractions were altered. The loss of the C_{15-} saturated hydrocarbons could be related to evaporation due to long-term sample storage and/or sample handling. The data further suggests that the SFNY petroleum probably has experienced incipient biodegradation as mirrored in the unusual selective depletion in the long chain alkylbenzenes (C_{15+}), while similar molecular weight n-alkanes and other paraffins remain intact. However, the deep burial of the SFNY shallow reservoir in the Miocene and heating to temperatures up to 76°C prior to uplift was probably the reason that ceased the microbial activities and preserved the SFNY oils from being severely degraded.

The variations in the $\delta^{34}S$ and the $\delta^{13}C$ of the SFNY whole oils fall within the instrument error range, and hence indicate the very limited utility of both the $\delta^{13}C$ & $\delta^{34}S$ composition of the whole oils in verifying the slight degree of biodegradation on this sample set.

Several "classical" gradient-inducing processes were investigated to determine which among these processes caused the dramatic gradients observed in some of the C_{15-} polycyclic aromatic hydrocarbon fractions (C_0-C_2 naphthalenes, BP, DBF, C_0-C_2 DBT) of the studied samples towards the oil water contact zone (OWCZ). These processes included: petroleum charging and compartmentalization, biodegradation and water washing. The results of this study revealed that petroleum charging and compartmentalization is likely not responsible for the gradient profiles observed in the LMW polycyclic aromatic hydrocarbon families of the SFNY oils as the samples show similarity in all source and maturity parameters indicating a homogenized oil column. Similarly, biodegradation was ruled out as a possible process responsible for these vertical gradients as there was no evidence for a sulfate reducing biodegradation that usually alters the LMW polycyclic aromatic hydrocarbons prior to the substantial destruction of n-alkanes and isoprenoids.

The depletion patterns in the LMW aromatic hydrocarbons in the studied SFNY petroleum follow the observations and conclusions made from studies and experiments which researched the effect of waterwashing on petroleum to some extent. These depletion patterns, along with the absence

of isomeric discrimination in the loss profiles of the LMW polycyclic aromatic hydrocarbons, suggest that these gradients might be associated with water washing. However, the volume of water calculations based on partition coefficients show that large volumes of water are required to justify the concentration reduction of these compounds in the studied samples. For example, to reduce the DBT concentration in the studied oils from 41μg/g to 13μg/g, a minimum of 27542.3 m^3 of equilibrated water is needed, which cannot be met in an intrashelf basin where no active meteoric water drive is present.

The unrealistic volumes of water lead to the conclusion that the main process resulting in the compositional heterogeneities observed in the LMW polycyclic aromatic hydrocarbons across the SFNY reservoir remains a mystery. Therefore, a detailed study on the hydrology of the Arabian Basin involving a hydrogen and oxygen isotope analysis of water samples, and oil/water partition coefficient actual measurements of the aromatic hydrocarbon compounds under subsurface conditions, is required to better understand the interactions between static water and the different compound classes of petroleum and hence to draw a firm conclusion on whether water washing was the main cause for the compositional gradients observed in the LMW aromatic hydrocarbons of the studied oils from the SFNY reservoir.

REFERENCES

Abu-Ali, M. A., Rudkiewicz, J. L. L., McGillivray, J. G., and Behar, F. (1999). Paleozoic petroleum system of central Saudi Arabia. GeoArabia, v. 4, p. 321–336.

Adams, J. (2008). The impact of Geological and Microbiological Processes on Oil Composition and Fluid Property Variations in Heavy Oil and Bitumen Reservoirs, Ph.D. thesis, Geosciences. University of Calgary, Calgary, p. 737.

Ahsan, S.A., Karlsen, D.A., Mitchell, A.W., and Rothwell, N. (1998). Inter and intrafield hydrocarbon compositional variations in the Ula and the Gyda fields (Central Graben-North Sea)-implication for understanding the controls on hydrocarbon distribution within and between these fields. Organic geochemistry, 29(1), 429-448.

Aitken, C.M., Jones, D.M., and Larter, S.R. (2004). Anaerobic hydrocarbon biodegradation in deep subsurface oil reservoirs. Nature 431, 291-294.

Akkurt, R., Seifert, D., Al-Harbi, A., Al-Beaiji, T. M., Kruspe, T., Thern, H., and Kroken, A. (2009). Real-time detection of tar in carbonates using LWD triple combo, NMR and formation tester in highly-deviated wells. Petrophysics, 50(2).

Ala, M.A. (1982). Chronology of trap formation and migration of hydrocarbons in Zagros sector of southwest Iran. AAPG Bulletin, 66(10), 1535-1541.

AlGeer, R.A. (2011). Stable Carbon Isotope Analysis of Biodegraded Oils from Alberta and The Liaohe Sedimentary Basins.(unpublished manuscript, University of Calgary,Calgary).

Allan, J., and Creaney, S. (1991). Oil families of the Western Canada Basin. Bulletin of Canadian Petroleum Geology 39, 107-122.

Alsharhan, A.S., and Kendall, C.G.St.C. (1986). Precambrian to Jurassic rocks of the Arabian Gulf and adjacent areas: their facies, depositional setting and hydrocarbon habitat. American Association of Petroleum Geologists Bulletin, U.S.A., v. 70, pp. 977-1002.

Alsharhan, A.S., and Nairn, A. E. M. (1997). Sedimentary basins and petroleum geology of the Middle East. Elsevier Science B.V., Amsterdam, 843 p 521-639.

AlUmran, M.I., AlDossari, K. A., and NasrElDin, H.A., (2005). Successful Treatments to Enhance the Performance of Horizontal Wells Drilled Near Tarmat Areas. International Petroleum Technology Conference held in Qatar,10188-MS.

Andrusevich, V.E., Engel, M.H., and Zumberge, J.E. (2000). Effects of paleolatitude on the stable carbon isotope composition of crude oils. Geology, 28(9), 847-850.

Ayres, M.G., Bilal, M., Jones, R. W., Slentz, L. W., Tartir, M., and Wilson, A. O., (1982). Hydrocarbon habitat in main producing areas, Saudi Arabia. AAPG Bull., v. 66, p. 1-9.

Azim, S., Al-Anzi, S., Hassan, Y., James, S., Mandal, D., and Al-Ajmi, H., (2006). Identification, Origin and Distribution of Tarmats in Upper Zubair Sand Reservoir, Raudhatain Field, North Kuwait. In Abu Dhabi International Petroleum Exhibition and Conference.

Bastow, T. P., Van Aarssen, B. G., and Lang, D. (2007). Rapid Small-Scale Separation of Saturate, Aromatic and Polar Components in Petroleum. Organic Geochemistry, Vol. 38, pp. 1235-1250.

Beach, F., Peakman, T.M., Abbott, G.D., Sleeman, R., and Maxwell, J.R. (1989). Laboratory thermal alteration of triaromatic steroid hydrocarbons. Organic geochemistry, 14(1), 109-111.

Bennett, B., and Larter, S.R. (2000). Quantitative separation of aliphatic and aromatic hydrocarbons using silver ion-silica Solid-Phase Extraction. Anal. Chem., 72: 1039–1044.

Bennett, B., Chen, M., Brincat, D., Gelin, F.J.P., and Larter, S.R. (2002). Fractionation of benzocarbazoles between source rocks and petroleums. *Organic Geochemistry*, 33(5), 545-559.

Bennett, B., Fustic, M., Farrimond, P., Huang, H., and Larter, S.R. (2006). 25-Norhopanes: Formation during biodegradation of petroleum in the subsurface. Organic Geochemistry 37, 787-797

Beydoun, Z.R. (1991). Arabian Plate hydrocarbon geology and potential: A plate tectonic approach. AAPG, 77 p.

Bilal, A. (2013). Time-seismicity evolution and seismic risk assessment of the Arabian Plate. Natural Science, Vol.5, No.9, 1019-1024.

Blanc, P., and Connan, J., (1994). Preservation, degradation and destruction of trapped oil. In: Magoon, L. B. & Dow, W. G. (eds) The Petroleum System from source to trap, AAPG Memoir 60, 237-246.

Bray, E.E., and Evans, E.D. (1961). Distribution of< i> n</i>-paraffins as a clue to recognition of source beds. Geochimica et Cosmochimica Acta, 22(1), 2-15.

Brooks, P.W., Fowler, M.G., and Macqueen, R.W. (1988). Biological marker and conventional organic geochemistry of oil sands/heavy oils, Western Canada Basin. Organic Geochemistry 12, 519-538.

Cagatay, M.N., Saner, S., Al-Saiyed, I., and Carrigan, W.J. (1995). Diagenesis of the Safaniya Sandstone Member (mid-Cretaceous) in Saudi Arabia, Sedimentary Geology 105, 221-239

Cantrell, D.L., Nicholson, P.G, Hughes, G.W., Miller, M.A., Bhullar, A.G., AbdelBagi, S.T., and Norton, A.K. (2013 in press). Tethyan Petroleum Systems of Saudi Arabia. In: Petroleum systems of the Tethyan region, AAPG Special Publication.

Carpentier, B., Huc, A.-Y., Marquis, F., (1998). Distribution and origin of a tar mat in the S. Field (Abu Dhabi, U.A.E.). SPE Paper, vol. 49472.

Carrigan, W.J., Cole, G.A., Colling, E.L., and Jones, P.J. (1995). Geochemistry of the Upper Jurassic Tuwaiq Mountain and Hanifa Formation Petroleum Source Rocks of Eastern Saudi Arabia. In Petroleum Source Rocks (pp. 67-87). Springer Berlin Heidelberg

Cassani, F., and Eglinton, G. (1991). Organic geochemistry of Venezuelan extra-heavy crude oils 2. Molecular assessment of biodegradation. Chemical geology, 91(4), 315-333.

Chung, H.M., Rooney, M.A., Toon, M.B., and Claypool, G.E. (1992). Carbon isotope composition of marine crude oils. AAPG Bulletin 76, 1000-1007

Connan, J. (1984). Biodegradation of crude oils in reservoirs. In: Brooks, J., Welte, D.H. (Eds.), Advances in Petroluem Geochemistry; Volume 1. Academic Press, London, pp. 299-335.

Connan, J., and Cassou, A.M. (1980) Properties gases and petroleum liquids derived from terrestrial kerogen at various maturation levels. Geochimica et Cosmochimica Acta , 44, 1-23.

Connan, J., Restle, A., and Albrecht, P. (1980). Biodegradation of crude oils in the Aquitaine basin. In: Advances in Organic Geochemistry 1979 (Ed. by A.G. Douglas and J.R. Maxwell), pp. 1-17. Pergamon, Oxford.

Cubitt, J. M., & England, W. A. (Eds.). (1995). The geochemistry of reservoirs. Geological Society.

Dahl, J.E., Moldowan, J.M., Peters, K.E., Claypool, G.E., Rooney, M.A., Michael, G.E., Mello, M.R., and Kohnen, M.L. (1999). Diamondoid hydrocarbons as indicators of natural oil cracking: Nature, v. 399, p. 54-57.

Demaison, G.J. (1977). Tar sands and supergiant oil fields. American Association of Petroleum Geologists Bulletin, v. 61, no. 11, p. 1950-1961.

Didyk, B., Simoneit, B.R.T., Brassell, S.C., and Eglinton, G. (1978). Organic geochemical indicators of palaeoenvironmental conditions of sedimentation. Nature, 272, 216– 222.

Eganhouse, R.P., and Calder, J.A. (1976). The solubility of medium molecular weight aromatic hydrocarbons and the effects of hydrocarbon co-solutes and salinity. Geochimica et Cosmochimica Acta, 40(5), 555-561.

England, W.A., Mackenzie, A.S., Mann, D.M., and Quigley, T. M. (1987). The movement and entrapment of petroleum fluids in the subsurface. Journal of the Geological Society,

144(2), 327-347.

Evans, C.R., Rogers, M.A., and Bailey, N.J.L. (1971). Evolution and alteration of petroleum in Western Canada. Chemical Geology 8(3), 147-170.

Fisher, S.J., Alexander, R., Kagi, R.I. (1996). Biodegradation of alkylnaphthalenes in sediments adjacent to an off-shore petroleum production platform. Polycyclic Aromatic Compounds 11, 35-42.

Fisher, S.J., Alexander, R., Kagi, R.I., and Oliver, G.A. (1998). Aromatic hydrocarbons as indicators of petroleum biodegradation in North Western Australian reservoirs. In: Purcell, P.G., Purcell, R.R. (Eds.), The Sedimentary Basins of Western Australia. 2. Proceedings of Petroleum Exploration Society Symposium 1998, Perth, pp. 185–194.

Fuex, A.N. (1977). The use of stable carbon isotopes in hydrocarbon exploration. Journal of Geochemical Exploration, 7, 155-188.

Fustic, M. (2011). Geological controls on reservoir and bitumen heterogeneities in Athabasca oil sands deposit, Ph.D. thesis, Geosciences. University of Calgary, Calgary, p. 381.

George, S.C., Boreham, C.J., Minifie, S.A., and Teerman, S.C. (2002). The effect of minor to moderate biodegradation on C5 to C9 hydrocarbons in crude oils. Organic Geochemistry 33, 1293-1317.

Goldstein, T.P., and Aizenshtat Z. (1994). Thermochemical sulfate reduction, a review. Journal of Thermal Analysis 42, 241-290.

Goossens, H., De Leeuw, J.W., Schenck, P.A., and Brassell, S.C. (1984). Tocopherols as likely precursors of pristane in ancient sediments and crude oils. Nature, 312, 440– 442.

Grassineau, N.V., Mattey, D.P., and Lowry, D. (2001). Sulfur Isotope Analysis of Sulfide and Sulfate Minerals by Continuous Flow-Isotope Ratio Mass Spectrometry. Anal. Chem., v. 73, p. 220-225

Halpern, H. I., Jones, P. J., Al-Qathami, S. M., and Al-Malki, K. R., (2004). Applications of pyrolysis to optimize oil field development in Saudi Arabia; Part 1, Prior to drilling phase. Annual Meeting Expanded Abstracts - American Association Of Petroleum Geologists, 1357.

Haskett, C.E., and Tartera, M. (1965). A practical solution to the problem of asphaltene deposits -- Hassi Messaoud Field, Algeria. JPT 17, 387-391.

Head, I.M., Jones, D.M., and Larter, S.R. (2003). Biological activity in the deep subsurface and the origin of heavy oil. Nature 426, 344-352.

Heider, J., Spormann, A.M., Beller, H.R., and Widdel, F. (1998). Anaerobic bacterial metabolism of hydrocarbons. FEMS Microbiology Reviews 22, 459-473.

Hempton, M.R. (1987). Constraints on Arabian plate motion and extensional history of the Red Sea. Tectonics, 6(6), 687-705

Hodgson, G.W., and Barker, B.L. (1959). Geochemical aspects of petroleum migration in Pembina, Red Water, Joffre and Lloyd-Minster oil fields of Alberta Saskatchewan, Canada. Amer. Assoc. Petr. Geol. Bull. 43, 311-328.

Holba, A.G., Wright, L., Levinson, R., Huizinga, B., and Scheihing, M. (2004). Effects and impact of early-stage anaerobic biodegradation on Kuparuk River Field, Alaska. In: Cubitt, J.M., England, W.A., Larter, S. (Eds.), Understanding Petroleum Reservoirs: Toward an Integrated Reservoir Engineering
and Geochemical Approach, vol. 237. Geological Society, Special Publications, London, pp. 53–88

Horsfield, B., Schenk, H.J., Mills, N., and Welte, D.H. (1992). An investigation of the in-reservoir conversion of oil to gas: compositional and kinetic findings from closed-system programmed-temperature pyrolysis. Organic Geochemistry 19, 191–204.

Huang, H., and Pearson, M.J. (1999). Source rock palaeoenvironments and controls on the distribution of dibenzothiophenes in lacustrine crude oils, Bohai Bay Basin, Eastern China. In: Organic Geochemistry vol. 30 pp. 1455-1470.

Huang, H., Bowler, B.F., Oldenburg, T.B., and Larter, S.R. (2004). The effect of biodegradation on polycyclic aromatic hydrocarbons in reservoired oils from the Liaohe basin, NE China. Organic geochemistry, 35(11), 1619-1634.

Huang, H., Jin, G., Lin, C., and Zheng, Y. (2003). Origin of an unusual heavy oil from the Baiyinchagan depression, Erlian basin, northern China. Marine and petroleum geology, 20(1),1-12.

Huang, W.Y., and Meinschein, W.G. (1979). Sterols as ecological indicators. Geochimica et Cosmochimica Acta , 43, 739-745.

Huc, A. Y., Nederlof, P., Debarre, R., Carpentier, B., Boussafir, M., Laggoun-Defarge, F., Lenail-Chouteau, A., and Floch, N. B. L., (2000). Pyrobitumen occurrences and formation in a Cambro-Ordovician sandstone reservoir, Fahud Salt Basin, North Oman: Chemical Geology, v. 168, p.99-112.

Hughes, W.B., Holba, A.G., and Dzou, L.I. (1995). The ratios of dibenzothiophene to phenanthrene and pristane to phytane as indicators of depositional environment and lithology of petroleum source rocks. Geochimica et Cosmochimica Acta, 59(17), 3581-3598.

Hunt J. (1979). Petroleum Geochemistry and Geology. Freeman, San Francisco.

Hunter, R. J. (1989) Foundations of Colloid Science, Vol. 1, Oxford Science, New York, 673pp.

Instrumental techniques used in the ISL. 13/12C and 15/14N of organics by CF-EA-IRMS.

Retrieved October 15, 2013, from http://www.ucalgary.ca/uofcisl/techniques.

Instrumental techniques used in the ISL. 34/32S $BaSO_4$ or sulfide minerals by CF-EA-IRMS. Retrieved October 15, 2013, from: http://www.ucalgary.ca/uofcisl/techniques.

John Morris Scientific. Analytical Methods for Oxygen Bombs. Retrieved October 16, 2013, from http://www.johnmorris.com.au/files/files/PDFs/Parr%20Instruments/207m.pdf

Jones, D.M., Head, I.M., Gray, N.D., Adams, J.J., Rowan, A.K., Aitken, C.M., Bennett, B., Huang, H., Brown, A., Bowler, B.F.J., Oldenburg, T., Erdmann, M., and Larter, S.R. (2008). Crude-oil biodegradation via methanogenesis in subsurface petroleum reservoirs. Nature 451, 176-180

Jones, P.J., Al-Shafei, E.N., Halpern, H.I., Al-Dubaisi, J.M., Ballay, R.E., and Funk, J. J. (2004). U.S. Patent No. 6,823,298. Washington, DC: U.S. Patent and Trademark Office.

Jones, P.J., and Stump, T. (1999). Depositional and tectonic setting of the Lower Silurian hydrocarbon source rock facies, Central Saudi Arabia. AAPG. Bull., v. 83, p. 314-332.

Karlsen, D., and Larter, S.R. (1991). Analysis of petroleum fractions by TLC-FID: applications to petroleum reservoir description. Organic Geochemistry 17, 603-617.

Kaufman, R.L., Kabir, C.S., Abdul-Rahman, B., Quttainah, R., Dashti, H., and Pederson, M.S., (1998). Characterizing the Greater Burgan Field using geochemical and other field data. SPE 49216 Annual Technical Conference and Exhibition. New Orleans, Louisiana.

Kennicutt, I.I., and Mahlon, C. (1988). The effect of biodegradation on crude oil bulk and molecular composition. Oil and Chemical Pollution, 4(2), 89-112.

Killops, S.D., and Killops, V.J. (2005). An Introduction to Organic Geochemistry. 2nd ed. 393 p., Blackwell Publishing.

Koopmans, M. P., Larter, S. R., Zhang, C., Mei, B., Wu, T., and Chen, Y. (2002). Biodegradation and mixing of crude oils in Eocene Es3 reservoirs of the Liaohe basin, northeastern China. AAPG bulletin, 86(10), 1833-1843.

Kuo, L. C. (1994). An experimental study of crude oil alteration in reservoir rocks by water washing. Organic Geochemistry, 21(5), 465-479

Lafargue, E., and Barker, C. (1988). Effect of water washing on crude oil composition, AAPG Bulliten, V 72, pp. 263–276.

Larter, S.R., Adams, J.J., Gates, I.D., Bennett, B., and Huang, H. (2008). The Origin, Prediction and Impact of Oil Viscosity Heterogeneity on the Production Characteristics of Tar Sand and Heavy Oil Reservoirs: Journal of Canadian Petroleum Technology, 47 (1), 52-61.

Larter, S. R., and Aplin, A.C. (1995). Reservoir geochemistry: methods, applications and opportunities. Geological Society, London, Special Publications, 86(1), 5-32.

Larter, S.R., Gates, I., Adams, J., Bennett, B., Huang, H., Koksalan, T., and Fustic, M. (2006a). Reservoir fluid characterization of tar sand and heavy oil reservoirs-impact of fluid heterogeneity on production characteristics. American Association of Petroleum Geologists 2006 Annual Convention – Perfecting the Search – Delivering on Promises, April 9–12. George R. Brown Convention Center,
Houston, Texas, USA.

Larter, S.R., Huang, H., Adams, J.J., Bennett, B., Jokanola, O., Oldenburg, T.B.P., Jones, M., Head, I.M., Riediger, C.L., and Fowler, M.G. (2006b). The controls on the composition of biodegraded oils in the deep subsurface. Part II – geological controls on subsurface biodegradation fluxes and constraints on reservoir-fluid property prediction. American Association of Petroleum Geologists Bulletin 90, 921–938.

Larter, S.R., Huang, H., Adams, J.J. Bennett, B., Snowdon, L.R., (2012). A practical biodegradation scale for use in reservoir geochemical studies of biodegraded oils. Organic Geochemistry 45, 66–76"

Larter S.R., Solli H., Douglas A.G., de Lange F., and de Leeuw J.W. (1979) Occurrence and significance of pristlene in kerogen pryolysates. Nature 279, 405-408.

Larter, S.R., Wilhelins, A., Head, I., Koopmans, M., Aplin, A., Di Primio, R., Zwach, C., Erdmann, M., and Telnaes, N. (2003). The controls on the composition of biodegraded oils in the deep subsurface -part 1: biodegradation rates in petroleum reservoirs. Organic Geochemistry 34, 601-613.

Lewan, M.D. (1998). Sulphur-radical control on petroleum formation rates. Nature 391, 164–166.

Li, M., Larter, S.R., Taylor, P., Jones, D.M., Bowler, B., and Bjorøy, M. (1995). Biomarkers or not biomarkers? A new hypothesis for the origin of pristane involving derivation from methyltrimethyltridecylchromans (MTTCs) formed during diagenesis from chlorophyll and alkylphenols. Organic Geochemistry, 23(2), 159-167.

Machel, H.G. (2001) Bacterial and thermochemical sulfate reduction in diagenetic settings: old and new insights. Sediment. Geol. 140, 143–175.

Mackenzie, A.S. (1984). Application of biological markers in petroleum geochemistry. In: Brooks, J.,Welte, D. (Eds.) Advances in Petroleum Geochemistry, Vol 1. Academic Press, London, pp. 115–214.

Mackenzie, A.S., Brassell, S.C., Eglinton, G., and Maxwell, J.R. (1982). Chemical fossils: the geological fate of steroids. Science, 217:491–504.

Mahmoud, M. D., Vaslet, D., and Al-Husseini, M. I. (1992). The Lower Silurian Qalibah Formation of Saudi Arabia-An important hydrocarbon source rock. AAPG Bull., v. 76, no. 10, p. 1491–1506.

Manowitz, B., Krouse, H.R., Barker, C., and Premuzic, E.T. (1990). Sulfur isotope data-analysis of crude oils from the Bolivar coastal fields (Venezuela), in: Orr, W.L., White, C.M. (Eds.), Geochemistry of Sulfur in Fossil Fuels, pp. 592-612

Marcano, N. (2011). Isotopic and Molecular Studies of Biodegraded Oils and the Development of Chemical Proxies for Monitoring in situ Upgrading of Bitumen. Department of Geoscience (Doctoral dissertation, PhD. Thesis, University of Calgary, Calgary).

May, W.E., Wasik, S.P., and Freeman, D.H. (1978). Determination of the solubility behavior of some polycyclic aromatic hydrocarbons in water. *Analytical Chemistry, 50*(7), 997-1000.

Miles, L.B. (1961). History of the exploration and development of the Khursaniyah field, Saudi Arabia. SPE.

Milner, C.W.D., Rogers, M.A., and Evans, C.R. (1977). Petroleum transformations in reservoirs. J. of Geochemical Exploration, v. 7, p. 101-153.

Moldowan, J.M., Lee, C.Y., Sundararaman, P., Salvatori, R., Alajbeg, A., Gjukic, B., Demaison, G.J., Slougui, N.E., and Watt, D.S. (1992). Source correlation and maturity assessment of select oils and rocks from the Central Adriatic basin (Italy and Yugoslavia). In: Moldowan, J.M., Albrecht, P., Philp, R.P. (Eds.), Biological Markers in Sediments and Petroleum. Prentice Hall, Englewood Cli.s, NJ, pp. 370±401.

Montgomery, J.H. (2010). Groundwater chemicals desk reference. CRC Press.

NASA (2013). The Gateway to Astronaut Photography of Earth. Retrieved November 17, 2013, from http://eol.jsc.nasa.gov/handbooks/arabianpages/arabianintro.htm

Okasha, T.M., Menouar, H.K., and Abu-Khamsin, S.A., (1998). Oil recovery from Tarmat reservoirs using hot water and solvent flooding. Journal of Canadian Petroleum Technology 37 (4), 33–40.

Orr, W.L. (1986). Kerogen/asphaltene/sulfur relationships in sulfur-rich Monterey oils. In Advances in Organic Geochemistry 1985 (Edited by Leythaeuser D. and Rullkftter J.). Org. Geochem. 10, 499-516. Pergamon Press, Oxford.

Ourisson, G., Albrecht, P., and Rohmer, M. (1984). The microbial origin of fossil fuels. Scientific American , 251, 44-51.

Palmer, S.E. (1984). Effect of water washing on C~5 hydrocarbon fraction of crude oils from northwest Palawan, Philippines. AAPG Bull. 68, 137-149.

Palmer, S.E. (1993). Effects of biodegradation and water washing on crude oil composition.Engel MH, Macko SA (eds) Organic Geochemistry Plenum Press, New York. pp 511-533.

Peters, K.E., and Fowler, M. G., (2002). Applications of petroleum geochemistry to exploration and reservoir management; Organic Geochemistry, 33, 5-36

Peters, K.E., and Moldowan, J.M. (1993). The Biomarker Guide, Interpreting molecular fossils in petroleum and ancient sediments, Prentice Hall, 363.

Peters, K.E., Moldowan, J.M., and Sundararaman, P. (1990). Effects of hydrous pyrolysis on biomarker thermal maturity parameters: Monterey phosphatic and siliceous members. Org. Geochem., 15, 249-265.

Peters, K.E., Snedden, J.W., Sulaeman, A., Sarg, J.F., and Enrico, R.J. (2000). New geochemicalsequence stratigraphic model for the Mahakam Delta and Makassar Slope, Kalimantan. AAPG Bulletin 84, 12-44.

Peters, K.E., Walters, C.C., and Moldowan, J.M. (2005). The biomarker guide. 2nd edition, volume 2: biomarkers and isotopes in petroleum exploration and earth history. Cambridge University Press,Cambridge pp 483-699.

Pollastro, R.M. (2003). Total petroleum systems of the Paleozoic and Jurassic, greater Ghawar uplift and adjoining provinces of central Saudi Arabia and northern Arabian- Persian Gulf. U.S. Geological Survey Bulletin 2202-H, 100p.

Powell, T.G., and McKirdy, D.M. (1973). Relationship between ratio of pristane to phytane, crude oil composition and geological environment in Australia. Nature Phys. 5c/., 243:37-39.

Powers, R.W., Ramirez, L.F., Redmond, D. D., and Elberg Jr., E. L. (1966). Geology of the Arabian peninsula, sedimentary geology of Saudi Arabia. U. S. Geological Survey Professional Paper, 560-D, 150 p.

Price, L.C. (1976). Aqueous solubility of petroleum as applied to its origin and primary migration: American Association of Petroleum Geologists Bulletin, v. 60, p. 213-244

Radke, M., and Welte, D.H. (1983). The methylphenanthrene index (MPI): a maturity parameters based on aromatic hydrocarbons. In: Bjoroy, M. (Ed.), Advances in Organic Geochemistry 1981. Wiley, Chichester, pp. 504–512.

Riley, C.M., Rodgers, M.A., and Young, W.A., (1977). Physical-Chemical Characteristics of Tar at Uthmaniyah Area, Ghawar Field, Saudi Arabia -- Explanatory and Predictive Model for Such Occurrences. Report EPR.47ES.77, Exxon Production Research Company, Houston, Texas.

Rogers, M.A., McAlary, J.D., and Bailey, N.J.L. (1974). Significance of reservoir bitumens to thermal-maturation studies, Western Canada Bain: AAPG Bulletin, v. 5, p.1806-1824.

Rubinstein, I., Sieskind, O., and Albrecht, P. (1975). Rearranged sterenes in a shale: Occurrence and simulated formation. In: Journal of the Chemical Society vol. 1 pp. 1833-1836.

Rullkötter, J., Meyers, P.A., Schaefer, R.G., and Dunham, K.W. (1986). Oil generation in the

Michigan Basin: A biological marker carbon and isotope approach. Organic Geochemistry, 10, 359-375.

Rullkötter, J., Mukhopadhyay P.K., Schaefer R.G., and Welte D.H. (1984). Geochemistry and petrography of organic matter in sediments from Deep Sea Drilling Project Sites 545 and 547, Mazagan Escarpment, in: Hinz, K., Winterer, E. L. et al. (eds.), Initial Reports of the Deep Sea Drilling Project: U.S. Government Printing Office, Washington, 79, 775–806.

Sangster, J. (1997). Octanol-water partition coefficients—fundamentals and physical chemistry: New York, Wiley, 170 p.

Saudi Geological Survey (2013). Retrieved November 17, 2013, from http://www.sgs.org.sa/english/geology/pages/arabianshield.aspx

Seifert, W.K., and Moldowan, J.M. (1978). Applications of steranes, terpanes and monoaromatics to the maturation, migration and source of crude oils. Geochimica et Cosmochimica Acta, 42(1), 77-95.

Seifert, W.K., and Moldowan, J.M. (1986). Use of biological markers in petroleum exploration. Methods in geochemistry and geophysics, 24, 261-290.

Seifert, D.J., Qureshi, A., Zeybek, M., Zuo, J.Y., Pomerantz, A.E., and Mullins, O.C., (2012). Mobile Heavy Oil and Tar Mat Characterization Within a Single Oil Column Utilizing Novel Asphaltene Science. SPE Kuwait International Petroleum Conference and Exhibition, Kuwait City, Kuwait, 163291-MS.

Schlumberger (2006). Highlighting Heavy Oil. Oilfield Review. Retrieved August 26, 2012, from http://www.slb.com/~/media/Files/resources/oilfield_review/ors06/sum06/heavy_oil.pdf

Sinninghe Damsté, J.S., Irene, W., Rijpstra, C., de Leeuw, J.W., and Schenck, P.A. (1988). Origin of organic sulphur compounds and sulphur-containing high molecular weight substances in sediments and immature crude oils. Organic Geochemistry 13, p. 593-606.

Sinninghe Damsté, J.S., Kenig, F., Koopmans, M.P., Köster, J., Schouten, S., Hayes, J.M. and de Leeuw, J.W. (1995) Evidence for gammacerane as an indicator of water column stratification. Geochimica et Cosmochimica Acta , 59(9), 1895-1900.

Sinninghe Damsté, J.S., Strous, M., Rijpstra, W.I.C., Hopmans, E.C., Geenevasen, J.A., van Duin, A.C., and Jetten, M.S. (2002). Linearly concatenated cyclobutane lipids form a dense bacterial membrane. Nature, 419(6908), 708-712

Sofer, Z. (1984). Stable carbon isotope compositions of crude oils; application to source depositional environments and petroleum alteration. AAPG Bulletin, 68(1), 31-49.

Stainforth, J.G. (2004). New insights into reservoir filling and mixing processes. Geological Society, London, Special Publications, 237(1), 115-132.

Sun, Y., Chen, Z., Xu, S., and Cai, P. (2005). Stable carbon and hydrogen isotopic fractionation of individual n-alkanes accompanying biodegradation: evidence from a group of progressively biodegraded oils. Organic Geochemistry 36, 225-238.

Tannenbaum E., and Aizenshtat Z. (1985). Formation of immature asphalt from organic-rich carbonate rocks--I. Geochemical correlation. Org. Geochem. 8, 181-192.

Ten Haven, H.L., de Leeuw, J.W., Peakman, T. M., & Maxwell, J. R. (1986). Anomalies in steroid and hopanoid maturity indices. Geochimica et Cosmochimica Acta, 50(5), 853-855.

Ten Haven, H.L., de Leeuw, J.W., Rullkötter, J., and Sinninghe Damste, J.S. (1987). Restricted utility of the pristane/phytane ratio as a paleoenvironmental indicator: Nature, v. 330, p. 641-643.

Tissot, B.P., and Welte, D.H. (1978). Petroleum formation and occurrence. Berlin, Springer-Verlag, 538, P. 409-419.

Tissot, B.P., Pelet, R., and Ungerer, P. (1987). Thermal history of sedimentary basins,maturation indices, andkinetics of oil and gas generation. Am. Assoc. Petrol. Geol. Bull. 71, 1445–1466.

Tobey, M.H., Halpern, H.I., Cole, G.A., Lynn, J.D., Al-Dubaisi, J.M., and Sese, P.C., (1993). Geochemical Study of Tar in the Uthmaniyah Reservoir. SPE Middle East Oil Technical Conference & Exhibition held in Bahrain, 25609, pp. 131-140.

Tomic, J., Behar, F., Vandenbroucke, M., and Tang, Y. (1995). Artificial maturation of Monterey kerogen (TypeII-S) in a closed system and comparison with Type II kerogen: implications on the fate of sulfur. Org.Geochem. 23, 647–660.

U.S. Geological Survey (2003). Heavy Oil and Natural Bitumen-Strategic Petroleum Resources. Retrieved November 15, 2013, from http://pubs.usgs.gov/fs/fs070-03/fs070-03.html

Volkman, J.K., Alexander, R., Kagi, R.I., and Woodhouse, G.W. (1984).Biodegradation of aromatic hydrocarbons in crude oils from the Barrow Sub-basin of Western Australia.In: Schenck, P.A., de Leeuw, J.W. (Eds.), Advances in Organic Geochemistry 1983.Pergamon Press, Oxford, pp.619–632.

Wang, T.-G., He, F., Wang, Ch., Zhang, W., and Wang, J. (2008). Oil filling history of the Ordovician oil reservoir in the major part of the Tahe Oilfield, Tarim Basin, NW China. Organic Geochemistry 39, 1637–1646.

Waples, D.W. (1985). Geochemistry in petroleum exploration. Int. Human Res. Devel. Corp., Boston, 232 pp.

Wenger, L.M., and Isaksen, G.H. (2002). Control of hydrocarbon seepage intensity on level of biodegradation in sea bottom sediments. Organic Geochemistry, 33, 1277-1292.

Wenger, L.M., Davies, C.I., and Isaksen, G.H. (2002). Multiple controls on petroleum biodegradation and impact on oil quality. SPE Reservoir Evaluation and Engineering, 5, 375-383.

Wilhelms, A.S., and Larter, S.R. (1994). Origin of tar mats in petroleum reservoirs. Part II: formation mechanisms for tar mats. Marine and Petroleum Geology, 11 (1994), pp. 442–456.

Wilhelms, A., and Larter, S.R (2004). Shaken but not always stirred. Impact of petroleum charge mixing on reservoir geochemistry. Geological Society, London, Special Publications, 237(1), 27-35.

Wilhelms, A.S., Larter, I. Head, P. Farrimond, C. Zwach, and R. Di Primio, (2001a). Paleopasteurisation and the base of the biosphere - A petroleum geochemical viewpoint, 20th.

Wingert, W.S., and Pomerantz, M. (1986). Structure and significance of some twenty-one and twenty-two carbon petroleum steranes. Geochimica et Cosmochimica Acta 50, 2763–2769.

Zhang, T., Ellis, G.S., Wang, K.S., Walters, C.C., Kelemen, S.R., Gillaizeau, B., and Tang, Y. (2007). Effect of hydrocarbon type on thermochemical sulfate reduction. Organic Geochemistry, 38(6), 897-910

APPENDIX 1: GC-MS IDENTIFICATION OF COMPOUNDS

1.1 Aromatic hydrocarbons

Table A1.1-1: Naphthalene and Alkylnaphthalenes m/z 128, 142, 156, 170, 184 &198

Peak	m/z	Compound ID	Compound Name	Retention Time (min)
1	128	N	Naphthalene	20.274
2	142	2MN	2-methylnaphthalene	24.196
3	142	1MN	1-methylnaphthalene	24.766
4	156	2EN	2-ethylnaphthalene	27.504
5	156	1EN	1-ethylnaphthalene	27.616
6	156	26,27DMN	2,6-+2,7-dimethylnaphthalene	27.85
7	156	13,17DMN	1,3-+1,7-dimethylnaphthalene	28.308
8	156	16DMN	1,6-dimethylnaphthalene	28.409
9	156	14,23DMN	1,4-+2,3-dimethylnaphthalene	28.912
10	156	15DMN	1,5-dimethylnaphthalene	29.012
11	156	12DMN	1,2-dimethylnaphthalene	29.381
12	170	137TMN	1,3,7-trimethylnaphthalene	31.583
13	170	136TMN	1,3,6-trimethylnaphthalene	31.717
14	170	135,146TMN	1,3,5-+1,4,6-trimethylnaphthalene	32.186
15	170	236TMN	2,3,6-trimethylnaphthalene	32.264
16	170	127,167,126TMN	1,2,7-+1,6,7-+1,2,6-trimethylnaphthalene	32.734
17	170	124TMN	1,2,4-trimethylnaphthalene	33.158
18	170	125TMN	1,2,5-trimethylnaphthalene	33.359
19	170	123TMN	1,2,3-trimethylnaphthalene	33.862
20	184	1357TeMN	1,3,5,7-tetramethylnaphthalene	35.136
21	184	1367TeMN	1,3,6,7-tetramethylnaphthalene	35.729
22	184	1246,1247,1467TeMN	1,2,4,6-+1,2,4,7-+1,4,6,7-tetramethylnaphthalene	36.164
23	184	1257TeMN	1,2,5,7-tetramethylnaphthalene	36.276
24	184	2367TeMN	2,3,6,7-tetramethylnaphthalene	36.421
25	184	1267TeMN	1,2,6,7-tetramethylnaphthalene	36.712
26	184	1237TeMN	1,2,3,7-tetramethylnaphthalene	36.835
27	184	1236TeMN	1,2,3,6-tetramethylnaphthalene	36.969
28	184	1256,1235TeMN	1,2,5,6-+1,2,3,5-tetramethylnaphthalene	37.405
29	198	12467PMN	1,2,4,6,7-pentamethylnaphthalene	39.852
30	198	12357PMN	1,2,3,5,7-pentamethylnaphthalene	40.087
31	198	12367PMN	1,2,3,6,7-pentamethylnaphthalene	40.679
32	198	12356PMN	1,2,3,5,6-pentamethylnaphthalene	41.182

Table A1.1-2: Phenanthrene and Alkylphenanthrenes, Dibenzothiophene and Alkyldibenzothiophenes m/z 178, 192, 206, 184, 198 &212

Peak	m/z	Compound ID	Compound Name	Retention Time (min)
33	178	P	Phenanthrene	38.522
34	192	3MP	3-methylphenanthrene	41.45
35	192	2MP	2-methylphenanthrene	41.584
36	192	9MP	9-methylphenanthrene	42.042
37	192	1MP	1-methylphenanthrene	42.165
38	206	3EP	3-ethylphenanthrene	43.752
39	206	36,92DMP,1EP	3,6-+9,2-dimethylphenanthrene+1-ethylphenanthrene	44.121
40	206	35,26DMP	3,5-+2,6-dimethylphenanthrene	44.355
41	206	27DMP	2,7-dimethylphenanthrene	44.456
42	206	13,39,210,310DMP	1,3-+3,9-+2,10-+3,10-dimethylphenanthrene	44.78
43	206	25,29,16DMP	2,5-+2,9+1,6-dimethylphenanthrene	44.925
44	206	17DMP	1,7-dimethylphenanthrene	45.059
45	206	23DMP	2,3-dimethylphenanthrene	45.216
46	206	19,49,410DMP	1,9-+4,9-+4,10-dimethylphenanthrene	45.316
47	206	18DMP	1,8-dimethylphenanthrene	45.607
48	206	12DMP	1,2-dimethylphenanthrene	45.976
49	184	DBT	Dibenzothiophene	37.807
50	198	4MDBT	4-methyldibenzothiophene	40.411
51	198	2,3MDBT	2,3-methyldibenzothiophene	40.936
52	198	1MDBT	1-methyldibenzothiophene	41.483
53	212	46DMDBT	4,6-dimethyldibenzothiophene	42.903
54	212	24DMDBT	2,4-dimethyldibenzothiophene	43.227
55	212	26,2EDBT,36DMDBT	2,6-+2-ethyldibenzothiophene+3,6-dimethyldibenzothiophene	43.428
56	212	28,27,37DMDBT	2,8-+2,7-+3,7-dimethyldibenzothiophene	43.875
57	212	16,18,14DMDBT	1,6-+1,8-+1,4-dimethyldibenzothiophene	43.998
58	212	13,34DMDBT	1,3-+3,4-dimethyldibenzothiophene	44.322
59	212	17DMDBT	1,7-dimethyldibenzothiophene	44.411
60	212	23DMDBT	2,3-dimethyldibenzothiophene	44.802
61	212	12DMDBT	1,2-dimethyldibenzothiophene	45.316

Table A1.1-3: Triaromatic and Monoaromatic Steroid Hydrocarbons m/z 231& 253

Peak	m/z	Compound ID	Compound Name	Retention Time (min)
62	231	20TAS	C_{20}-triaromatic steroid hydrocarbon	53.273
63	231	21TAS	C_{21}-triaromatic steroid hydrocarbon	55.117
64	231	26STAS	C_{26} 20S triaromatic steroid hydrocarbon	62.034
65	231	26R,27STAS	C_{26} 20R+C_{27} 20S triaromatic steroid hydrocarbon	63.207
66	231	28STAS	C_{28} 20S triaromatic steroid hydrocarbon	64.191
67	231	27RTAS	C_{27} 20R triaromatic steroid hydrocarbon	64.693
68	231	28RTAS	C_{28} 20R triaromatic steroid hydrocarbon	65.9
69	253	21MAS	C_{21}-monoaromatic steroid hydrocarbon	47.652
70	253	22MAS	C_{22}-monoaromatic steroid hydrocarbon	49.351
71	253	27bSMAS	C_{27} 14β(H) 20S monoaromatic steroid hydrocarbon	56.648
72	253	27bRMAS	C_{27} 14β(H) 20R monoaromatic steroid hydrocarbon	57.877
73	253	28bSMAS	C_{28} 14β(H) 20S monoaromatic steroid hydrocarbon	58.179
74	253	29bS,28bRMAS	C_{29} 14β(H) 20S+C_{28} 14β(H) 20R monoaromatic steroid hydrocarbon	59.486
75	253	29aSMAS	C_{29} 14α(H) 20S monoaromatic steroid hydrocarbon	60.548
76	253	29bR,28aRMAS	C_{29} 14β(H) 20R+C_{28} 14α(H) 20R monoaromatic steroid hydrocarbon	60.838
77	253	29aRMAS	C29 14α(H) 20R monoaromatic steroid hydrocarbon	62.123

1.2 Saturated hydrocarbons

Table A1.2-1: Acyclic alkanes m/z 85

Peak	m/z	Compound ID	Compound Name	Retention Time (min)
78	**85**	n-C13	C_{13} normal alkane	24.587
79	85	n-C14	C_{14} normal alkane	27.873
80	85	n-C15	C_{15} normal alkane	30.968
81	85	n-C16	C_{16} normal alkane	33.896
82	85	n-C17	C_{17} normal alkane	36.667
83	85	Pr	Pristane	36.835
84	85	n-C18	C_{18} normal alkane	39.304
85	85	Ph	Phytane	39.55
86	85	n-C19	C_{19} normal alkane	41.819
87	85	n-C20	C_{20} normal alkane	44.221
88	85	n-C21	C_{21} normal alkane	46.523
89	85	n-C22	C_{22} normal alkane	48.725
90	85	n-C23	C_{23} normal alkane	50.837
91	85	n-C24	C_{24} normal alkane	52.859
92	85	n-C25	C_{25} normal alkane	54.815
93	85	n-C26	C_{26} normal alkane	56.704
94	85	n-C27	C_{27} normal alkane	58.514
95	85	n-C28	C_{28} normal alkane	60.268
96	85	n-C29	C_{29} normal alkane	61.956
97	85	n-C30	C_{30} normal alkane	63.598
98	85	n-C31	C_{31} normal alkane	65.185
99	85	n-C32	C_{32} normal alkane	66.716
100	85	n-C33	C_{33} normal alkane	68.202
101	85	n-C34	C_{34} normal alkane	69.655
102	85	n-C35	C_{35} normal alkane	71.063

Table A1.2-2: Terpanes m/z 191

Peak	m/z	Compound ID	Compound Name	Retention Time (min)
103	191	21TT	C_{21}-Tricyclic terpane	46.702
104	191	22TT	C_{22}-Tricyclic terpane	48.557
105	191	23TT	C_{23}-Tricyclic terpane	50.658
106	191	24TT	C_{24}-Tricyclic terpane	51.775
107	191	25TT	C_{25}-Tricyclic terpane	54.033
108	191	24TeT	C_{24}-Tetracyclic terpane	55.463
109	191	26TTa	C_{26}-Tricyclic terpane	55.653
110	191	26TTb	C_{26}-Tricyclic terpane	55.787
111	191	28TTa	C_{28}-Tricyclic terpane	59.24
112	191	28TTb	C_{28}-Tricyclic terpane	59.519
113	191	29TTa	C_{29}-Tricyclic terpane	60.313
114	191	29TTb	C_{29}-Tricyclic terpane	60.603
115	191	Ts	C_{27} 18α(H)-22,29,30- trisnorneohopane	61.319
116	191	Tm	C_{27} 17α(H)-22,29,30- trisnorneohopane	61.978
117	191	30TTa	C_{30}-Tricyclic terpane	62.235
118	191	30TTb	C_{30}-Tricyclic terpane	62.47
119	191	28BH	C_{28}-Bisnorhopane	63.52
120	191	29H	C_{29}17α(H),21β(H) hopane	64.235
121	191	29Ts	C_{29}18α(H)-30-norneohopane	64.347
122	191	30DiaH	C_{30}17α diahopane	64.526
123	191	29M	C_{29}17β(H),21α(H) hopane	65.017
124	191	30H	C_{30}17α(H), 21β(H) hopane	65.587
125	191	30M	C_{30}17β(H),21α(H) hopane	66.202
126	191	31HS	C_{31}17α(H), 21β(H) 22S homohopane	67.163
127	191	31HR	C_{31}17α(H), 21β(H) 22R homohopane	67.353
128	191	GAM	Gammacerane	67.576
129	191	32HS	C_{32} 17α(H), 21β(H) 22S homohopane	68.392
130	191	32HR	C_{32} 17α(H), 21β(H) 22R homohopane	68.66
131	191	33HS	C_{33} 17α(H), 21β(H) 22S homohopane	69.823
132	191	33HR	C_{33} 17α(H), 21β(H) 22R homohopane	70.191
133	191	34HS	C_{34} 17α(H), 21β(H) 22S homohopane	71.298
134	191	34HR	C_{34} 17α(H), 21β(H) 22R homohopane	71.745
135	191	35HS	C_{35} 17α(H), 21β(H) 22S homohopane	72.75
136	191	35HR	C_{35} 17α(H), 21β(H) 22R homohopane	73.287

Table A1.2-3: Steranes and Diasteranes m/z 217

Peak	m/z	Compound ID	Compound Name	Retention Time (min)
142	217	21PREG	C_{21} Pregnane	48.848
143	217	22PREG	C_{22} Pregnane	51.161
144	217	27baS	C_{27} βα 20S diasterane	57.463
145	217	27baR	C_{27} βα 20R diasterane	58.111
146	217	27abS	C_{27} αβ 20S sterane	58.536
147	217	27abR	C_{27} αβ 20R sterane	59.017
148	217	28baS	C_{28} βα 20S diasterane	59.128
149	217	28baR	C_{28} βα 20R diasterane	59.754
150	217	28abS+27aaaS	C_{28} αβ 20S sterane + C_{27} 5α,14α,17α (H) 20S sterane	60.201
151	217	29baS+27abbR	C_{29} βα 20S diasterane +C_{27} 5α, 14β, 17β (H) 20R sterane	60.391
152	217	28abR+27abbS	C_{28} αβ 20R sterane + C_{27} 5α, 14β, 17β (H) 20S sterane	60.547
153	217	27aaaR	C_{27} 5α, 14α, 17α (H) 20R sterane	60.927
154	217	29baR	C_{29} βα 20R diasterane	61.151
155	217	29abS	C_{29} αβ 20S sterane	61.464
156	217	28aaaS	C_{28} 5α,14α,17α (H) 20S sterane	61.978
157	217	29abR+28abbR	C_{29} αβ 20R sterane + C_{28} 5α, 14β, 17β (H) 20R sterane	62.123
158	217	28abbS	C_{28} 5α, 14β, 17β (H) 20S sterane	62.268
159	217	28aaaR	C_{28} 5α, 14α, 17α (H) 20R sterane	62.738
160	217	29aaaS	C_{29} 5α, 14α, 17α (H) 20S sterane	63.218
161	217	29abbR	C_{29} 5α, 14β, 17β (H) 20R sterane	63.531
162	217	29abbS	C_{29} 5α, 14β, 17β (H) 20S sterane	63.643
163	217	29aaaR	C_{29} 5α, 14α, 17α (H) 20R sterane	64.224

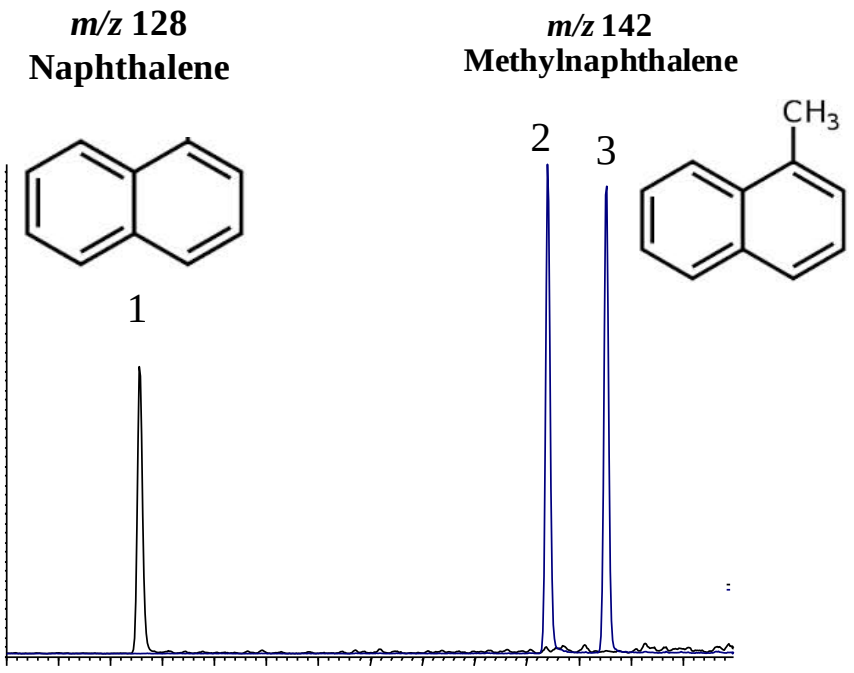
m/z 128
Naphthalene
m/z 142
Methylnaphthalene
CH3
1
2
3

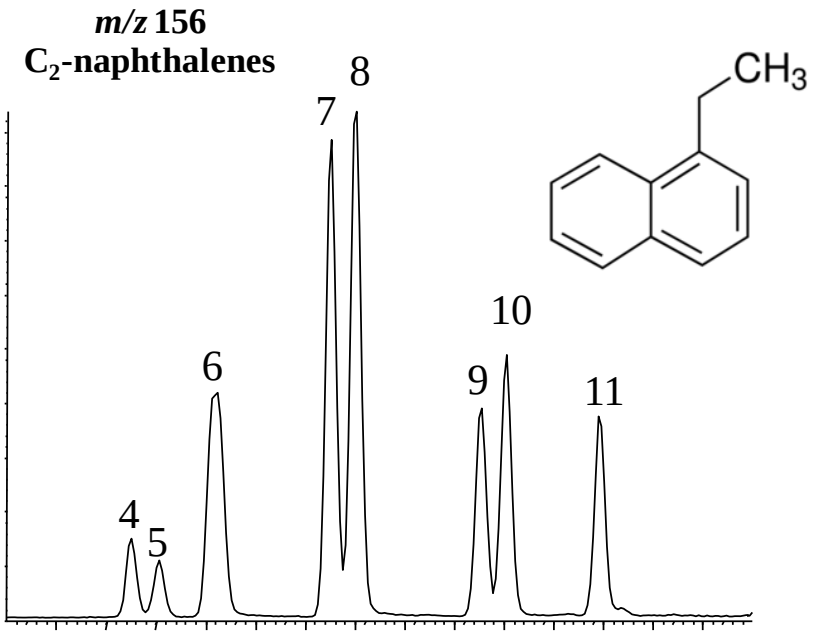
m/z 156
C2-naphthalenes
CH3
4
5
6
7
8
9
10
11

***m/z* 170**
C_3-methylnaphthalenes

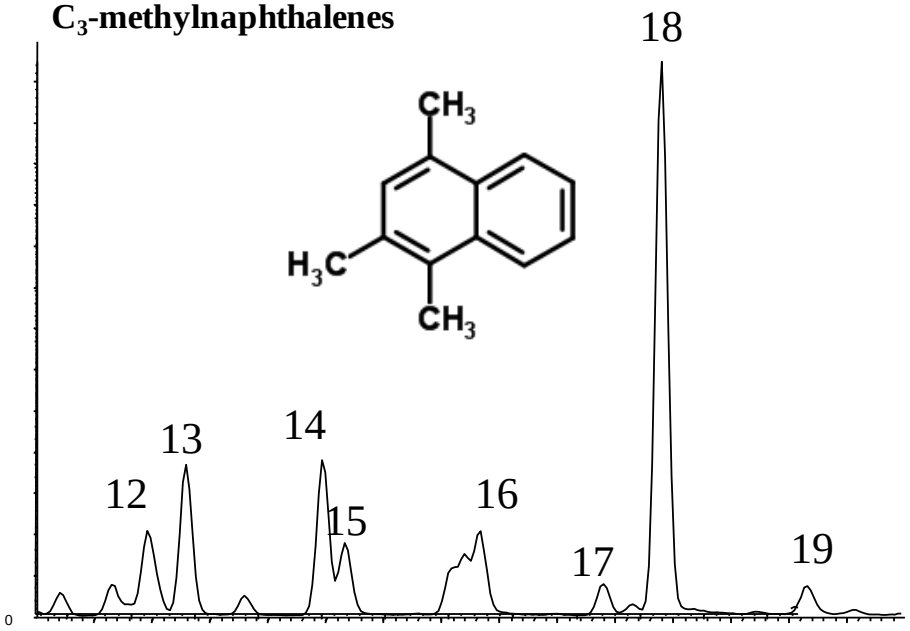

***m/z* 184**
C_4-methylnaphthalenes +DBT

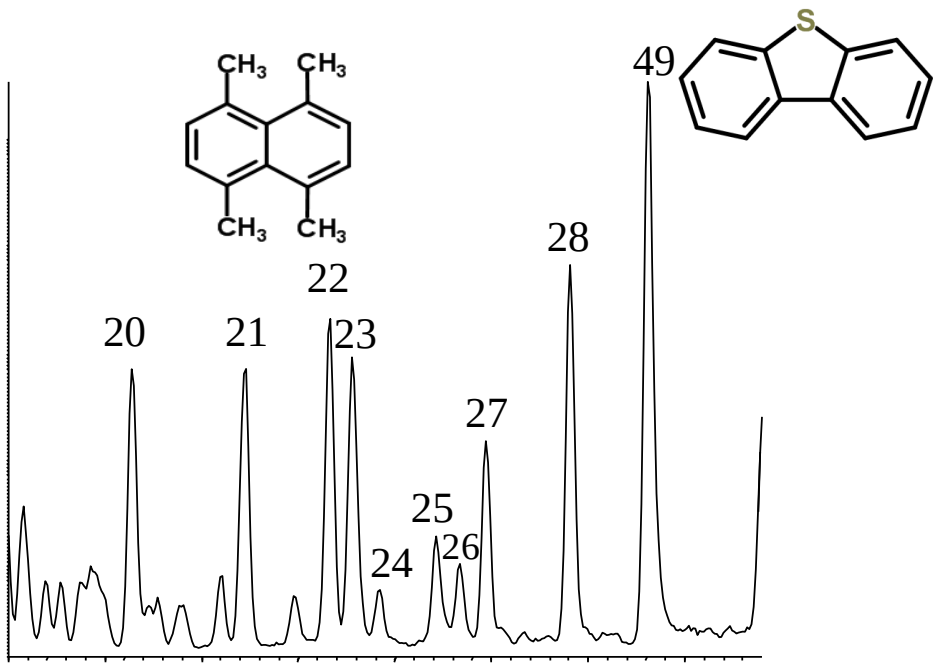

***m/z* 198**
C_5-methylnaphthalene

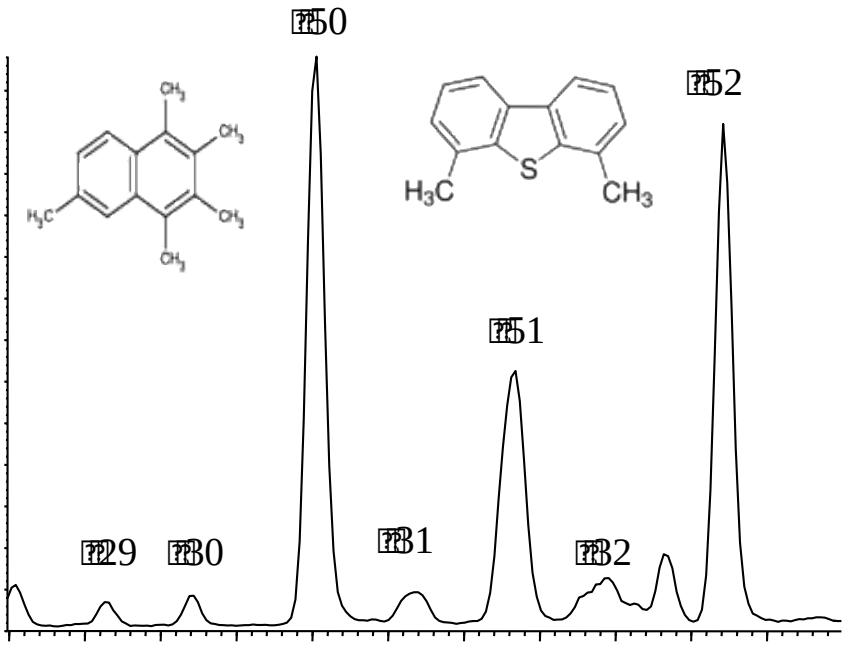

***m/z* 178**
Phenanthrene

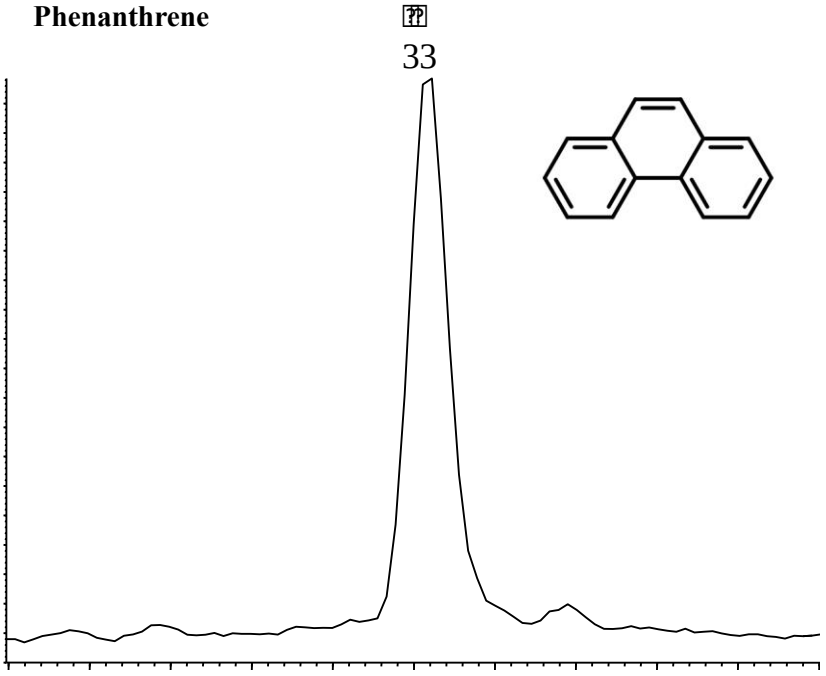

***m/z* 192**
C_1-phenanthrene

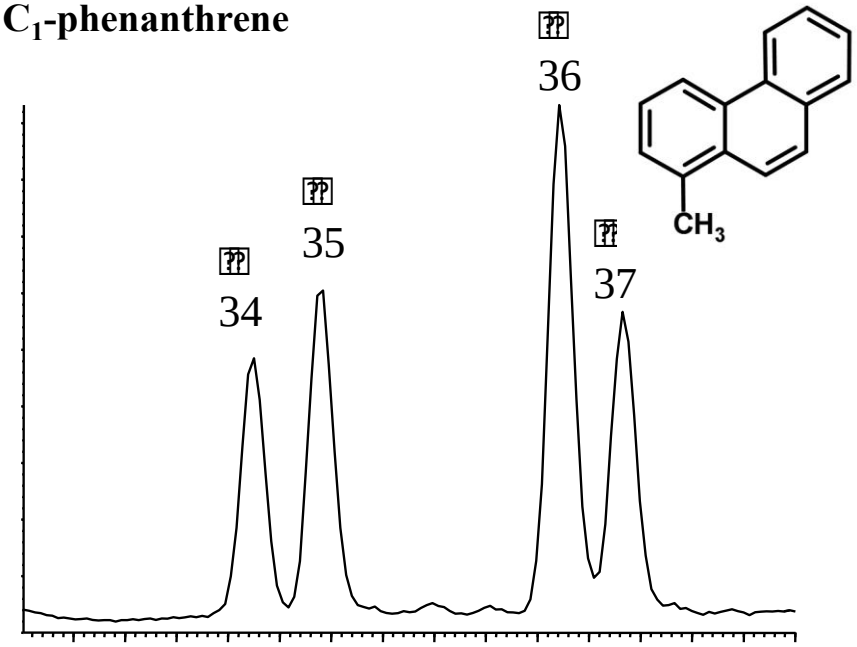

***m/z* 206**
C_2-phenanthrene

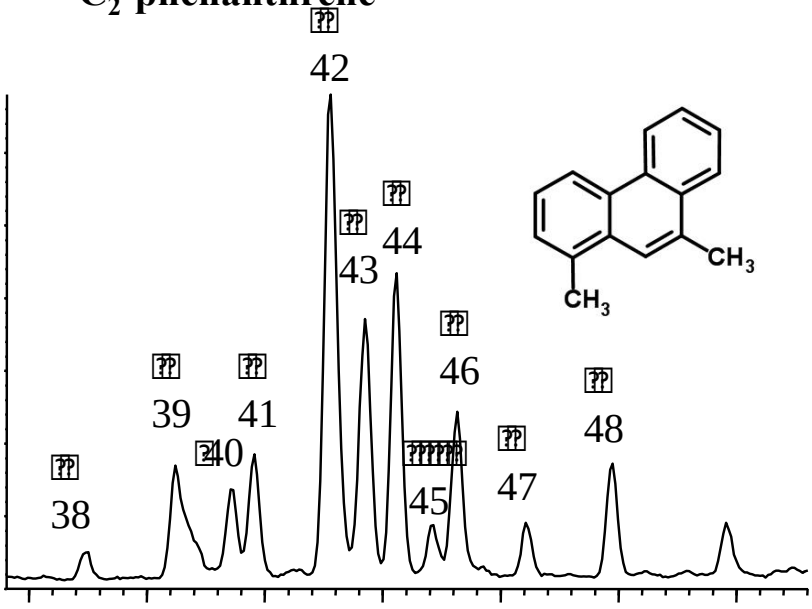

***m/z* 212**
C_2-dibenzothiophenes

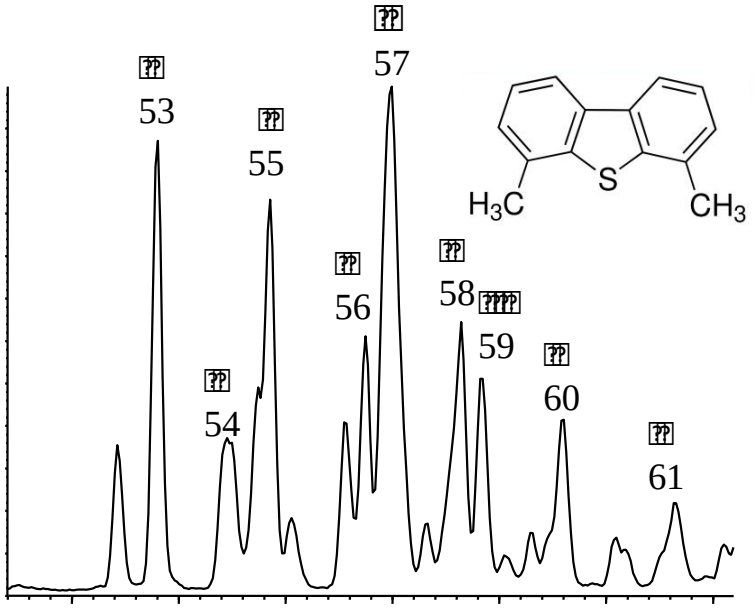

***m/z* 231 Triaromatic Steroids**

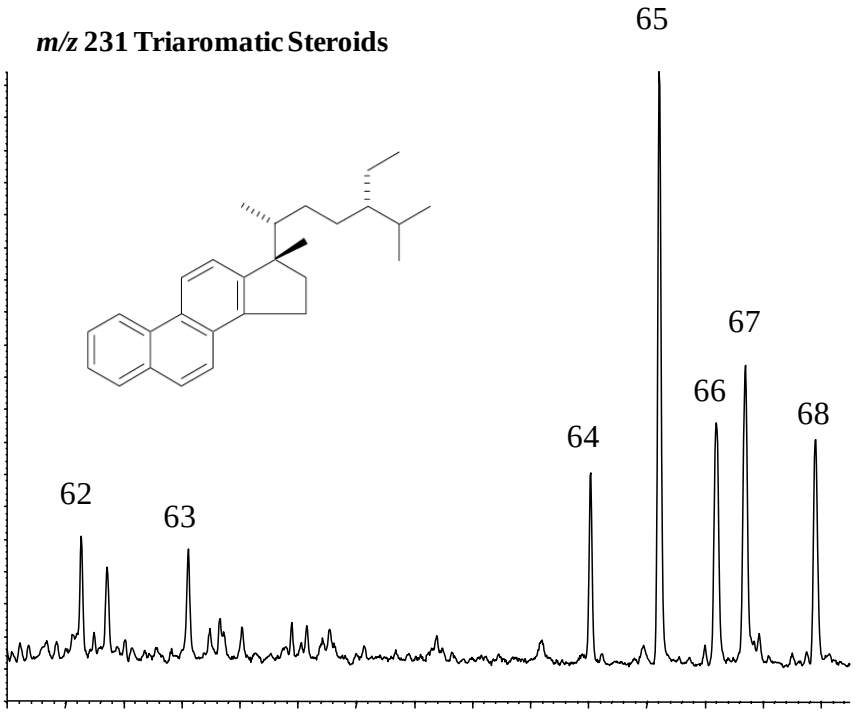

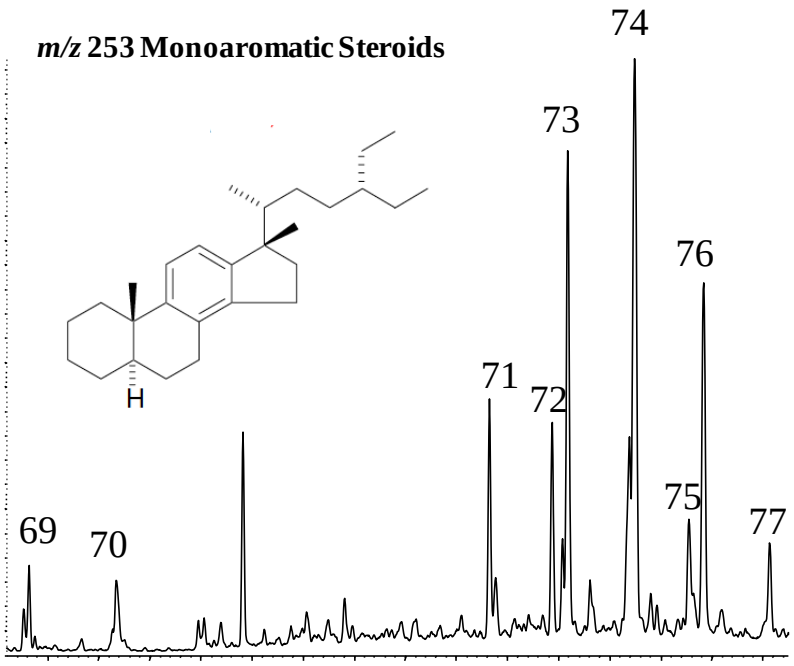
m/z 253 Monoaromatic Steroids
74
73
76
71
72
75
77
69
70
H

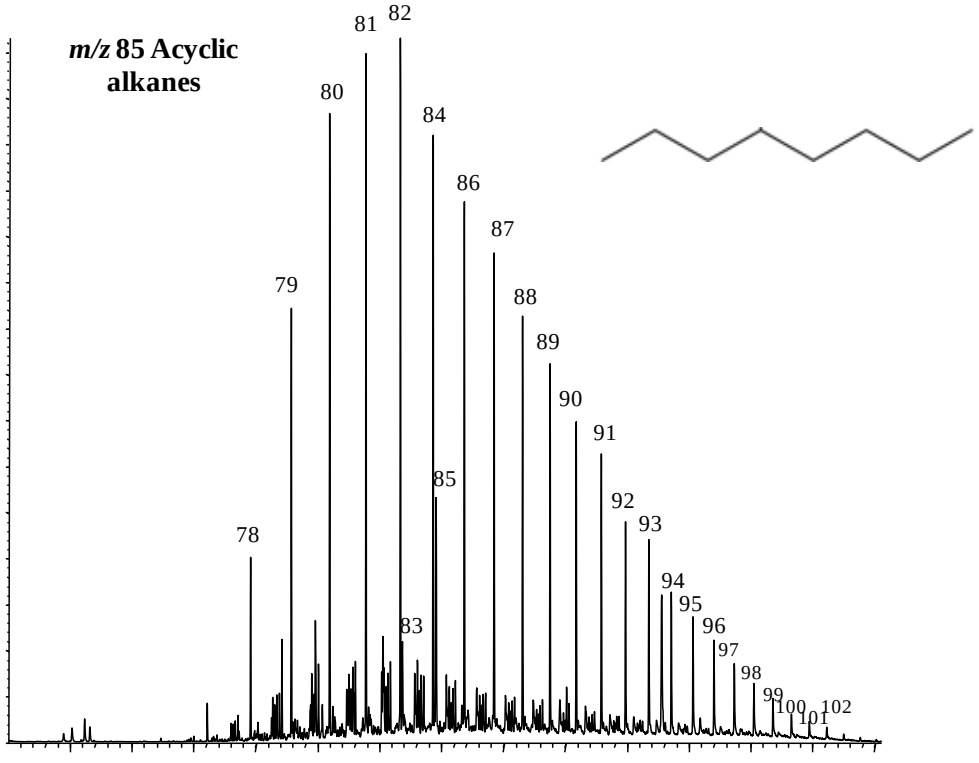
m/z 85 Acyclic alkanes
81
82
80
84
86
87
79
88
89
90
91
85
92
93
78
94
95
96
83
97
98
99
100
101
102

***m/z* 191 Terpanes**

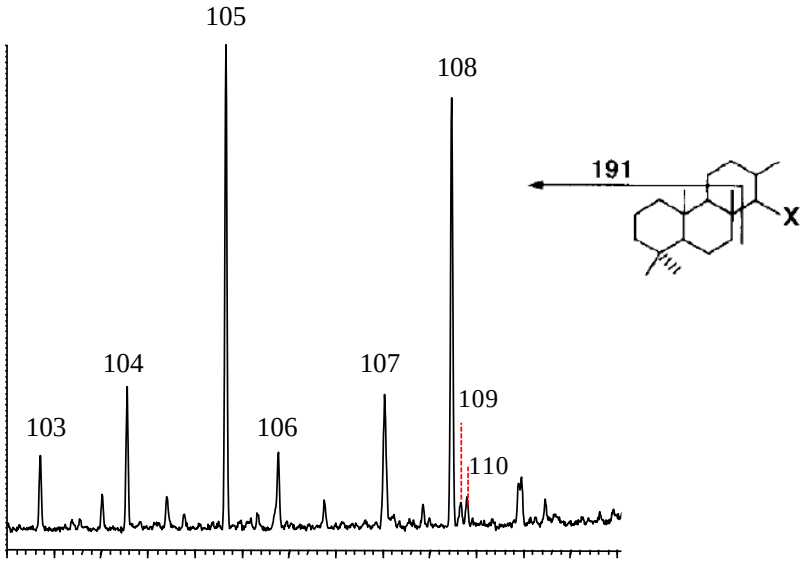

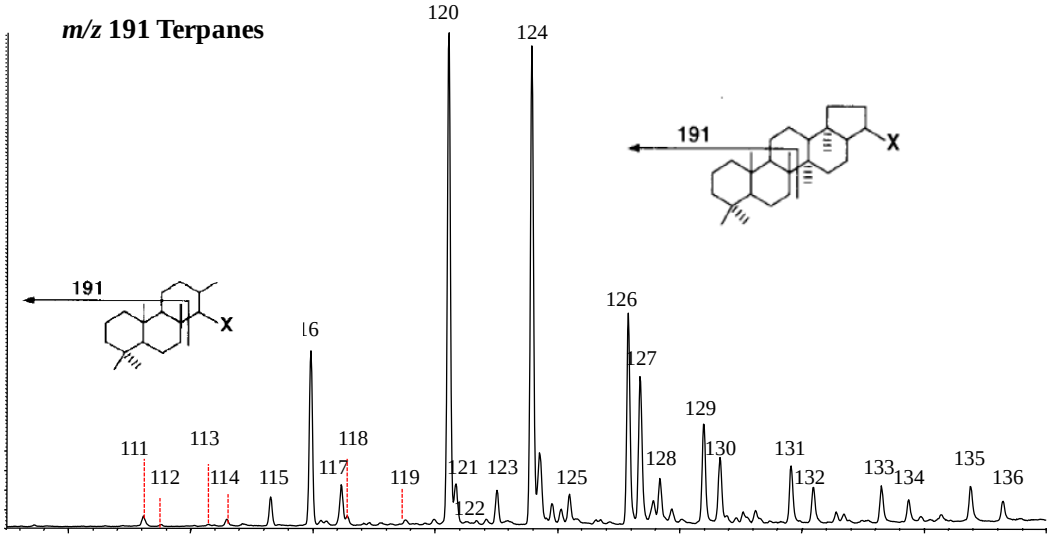

***m/z* 217 Steranes**

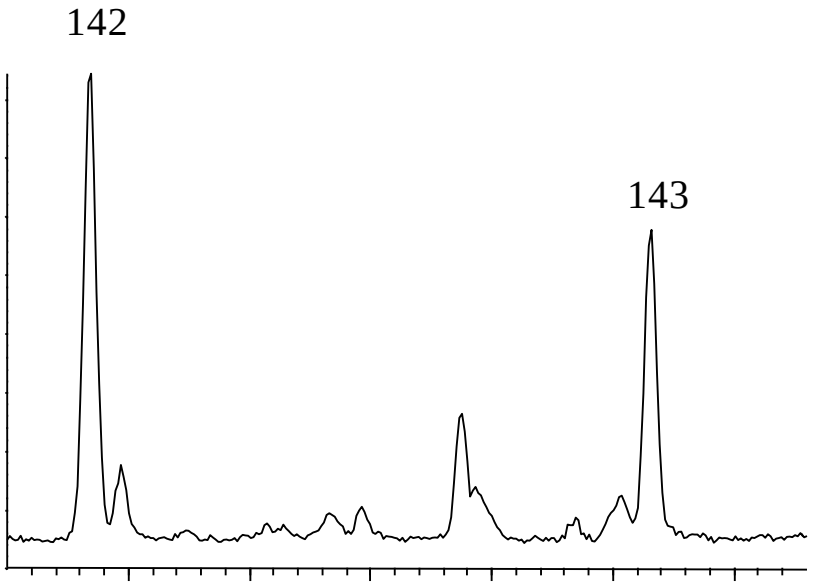

***m/z* 217 Steranes & Diasteranes**

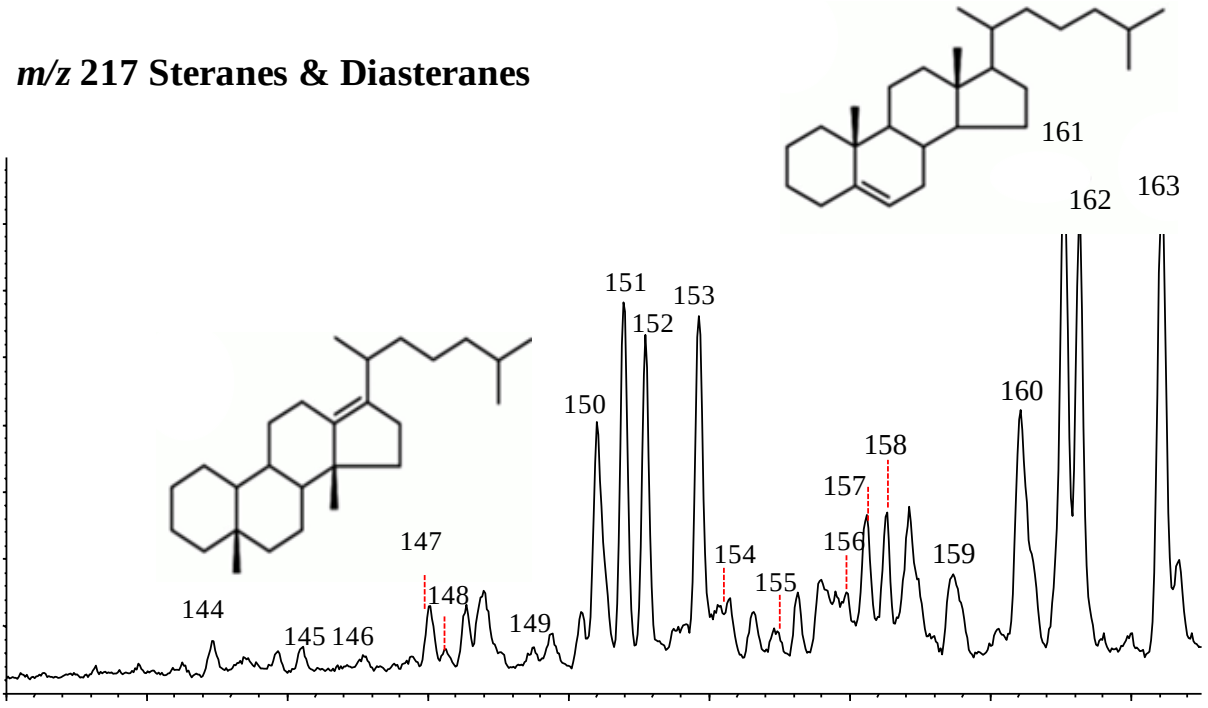

APPENDIX 2

APPENDIX 2: MOLECULAR CONCENTRATIONS IN HEAVY OIL from the SFNY RESERVOIR

Tables A2.1-A2.4: Absolute Concentrations (μg/g) of the families of compounds analyzed in the core-extracted bitumen and produced oil from the SFNY reservoir. Concentrations of individual compounds are available upon request.

Table A2.1:

Sample #	Sample Type	Depth (ft)	N	EN	MN	DMN	TMN	TetMN	PMN
1	Rock Extract	3373.1	55.94	12.65	117.31	164.48	241	90	27
2	Rock Extract	3375.5	75.14	18.93	164.68	225.96	350	101	25
3	Rock Extract	3377.6	38.01	9.17	78.63	113.86	272	77	25
4	Rock Extract	3380.3	47.44	10.35	91.35	125.67	203	85	23
5	Rock Extract	3382.2	45.48	11.10	96.41	134.37	202	78	23
6	Rock Extract	3385.1	38.21	9.25	79.29	118.50	200	87	23
7	Rock Extract	3389.8	42.16	12.88	104.50	169.04	278	106	26
8	Rock Extract	3392.8	39.29	12.57	102.36	161.66	254	93	22
9	Rock Extract	3433.4	6.17	8.81	46.42	132.96	287	110	24
10	Rock Extract	3435.7	2.76	4.79	19.95	81.97	211	92	22
11	Rock Extract	3437.5	8.77	8.24	52.20	117.06	210	84	21
12	Rock Extract	3440.5	12.59	10.62	67.86	153.65	290	115	23
13	Rock Extract	3466.2	4.62	7.05	35.86	111.13	249	108	22
14	Rock Extract	3469.9	2.51	6.30	25.26	108.46	228	88	21
15	Rock Extract	3471.2	2.71	9.20	43.69	154.03	293	107	19
16	Rock Extract	3473.2	1.34	5.57	12.94	127.92	256	107	21
17	Rock Extract	3479.3	1.79	1.60	8.53	49.83	284	96	22
18	Rock Extract	3480.2	1.26	2.99	6.05	80.55	221	96	21
19	Rock Extract	3482.9	1.55	4.32	9.64	103.92	241	97	22
20	Rock Extract	3484.1	1.63	3.60	8.81	85.58	296	96	20
21	Produced Oil	3370-3470	160.23	30.87	367.90	508.69	460	136	20

Table A2.2:

Sample #	Sample Type	Depth (ft)	DBT	MDBT	DMDBT	P	MP	DMP
1	Rock Extract	3373.1	38.42	176.48	310.57	17.76	53.15	103.23
2	Rock Extract	3375.5	34.35	160.02	521.22	16.73	49.73	108.42
3	Rock Extract	3377.6	29.46	138.50	348.99	16.86	51.05	100.72
4	Rock Extract	3380.3	27.78	132.33	287.28	17.68	50.05	106.42
5	Rock Extract	3382.2	28.92	132.16	557.10	16.87	51.43	102.33
6	Rock Extract	3385.1	32.71	155.41	333.77	16.92	50.17	106.52
7	Rock Extract	3389.8	40.72	180.52	347.96	18.46	53.85	106.07
8	Rock Extract	3392.8	27.31	130.71	327.49	16.43	49.43	102.55
9	Rock Extract	3433.4	20.20	99.50	242.67	17.36	51.26	99.27
10	Rock Extract	3435.7	14.98	69.30	221.60	16.63	50.05	103.27
11	Rock Extract	3437.5	12.57	60.08	214.12	16.24	49.68	101.57
12	Rock Extract	3440.5	15.05	67.16	158.83	16.91	48.03	100.57
13	Rock Extract	3466.2	16.70	74.02	178.78	17.27	48.12	101.10
14	Rock Extract	3469.9	21.9	92.48	204.62	16.93	48.16	99.34
15	Rock Extract	3471.2	26.40	85.35	166.45	17.89	49.50	98.81
16	Rock Extract	3473.2	22.40	86.89	174.12	18.21	48.44	92.54
17	Rock Extract	3479.3	16.79	75.40	255.28	18.93	48.43	92.32
18	Rock Extract	3480.2	15.24	74.05	243.37	17.61	48.26	99.88
19	Rock Extract	3482.9	16.99	73.16	228.85	18.74	50.36	100.22
20	Rock Extract	3484.1	15.02	72.37	232.04	18.05	47.64	99.37
21	Produced Oil	3370-3470	50.24	188.16	362.92	33.21	93.37	140.36

Table A2.3:

Sample #	Sample Type	Depth (ft)	n-C17	Pr	TAS	MAS	BP	DBF
1	Rock Extract	3373.1	1233.13	270	386.58	1339.33	2.8	9.83
2	Rock Extract	3375.5	1250.37	250	421.76	1565.62	2.3	7.37
3	Rock Extract	3377.6	1303.11	243	377.01	1348.84	1.8	4.64
4	Rock Extract	3380.3	1205.23	229	388.63	1385.68	1.7	4.97
5	Rock Extract	3382.2	1261.03	240	391.69	1388.82	2.0	7.58
6	Rock Extract	3385.1	1246.27	239	392.76	1318.14	2.0	5.52
7	Rock Extract	3389.8	1331.94	281	368.66	1342.28	2.1	7.87
8	Rock Extract	3392.8	1139.55	226	382.49	1372.63	2.0	6.98
9	Rock Extract	3433.4	1066.96	208	360.74	1450.45	1.0	3.66
10	Rock Extract	3435.7	1042.49	209	338.09	1374.11	0.7	4.70
11	Rock Extract	3437.5	1110.34	182	348.28	1376.75	1.3	4.93
12	Rock Extract	3440.5	1169.38	209	347.82	1354.19	1.4	3.84
13	Rock Extract	3466.2	1166.04	227	376.37	1532.91	1.3	3.80
14	Rock Extract	3469.9	1216.16	245	355.66	1460.44	1.5	4.12
15	Rock Extract	3471.2	1259.00	255	398.02	1408.26	1.3	4.77
16	Rock Extract	3473.2	1291.45	260	390.03	1391.17	1.4	4.26
17	Rock Extract	3479.3	1191.66	237	402.25	1499.31	0.9	3.14
18	Rock Extract	3480.2	1217.49	240	402.44	1518.23	0.8	3.33
19	Rock Extract	3482.9	1276.77	258	372.36	1482.00	1.3	3.96
20	Rock Extract	3484.1	1218.44	260	388.09	1473.50	1.0	3.94
21	Produced Oil	3370-3470	1882.59	421	337.94	1313.43	19.3	6.85

Table A2.4:

Sample #	Sample Type	Depth (ft)	Tricyclic Terpane	Hopane	Homohopane	Gammacerane	Sterane	Diasterane
1	Rock Extract	3373.1	233.48	1600.49	1322.12	55.05	427.83	54.72
2	Rock Extract	3375.5	234.73	1525.07	1274.59	53.95	422.69	54.39
3	Rock Extract	3377.6	230.25	1485.69	1259.86	56.57	428.23	53.56
4	Rock Extract	3380.3	207.58	1399.41	1176.72	53.59	394.37	48.72
5	Rock Extract	3382.2	199.37	1293.94	1162.23	51.75	364.71	45.30
6	Rock Extract	3385.1	232.63	1421.72	1154.36	49.64	402.38	52.83
7	Rock Extract	3389.8	202.41	1364.29	1116.64	49.59	358.77	45.19
8	Rock Extract	3392.8	192.88	1443.17	1243.37	53.51	363.24	44.37
9	Rock Extract	3433.4	212.01	1385.81	1216.67	55.83	375.35	46.71
10	Rock Extract	3435.7	197.15	1379.67	1175.79	52.88	359.44	44.21
11	Rock Extract	3437.5	200.58	1396.47	1180.93	54.86	368.80	43.64
12	Rock Extract	3440.5	205.32	1432.40	1181.47	49.94	350.37	44.46
13	Rock Extract	3466.2	223.98	1507.02	1138.55	50.84	394.56	50.00
14	Rock Extract	3469.9	206.43	1436.37	1160.06	54.87	378.90	48.90
15	Rock Extract	3471.2	204.48	1519.41	1310.31	58.39	384.12	46.60
16	Rock Extract	3473.2	203.32	1489.44	1276.39	57.45	371.88	46.42
17	Rock Extract	3479.3	211.10	1579.72	1341.62	58.82	391.26	48.69
18	Rock Extract	3480.2	214.79	1575.56	1336.32	58.02	391.99	48.62
19	Rock Extract	3482.9	212.24	1600.95	1364.36	58.17	396.01	49.16
20	Rock Extract	3484.1	207.81	1559.25	1327.94	59.63	388.27	48.55
21	Produced Oil	3370-3470	179.81	1292.18	1100.69	49.31	326.50	40.02